For New Technology Network

NTN®

TECHNICAL REVIEW

No. 71

Special Issue

Special Supplement to Industrial Machines

April 2004

ISSN 0915-0528 OSAKA,JAPAN

CONTENTS

Preface

Wasaburo SUGANUMA 1

Technical Papers

Improving Rolling Contact Fatigue Life of Bearing Steels Through Grain Refinement
Chikara OOKI, Kikuo MAEDA and Hirokazu NAKASHIMA 2

Dynamic analysis of Cage behavior in a Cylindrical Roller Bearing
Tomoya SAKAGUCHI and Kaoru UENO 8

New Products

Precision Bearings "ULTAGE" Series for Machine Tools
Futoshi KOSUGI 18

Bearings for High Speed CT Scanner
Yosuke OYA 28

Integrated Sensor Bearing Unit for Axleboxes
Masanori UENO 34

Bearings for Wind Turbine
Souichi YAGI 40

Insulated bearing "MEGAOHM" series
Hideji ITO 48

New High-Capacity HWTJ Type Pressed Cage and Needle Roller Assemblies
Katsufumi ABE 52

HK-F type drawn cup needle roller bearings
Hideki AKAMATSU 56

Hydrodynamic BEARPHITE Unit for HDD
Kiyotaka KUSUNOKI 62

High Angle Active Link
Keisuke SONE, Hiroshi ISOBE and Koji YAMADA 70

Technical Articles

Improvement of Leakage Magnetic Flux Resistance of Integrated Sensor Bearings
Takashi KOIKE, Tomomi ISHIKAWA, Hiroyoshi ITO and Noriyoshi MIZUTANI 74

Introduction of Grinding Swarf Recycling
Kanji NAKAMURA 80

New Products Information 84

[Preface]

Special Issue

Special Supplement to Industrial Machines

Wasaburo SUGANUMA
Executive Director

In the second half of the 20th century, when industry was booming, awareness began to increase about the effect that industrialization may have on the natural environment and on our social surroundings. It became clear that people strongly desired an environment where they could live comfortably and safely. Now that we are into the 21st century, industrial products are designed with safety and human convenience as primary considerations.

As a result of these changes in the atmosphere, industrial machine designs are also advancing to be more ecologically sound and people-friendly. For example, emphasis in the machine tool industry has been placed on considerations affecting the working environment –such as sound generation and air quality– in addition to strictly performance-related issues such as increasing speed and precision capabilities. The increased reliability of railroad vehicles has been achieved simultaneously with increased speed performance and maintenance intervals. Also, the use of sensors used for failure prediction, integrally designed with the bearings used, is on the rise. CT scanners, imaging equipment used in the medical field, are being widely used. To reduce patient stress during the exam, higher speed operation and lower noise levels are required by the scanner manufacturers. Furthermore, wind power generation systems are being installed worldwide as a clean source of energy.

NTN has been advancing bearing designs in step with technological innovations in all industrial machinery fields, and actively seeks improvement of various technologies for longer life and reduction of size, weight, and friction for these applications. In this special issue, we introduce technology for bearing life improvement, high speed and precision, and environmental preservation, together with the basic technologies that allow these developments. Included are the following subjects:

- FA-treated bearings, with drastically prolonged rolling contact fatigue life due to grain refinement;
- ULTAGE series, which has gained a reputation for precision bearings in machine tools;
- Hydrodynamic BEARPHITE unit that is rapidly gaining acceptance in hard disk drive market;
- MEGAOHM series that features high insulation capability and reliability through the application of special ceramics and improvements in spray-coating methods

In the midst of global industrial structural changes, we hope that **NTN** can contribute, through bearings and other precision products, to a global environment and living conditions in which our children, who will be leaders in the coming decades, can live comfortably and safely.

Improving Rolling Contact Fatigue Life of Bearing Steels Through Grain Refinement

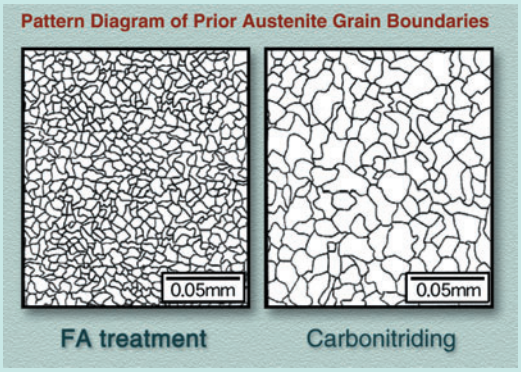

Chikara OOKI*
Kikuo MAEDA*
Hirokazu NAKASHIMA*

It is well known that yield strength can be improved by reducing the ferritic grain size (i.e. Hall-Petch's Law) and that through a reduction in the ferritic grain size an increase in a steel's fatigue life is observed. However, the specific effect of grain refinement on rolling contact fatigue life has not been thoroughly investigated. The primary obstacle in researching hardened steels (which possess a martensitic structure) has been the difficulty in obtaining small, uniform grain sizes. Recently, some new methods for the grain refinement of hardened steels have been discovered. One such method is called "Ausforming", which induces a large deformation at temperatures over Ac1. Unfortunately, this remarkable method is as yet unavailable for practical manufacturing. Keeping this in mind, we set out to develop a specialized heat-treatment process. The main objective was to obtain a grain refined martensitic structure within JIS-SUJ2 (SAE52100 equivalent) bearing steel, produced by a standard manufacturing process, while at the same time minimizing productivity loss. Thus far, we have succeeded in creating a prior austenite grain size of approximately 5 μm in diameter (half that of the conventional grain size). It is believed that the packet or block size of the martensite decreases proportionally with that of the prior austenite grain size. As a result, during RCF testing, the grain refined SUJ2 material demonstrated a fatigue life that was twice as long as carbonitrized steel under both clean and debris-contaminated conditions. In addition, the grain refined SUJ2 material was superior in fracture strength and aged dimensional stability. Therefore, it can be concluded that the grain refinement of existing bearing steels could prove to be very useful in greatly extending fatigue life.

1. Introduction

Steel is a polycrystalline substance, containing various microstructures such as prior austenite, martensite and ferritic grain boundaries. Many studies have been conducted detailing the effects of grain size variations on the macro-properties of steel. It is well known that yield strength of steel can be improved (as well as, the fatigue life) through a general reduction in the materials' grain size (i.e. Hall-Petch's Law) [1]. This technique is commonly referred to as "grain refinement".

By and large, there have been few detailed studies concerning the effects of grain refinement on steels' rolling contact fatigue (i.e. RCF) life. Primarily, because it was believed that a) the grains of quenched bearing steels were already considerably small, b) excessively small grains hindered the hardenability of steels, and c) specialized heat treatment processes such as "Ausforming" and the "Grange Method" [2] were required for further grain refinement. This paper summarizes the attempt to extend the RCF life of bearing steels through grain refinement via. a specialized heat-treatment process.

*Reserch & Development Center Technical Reserch Dept.

2. Refinement of Crystal Grains

Given that the size of crystalline grains are largely dependant upon the quenching temperature [3], it is assumed that a more refined grain structure can be produced if the quenching temperature is kept as low as possible but still above the austenite transformation temperature. However, to provide the steel with sufficient hardness, it is necessary for at least a minimum amount of carbon to be dissolved in martensite. Thus, the quenching temperature must be determined by taking into account both the amount of dissolved carbon and the degree of grain refinement required. This is the reason why it is not conventionally possible to perform quenching at considerably lower temperatures.

In this study, test specimens were initially nitrided to reduce the steel's Ac1 transformation temperature and maintain a sufficient amount of dissolved carbon in the martensite during the primary quenching process. The specimens were then heat treated at lower temperatures (in the secondary quenching process) to produce refined or smaller crystalline grains.

The adaptation of the grain-refining heat treatment method allowed the JIS-SUJ2 (SAE 52100 EQUIVALENT) test material to form prior austenite grain boundaries with an average size of 5mm or smaller and hardnesses of HV700 or higher (even after tempering at 180˚C for 2 hours). The steel processed as a result of this specialized heat treatment is hereafter referred to (within this study) as "FA-treated" material. **Photo 1** shows the prior austenite grain boundaries of a normally quenched material, carbonitrided material and FA-treated material. The FA-treated material possesses crystalline-grain diameters that are at least 50% smaller than that of the other two materials.

3. Point Contact Type Rolling Contact Fatigue Test

To investigate basic rolling contact fatigue characteristics, cylindrical specimens (ϕ 12×L22) were tested under clean lubrication conditions. SUJ2 (SAE 52100 EQUIVALENT) material was used to fabricate these test specimens; one exhibiting a normal level of cleanliness, the other possessing a lesser degree of cleanliness. **Fig. 1** shows the analytical results for the evaluation of non-metallic inclusions, conducted using **NTN**'s inclusion quantification unit [4]. Type Ⅰ refers to A-type inclusions with TiN, and Type Ⅱ refers to B and C-type inclusions without TiN. Regarding Type Ⅰ and Ⅱ, it was shown that the specimen with the lesser degree of cleanliness contained the greater percentage of inclusions.

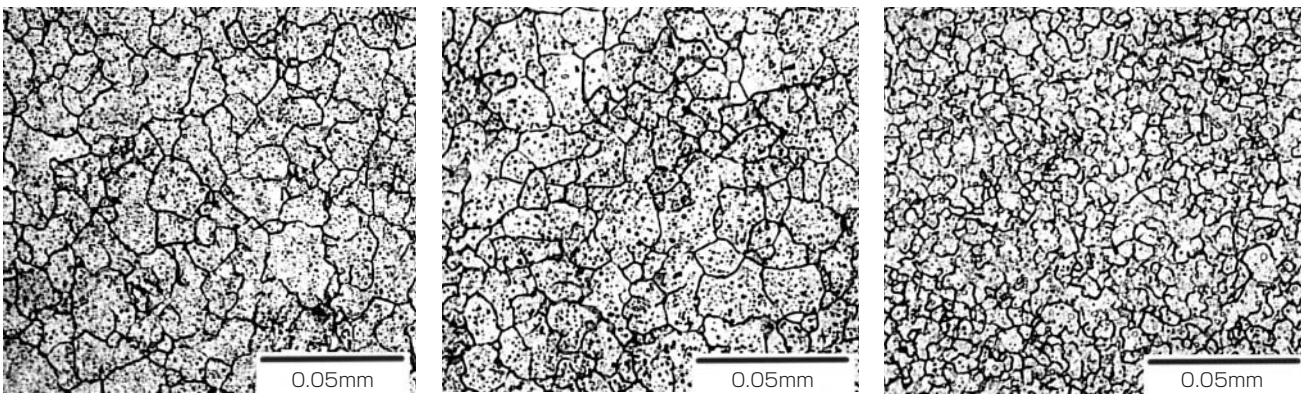

Normally quenched | Carbonitrided | **FA treated**

Photo 1 The prior austenite grain boundaries

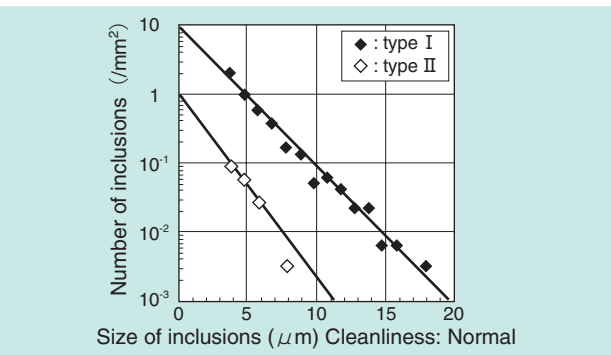

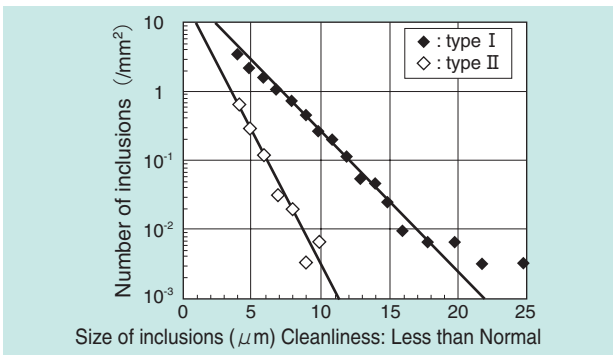

Fig. 1 Size distributions of non-metallic inclusions (Measurement area:1000mm^2)

Fig. 2 illustrates a schematic of the test rig, and **Table 1** shows the test conditions.

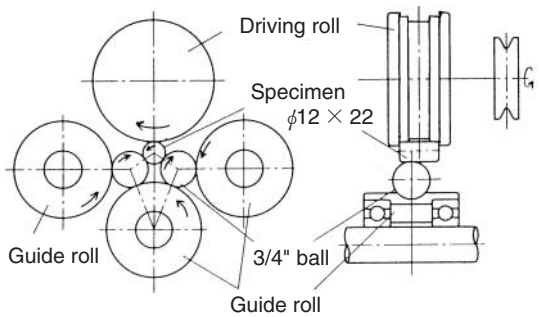

Fig. 2 ϕ 12 point contact type rolling contact fatigue test rig

Table 1 Test condition of point contact fatigue test

Specimen	Cylindrical specimen (ϕ 12 x L22)
Steel ball	3/4" (19.05mm)
Maximum contact stress (GPa)	5.88
Load speed (cpm)	46240
Lubricating oil	Turbine VG68, forced oil lubrication

Table 2 shows the results of a point contact type rolling contact fatigue test. Regarding the steel specimen possessing normal cleanliness, the L_{10} life of the carbonitrided material was found to be 3.1 times longer than the normally quenched material, while the FA-treated material was 5.4 times longer. In the case of the steel specimens possessing a lesser degree of cleanliness, the FA-treated material displayed an L_{10} life 3.5 times longer than that of carbonitrided material. Unfortunately, the testing of the normally quenched specimen (with a lesser degree of cleanliness) was suspended, due to surface peeling developing within the specimens early on in the testing. It is evident (from the above data) that RCF life can be prolonged by the refinement of crystalline grains.

4. Life Test Under Contaminated Lubrication Conditions

Since the cleanliness of steels has greatly improved due to the advancement of steel manufacturing processes, peeling that is due primarily to rolling contact fatigue rarely occurs [5].

However, given the increasingly hostile environments in which bearings are being subjected (especially in automotive applications), the entry of hard-particle debris is avoidable. It is clear that the main cause of damage to bearings today is due to flaking that starts from indentations formed by these particles. This section evaluates the benefits of FA-treated material within such applications.

L_{10} life testing was conducted with 6026-type ball bearings and 30206-type tapered bearings using lubrication contaminated with relatively large hard-particle debris.

4. 1 RCF-Test on 6206-Type Ball Bearing Under Contaminated Lubrication Conditions

The bearings used for the test were normally quenched, carbonitrided, and FA-treated 6206-type ball bearings manufactured from SUJ2 (SAE 52100 EQUIVALENT). **Table 3** shows the metallurgical constituents from each bearing sample. The amount of retained austenite in the FA-treated bearing was between those of the carbonitrided and FA-treated bearings.

Table 3 Metallurgical properties of ball bearing 6206 (0.05mm depth from surface)

Heat treatment	Prior austenite grain boundaries Average particle size (μm)	HV hardness	Residual stress (MPa)	Amount of retained austenite (%)
Normally quenched	10.5	746	+15	7.1
Carbonitrided	9.4	752	-110	25.5
FA treated	4.4	733	-122	18.9

Table 2 Test results of point contact fatigue test

Cleanliness	Heat treatment	N count	End face hardness (HRC)	L_{10} life (cycles)	L_{50} life (cycles)	L_{10} life ratio
Normal	Normally quenched	14	62.4	8017 $\times 10^4$	18648 $\times 10^4$	1
	Carbonitrided	7	63.0	24656	33974	3.1
	FA treated	6	61.6	43244	69031	5.4
Lower	Normally quenched	4	62.5	— 1)	—	—
	Carbonitrided	10	63.6	9018	21653	1.1
	FA treated	10	60.5	30327	55040	3.8

1) Life calculation was not possible due to peeling observed on specimens at an early stage of the testing.

Fig. 3 shows a schematic of the test rig, and **Table 4** shows the test conditions.

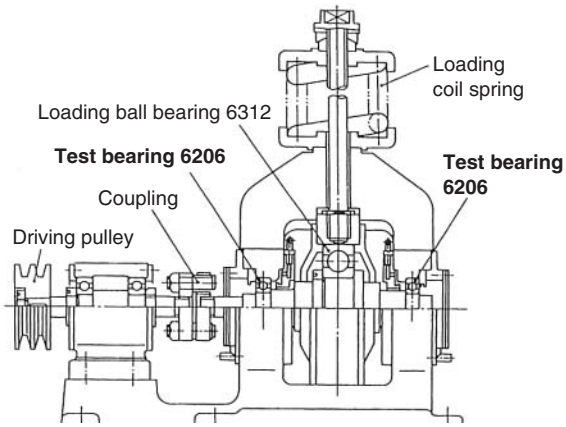

Fig. 3 NTN rolling contact fatigue test rig for ball bearing

Table 4 Test condition of 6206 ball bearing under contaminated lubrication

Load F_r (kN)	6.86
Maximum contact stress (GPa)	3.2
Rotation speed (min^{-1})	3000 (Inner ring rotation)
Lubricating oil	Turbine oil 56, oil bath, approx. 30ml
Contaminant amount	0.4g/L
Contaminant type	Gas atomized particles :Grain size 100 to 180 μm Hardness approx. HV800

Table 5 shows the results from the life testing. The L10 life of the FA-treated bearing was 3.7 times longer than that of the normally quenched bearing, and 2.1 times longer than that of the carbonitrided sample. It is once again evident, that RCF life can be prolonged by this specialized grain refinement method (i.e. FA-treatment). Even under contaminated lubrication conditions, which can produce indentation-originated peeling, it is seen that grain refinement can provide a positive effect.

Traditionally, it has been known that the greater the amount of retained austenite within steel, the higher the hardness and the longer the life under contaminated lubrication [6]. However, as shown in **Table 3**, the FA-treated bearing possesses a longer life even though it contains less retained austenite than the carbonitrided-bearing This again shows that grain refinement provides a compensatory effect for the reduction in life that occurs as a result of lower percentage of retained austenite.

Table 5 RCF-life test results of 6206 under contaminated lubrication

Heat treatment	N count	L_{10} life (h)	L_{50} life (h)	L_{10} life ratio (when the life of normally quenched bearing is 1.0)
Normally quenched	4	13.1	19.4	1.0
Carbonitrided	7	23.0	45.5	1.8
FA treated	7	48.0	87.2	3.7

4. 2 Life Test on 30206-Type Tapered Bearings Under Contaminated Lubrication Conditions

The bearings used for the test were normally quenched, carbonitrided and FA-treated 30206-type tapered bearings, manufactured from SUJ2 (SAE 52100 EQUIVALENT). **Table 6** shows the main metallurgical constituents from each bearing sample. Similar to the previous 6206-type ball bearings, the FA-treated bearing sample contains more retained austenite than the normally quenched bearing but less than the carbonitriding.

Table 6 Metallurgical properties of 30206 tapered roller bearing (0.05mm depth from surface)

Heat treatment	Prior austenite grain boundaries Average particle size (μm)	HV hardness	Residual stress (MPa)	Amount of retained austenite (%)
Normally quenched	11.8	792	+10	6.0
Carbonitrided	12.2	763	-140	32.4
FA treated	5.2	748	-118	23.3

Fig. 4 shows a schematic of the test rig, and Table 7 shows the test conditions.

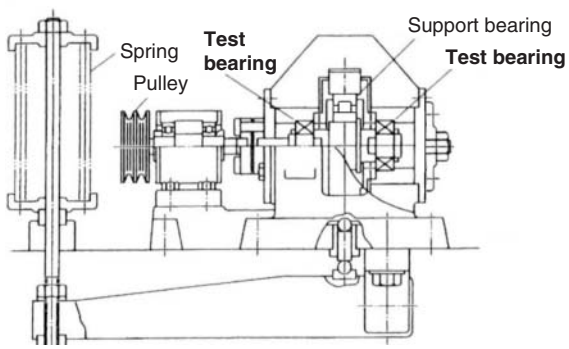

Fig. 4 NTN rolling contact fatigue test rig for tapered roller bearing

Table 7 Test condition of 30206 tapered roller bearing under contaminated lubrication

Load (kN)	F_r	17.64
	F_a	1.5
Maximum contact stress (GPa)		2.5
Rotating speed (min^{-1})		2000 (Inner ring rotation)
Lubricating oil		Turbine oil 56, oil bath, approx. 30ml
Contaminant amount		1.0g/L
Contaminant type		Gas atomized particles: 50 μm or smaller (80wt%) 100 to 180 μm (10wt%) Hardness approx. HV800

Table 8 shows the results of the life testing. The L_{10} life of the FA-treated bearing was 4.1 times longer than that of the normally-quenched bearing, and 2.0 times longer than that of the carbonitrided bearing.

Table 8 The RCF-life test results of 30206 tapered roller bearing under contaminated lubrication

Heat treatment	N count	L_{10} life (h)	L_{50} life (h)	L_{10} life ratio (when the life of normally quenched bearing is 1.0)
Normally quenched	6	101.2	117.3	1.0
Carbonitrided	6	211.6	284.5	2.1
FA treated	6	415.6	464.3	4.1

5. Dimensional Change Occurring at High Temperatures

When bearings operate at high temperatures for extended periods of time, very small dimensional changes can occur. One of the main causes for this dimensional change is an expansion in the material lattice size due to the transformation of retained austenite to martensite. Thus, the greater the percentage of retained austenite within bearing steel, the greater the dimensional change or instability, making it difficult to use them at higher temperatures. Since FA-treated bearings possess less retained austenite than carbonitrided bearings, it is expected that they will develop smaller dimensional changes.

To test dimensional stability, the outer rings of 6206-type bearings were held at 100˚C and 120˚C respectively, for 2500 hours, and then measured. The results are shown in **Table 9**. It is clear that the dimensional change ratio of the FA-treated specimen is smaller than that of the carbonitrided specimen. Specifically, with regards to samples tested at 100˚C, the dimensional change ratio of the FA-treated specimen is approximately 1.3 times less than that of the normally quenched material. Given the likelihood that bearings in the near future will be operating under more thermally unstable conditions, it will become extremely important to design units (such as the FA-treated specimen) with high-temperature dimensional stability.

Table 9 Dimensional change after 2500h-soak

Heat treatment	The amount of retained γ (%)	Dimensional change [1]	
		Temperature: 100˚C	Temperature: 120˚C
Normally quenched	7.0	1.0	1.0
Carbonitrided	27.7	1.8	2.5
FA treated	20.5	1.3	1.6

1) Ratio to the normally quenched bearing

6. Fracture Strength

Bearing ring components (outer diameter: ϕ 60, inner diameter: ϕ 45, width: 15) were manufactured from SUJ2 (SAE 52100 EQUIVALENT) and tested to evaluate their static fracture stress.

Investigation on impact strength was also conducted using JIS3 Charpy impact specimen (U-notched). As shown in **Table 10,** the carbonitrided specimen possessed a lower static fracture stress and Charpy impact strength than the normally quenched specimen. The strength of the FA-treated specimen was found to be almost equal to that of the normally quenched specimen, in spite of having a carbonitrided layer.

Table 10 Test results of fracture strength

Heat treatment	Static fracture stress (MPa)	Charpy impact strength (J/cm^2)
Normally quenched	2770	6.70
Carbonitrided	2330	5.33
FA treated	2840	6.65

7. Discussion

As explained in Sections 3 and 4, the FA-treated material possesses a longer RCF life than the conventional carbonitrided material. This is primarily due to the delaying of the rolling contact fatigue mechanism by the grain refinement.

As shown in **Fig. 1**, the grain size of prior austenite contained within the FA-treated material is 1/2 times or smaller than conventional material. However, because every structure of prior austenite contains some martensite, it is thought that these structures have a large influence upon the life and strength of the material. So, a FE-SEM/EBSP measuring instrument [7] was used to measure the distribution of crystal orientations, to ascertain the difference in martensite particle size between the carbonitrided and FA-treated materials.

Photo 2 shows an image obtained by FE-SEM/EBSP, and **photo 3** shows the distribution of crystalline orientation. It is clear (compared to the carbonitrided material) that the FA-treated material possesses smaller martensite particles. The areas within 10 degrees of crystal orientation were assumed to be the same crystal particles, and the diameter of a circle of the same area was assumed to be the particle size. The results reveal the average particle size of the carbonitrided material as being 0.66 mm, and that of

the FA-treated material as being 0.49 mm. Therefore; it can be considered that extension of RCF life through grain refinement is caused by the uniformly reduced particle size of martensite.

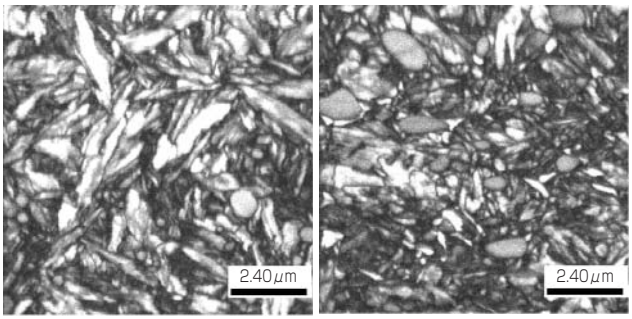

Carbonitrided **FA treated**

Photo 2 Image of FE-SEM/EBSP

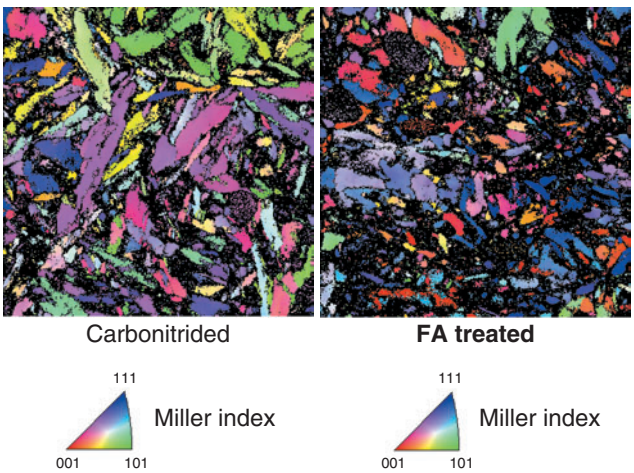

Carbonitrided **FA treated**

Photo 3 Distribution of crystal orientations by FE-SEM/EBSP

8. Conclusion

By double-quenching through-hardened steel after carbonitriding, we succeeded in reducing the size of prior austenite grain size to half that of conventional steels. Various tests that were conducted demonstrate the following properties of the grain-refined material.

1) FA-treated material has a RCF life that is approximately double the RCF life of carbonitrided material; irrespective of lubrication conditions.
2) FA-treated material developed fewer dimensional changes than that of the carbonitrided material (approximately 70%).
3) The static fracture stress and impact strength, that are reduced as a result of carbonitriding, can be restored.

NTN has begun to utilize this specialized grain-refined material within specific applications. We believe that as bearings begin to operate under increasingly hostile environments, the need for this technology will expand.

References

1) K.Tanaka, TETSU-TO- HAGANE, Vol.79, No.8 (1993), 908(in Japanese)
2) T.Yokota, TETSU-TO- HAGANE, Vol.86, No.7 (2000), 479(in Japanese)
3) The Japan Institute of Materials, KINZOKUBINRAN, (2000), 122(in Japanese)
4) H.Murakami, **NTN** TECHNICAL REVIEW, No.68 (2000), 58(in Japanese)
5) K.Maeda, **NTN** TECHNICAL REVIEW, No.65 (1996), 58(in Japanese)
6) N.Tsushima, SAE Technical paper series (1986), 860725
7) S.Suzuki, MTERE2, Vol.50, No.7 (2001), 612(in Japanese)

Photos of authors

Chikara OOKI
Technical Reserch Dept.
Reserch& Development Center

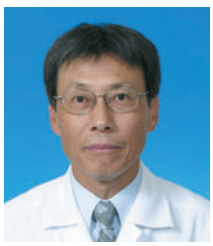

Kikuo MAEDA
Technical Reserch Dept.
Reserch& Development Center

Hirokazu NAKASHIMA
Technical Reserch Dept.
Reserch& Development Center

Dynamic Analysis of Cage Behavior in a Cylindrical Roller Bearing

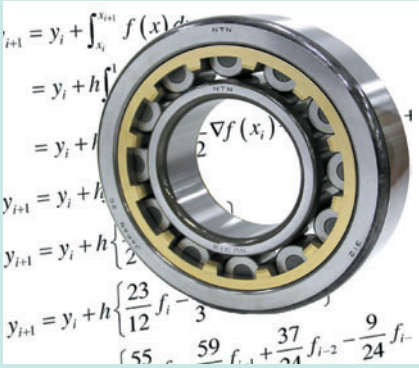

Tomoya SAKAGUCHI*
Kaoru UENO**

It is important to understand time-varying behavior and stress of a cage for an advanced design procedure of rolling bearings. A dynamic analysis tool is required for that purpose.

Hence, we introduced a commercial software "ADAMS (MSC. Software)" for virtual prototyping of a mechanical system. The environment provides a set of high-performance numerical integration solvers to resolve equations of motion as well as high-level visualization functions of the numerical results.

In this report, as a milestone for the development of dynamic analysis tools of various types of rolling bearings, we developed a code on ADAMS that can simulate real-time behavior of a cylindrical roller bearing assuming the motion of all the bearing elements is planar. Also, with regard to the cage behavior, we made a comparison between numerical and experimental results. The results show that interaction forces between the cage and the rollers traveling around the exit of the load zone have a major influence on the cage motion.

1. Introduction

It is important to understand time-varying behavior and stress of a cage for an advanced design procedure of rolling bearings. A dynamic analysis tool is required for that purpose.

Hence, we introduced commercial software "ADAMS [1)]" for virtual prototyping of a mechanical system. The environment provides a set of high-performance numerical integration solvers to resolve equations of motion as well as high-level visualization functions of the numerical results.

In this report, as a milestone for the development of dynamic analysis tools of various types of rolling bearings, we developed a code on ADAMS that can simulate real-time behavior of a cylindrical roller bearing assuming the motion of all the bearing elements is planar. Also, with regard to the cage behavior, we made a comparison between numerical and experimental results.

The results show that interaction forces between the cage and the rollers traveling around the exit of the load zone have a major influence on the cage motion.

2. Symbols

a_n : Amplitude of n-th order waviness of cage roundness, m

b : Hertz contact half-width, m

b_n : Phase of n-th order waviness of cage roundness, rad

C_r : Basic dynamic radial load rating, N

D : Non-dimensional Deborah number $[= \eta_0 e^{\alpha \bar{P}} \bar{u}/Gb]$

E : Young's modulus, Pa

E' : Equivalent Young's modulus, Pa

F_{EHLr} : Shearing force by viscosity of EHL film, N

*Technical Research Dept., Research & Development Center
**Industrial Engineering Department, Industrial Sales Headquarters

F_{hydro} : Viscous shearing force of oil film at cage guide, N
F_{px} : Rolling directional component of EHL film pressure, N
F_T : Tangential force at contact area, N
F_y, F_z : Force acting on cage at cage guide, N
f : Frequency, Hz
G : Dimensionless material parameter $[=\alpha_0 E']$
h : Oil film thickness, m
h_c : Central oil film thickness, m
$h_{c,iso}$: Isothermal central film thickness, m
k' : Thermal conductivity of lubricant, W/mK
l_{be} : Roller effective width, m
l_{co} : Effective width (one side) of cage guide face, m
L_T : Thermal load factor $[=\eta_0 \beta \bar{u}^2/k']$
$\bar{P}$: Mean pressure of Hertzian contact, Pa
P_{HZ} : Maximum pressure of Hertzian contact, Pa
Q : Normal force at contact area, N
R : Radius of curvature, m
R_{co} : Radius of cage outer diameter, m (Average value if an upper bar is present)
R_e : Equivalent radius, m
R_g : Radius of outer ring inner diameter, m
$\bar{S}$: Mean dimensionless shearing stress of contact areas $[=\tau_s/\tau_0]$
s : Slip ratio $[=|u_b-u_r|/\bar{u}]$
t : Time, s
U : Dimensionless velocity $[=\mu_0\bar{u}/(E'R)]$
u : Surface velocity, m/s
$\bar{u}$: Mean velocity, m/s $[=0.5\times|u_b+u_r|]$
W : Dimensionless load parameter $[=Q/(E'R_e l_{be})]$
X_c : Dimensionless length of EHL contact area $[=(D/\Sigma)\sinh^{-1}\Sigma]$
y_c, z_c : Geometric center position of cage, m
y_0, z_0 : Geometric center position of outer ring, m
N_z : Number of rolling elements
α : Viscosity pressure coefficient, 1/Pa
α_0 : Pressure viscosity index of lubricating oil under normal pressure, 1/Pa
β : Viscosity temperature-rise coefficient, 1/K
δ : Geometric interaction amount, m
ε : Eccentricity ratio for journal bearing model
η_0 : Viscosity under normal temperature and pressure, Pa・s
θ : Angle, rad
Λ : Film parameter (Ratio to oil film parameter, combined roughness)
Λ_{bd} : Maximum film parameter under boundary lubrication
Λ_{hd} : Minimum film parameter under hydrodynamic lubrication
μ_{bd} : Traction coefficient under boundary lubrication
μ_{hd} : Traction coefficient under hydrodynamic lubrication
μ_r : Traction coefficient at contact area
ν : Poisson's ratio
Σ : Dimensionless shearing velocity of lubricant $[=\eta_0 e^{\alpha p} s/(\tau_0 h_c)]$
τ_0 : Characteristic stress of lubricant, Pa
τ_r : Shearing stress by viscosity of EHL film during pure rolling, Pa
τ_s : Shearing stress by slip of EHL film, Pa
ϕ : Angle, rad
ϕ_c : Angle at cage center, rad
ϕ_r : Cage revolution angle, rad
ϕ_{TH} : Oil film thickness correction factor by shearing heat of EHL oil film
ϕ_{TR} : Correction factor by shearing heat of EHL rolling viscous resistance
ω : Revolution angle of each element, rad/s

Subscript

b : Roller
c : Cage
i : Inner ring
o : Outer ring
r : Raceway

3. Analysis Method for Cage Behavior

Fig. 1 shows a schematic of the test bearing and its coordinate system. All the coordinates are expressed in the right-handed Cartesian coordinate system. While the outer ring is fixed in space, the inner ring rotates clockwise about the -X axis and the radial load is in the +Z direction. Gravity is in the -Z direction.

Principal assumptions are given below.

1. The inner ring and cage can move on the radial plane (Y-Z plane in **Fig. 1**) only.
2. Contact force in geometric interaction areas conforms to the elastic contact theory.
3. Traction characteristic conforms to Formula [2] set by Mr. Muraki et.al..
4. Rolling viscous resistance [3] by EHL film exists in the contact area between the rollers and raceway.
5. The interaction model at the cage guide is expressed using the theory of short-width journal bearing with squeeze effect and cage's outer diameter roundness taken into account, and Gümbel's boundary condition is adopted.
6. Gravity is taken into account.

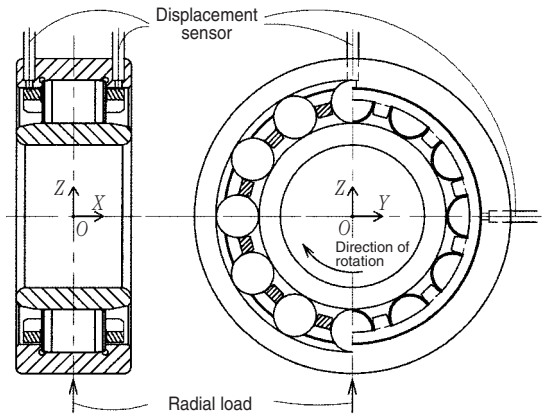

Fig.1 Schematic of test bearing and its coordinate system

As the initial condition for numerical integration solvers of equations of motion, it is assumed that the rollers and cage rotate on their own axis or rotate around the other at mechanics theoretical speed. It is also assumed that the cage is centered at the outer raceway and the rollers are located on the pitch circle line as well as the center of the cage pocket. Rotational displacement was forced to the inner ring at a constant angular velocity.

Physical observation time was set to 0.3 seconds and data recording was performed at 0.5-ms intervals.

Calculation model for each interaction area is shown below.

3.1 Interaction Force between Roller Rolling Contact Surface and Raceway

The model of interaction force between roller rolling contact surface and raceway is based on the following assumptions.

1) Because of the relative positions of the rollers and raceway given by time t, normal force by contact and tangential force and rolling viscous resistance [3] by EHL film will occur between the two objects only when geometrical interaction occurs. For analysis of dynamics, squeeze effect (dependant of speed) by EHL film must be taken into account. However, this is not considered since doing so will require accurate EHL calculation that necessitates tremendous cost.
2) If the EHL film is so thin that it will tear, friction by solid contact must be taken into account for the tangential force.
3) Consider that line contact of the roller's effective length (l_{be}) occurs if geometrical interaction amount (δ) is given, and calculate normal force Q using Palmgren's simplified equation. Determine non-dimensional load variable W based on Q, and then calculate the film thickness using the Pan-Hamrock's formula for isothermal central film thickness of EHL in line contact [4] and Ghosh-Pandey's thermal correction factor equation [5].

$$\delta_{i,o} = 0.39\left(\frac{8}{E'}\right)^{0.9}\frac{Q^{0.9}}{l_{be}^{0.8}} \quad \cdots\cdots (1)$$

$$h_c = \phi_{TH} h_{c,iso} = \phi_T \cdot 2.922\, W^{-0.166} U^{0.692} G^{0.47} R_e \quad (2)$$

where,

$$R_e^{-1} = \begin{cases} \dfrac{1}{R_b} + \dfrac{1}{R_i} & \text{for Roller/Inner race} \\ \dfrac{1}{R_b} - \dfrac{1}{R_o} & \text{for Roller/Outer race} \end{cases} \quad \cdots\cdots (3)$$

$$E' = 2\left[\frac{1-\nu_b^2}{E_b} + \frac{1-\nu_r^2}{E_r}\right]^{-1} \quad \cdots\cdots (4)$$

$$\phi_{TH} = [1 + 1.6\, W^{0.152} L_T^{0.379} (1 + 3.96 s^{0.96})]^{-1} \quad (5)$$

4) From this calculated film thickness, obtain traction coefficient (μ_{hd}) for hydrodynamic lubrication using Muraki-Kimura's simplified equations[2] shown below.

$$X_c \geq 2 : \bar{S} = D/\Sigma \quad \cdots\cdots (6)$$

$$X_c < 2 : \bar{S} = \sinh^{-1}\Sigma\{1 - (D/4\Sigma)\sinh^{-1}\Sigma\} \quad \cdots (7)$$

$$\mu_{hd} = \tau_0 \bar{S}/\bar{P} \quad \cdots\cdots (8)$$

Where, $X_c = (D/\Sigma)\sinh^{-1}\Sigma$ indicates the dimensionless length of EHL contact area.

For equation (7), it is necessary to consider temperature rise caused by self heating of the film, therefore, convergence calculation is required. From this, the traction coefficient of the EHL film can be determined.

As shown in assumption 2), the traction coefficient (μ_r) for the entire set of all lubrication regimes can be approximated by equation (9), with influences of boundary lubrication and mixed lubrication taken into account.

$$\mu_r = \begin{cases} \mu_{bd} & \text{if } \Lambda < \Lambda_{bd} \\ \left\{\dfrac{\mu_{bd} - \mu_{hd}}{(\Lambda_{bd} - \Lambda_{hd})}(\Lambda - \Lambda_{hd})^6 + \mu_{hd}\right\} & \text{if } \Lambda_{bd} \leqq \Lambda < \Lambda_{hd} \\ \mu_{hd} & \text{if } \Lambda_{hd} \leqq \Lambda \end{cases} \quad \cdots\cdots (9)$$

The tangential force (F_T) with μ_{bd} = 0.1, Λ_{bd} = 0.06, Λ_{hd} = 3.0 can be calculated by equation (10).

$$|F_T| = \mu_r Q \quad \cdots\cdots (10)$$

5) For the EHL rolling viscous resistance, use Zhou-Hoeprich's equation (11) [3]. The direction of F_{EHLr} is the same for both objects, and is opposite to the composite velocity vector on the contact surface of the two objects. For the rotating two objects, the force (F_{px}) caused by the pressure component in the EHL film rolling direction must be taken into account [3].

$$F_{EHLr} = \phi_{TR} \frac{29.2 R_e l_{be} (GU)^{0.648} W^{0.246}}{\alpha_0} \quad \cdots\cdots \quad (11)$$

Provided that, $\phi_{TR} = \dfrac{1 - 13.2(P_{HZ} - / E')L_T^{0.42}}{1 + 0.213(1 + 2.23s^{0.83})L_T^{0.64}}$

$$F_{pxb,r} = -\frac{2R_e}{R_{b,r}} F_{EHLr} \quad \cdots\cdots\cdots\cdots\cdots\cdots\cdots\cdots\cdots \quad (12)$$

3.2 Interaction Force between Rollers and Cage Pocket

The interaction force model is almost the same as the one between roller rolling contact surface and raceway. However, since the traction force is dominant due to large slip ratio, the EHL rolling viscous resistancet [3] can be ignored. The model for interaction force between rollers and cage pocket is given below.

1) Because of the relative positions of the rollers and cage pocket given by time t, normal force by contact and tangential force by EHL film will occur between the two objects only when geometrical interaction occurs. Squeeze effect for these objects is ignored.
2) If the EHL film is so thin that it will tear, friction by solid contact must be taken into account for the tangential force.
3) Consider that line contact of the roller's effective length (lbe) occurs if geometrical interaction amount δ is given, and calculate normal force Q in the same way as 3.1, "Interaction Force between Roller Rolling Contact Surface and Raceway".
4) From this calculated film thickness, obtain traction coefficient using Muraki-Kimura's simplified equations (6) to (8) [2].
5) If the center of the rollers comes out of the oblique-line area (see **Fig. 2**) enclosed by the pocket center and pocket ends, only the interaction force caused by solid contact between the roller and pocket edge must be taken into account.

3.3 Interaction Force between Cage and Outer Ring (Guiding surface)

Since the outer ring guide type cage is used, only the interaction force between the cage and outer ring's rib inner diameter can be taken into account. The assumptions are given below.

1) Since the guide's width is smaller than the diameter, a short-width journal bearing theory is used.
2) The bearing is placed under a hydrodynamic lubrication for an isoviscous-rigid regime and a laminar flow, and the squeeze effect and cage's outer diameter roundness must be taken into account. The cage's outer diameter roundness is expressed by equation (13).

$$R_{co}(\theta) = \overline{R_{co}} + \sum_{n=1}^{m} a_n \cos(n\theta + b_n) \quad \cdots\cdots\cdots \quad (13)$$

3) Only positive pressures among those obtained by Reynolds equation are taken into account (Gümbel's boundary condition).
4) If the clearance is infinitely small in the case of journal bearing, an infinitely large interaction force will occur theoretically. Thus, the interaction force caused by direct contact between the cage and outer ring can be ignored.

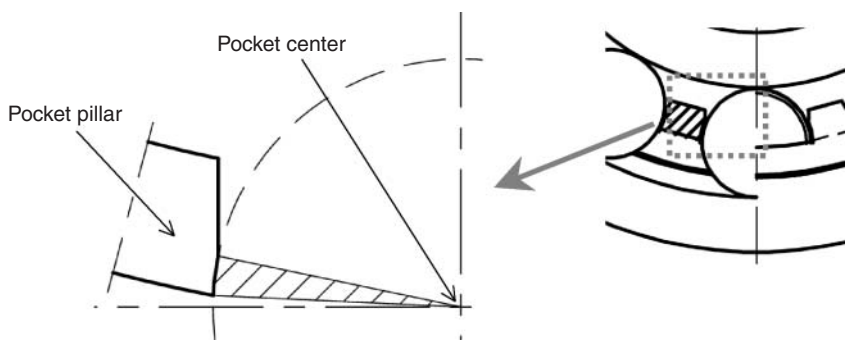

Fig. 2 Cross section of cage pocket

Equations for the short-width journal bearing based on the above assumptions are given below. The coordinate system for this model is shown in **Fig. 3**. The force given on the cage by the film is expressed by a sum of two equivalent journal bearings, and is obtained by equation (14) by y-z plane.

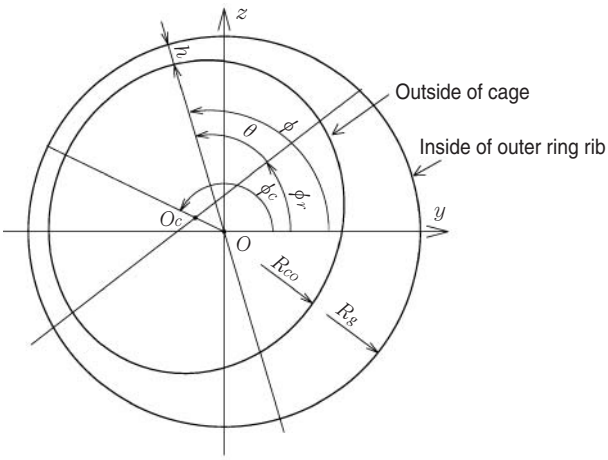

Fig. 3 Journal bearing coordinate system for outer ring land riding cage

$$\begin{bmatrix} F_y \\ F_z \end{bmatrix} = \eta_0 R_{co} l_{co}^3 \int_0^{2\pi} g(\phi) \begin{bmatrix} \cos\phi \\ \sin\phi \end{bmatrix} d\phi \quad \cdots\cdots (14)$$

$$g(\phi) = \frac{1}{h^3}\left[\omega_c \frac{\partial h}{\partial \phi} + 2\frac{\partial h}{\partial t}\right] \quad \cdots\cdots\cdots\cdots (15)$$

$$g(\phi) = \begin{cases} g(\phi) & \text{if } g(\phi) < 0 \\ 0 & \text{otherwise} \end{cases} \quad \cdots\cdots\cdots\cdots (16)$$

$$h = (R_g - R_{co}(\phi - \phi_r)) - (y_c - y_o)\cos\phi - (z_c - z_o)\sin\phi \quad \cdots\cdots\cdots\cdots (17)$$

$$\frac{\partial h}{\partial \phi} = \sum_{n=2}^{m}\left[n a_n \sin\left\{n(\phi - \phi_r) + b_n\right\}\right] + (y_c - y_o)\sin\phi - (z_c - z_o)\cos\phi \quad \cdots\cdots\cdots\cdots (18)$$

$$\frac{\partial h}{\partial t} = \sum_{n=2}^{m}\left[-n\,\omega_c a_n \sin\left\{n(\phi - \omega_c t) + b_n\right\}\right] - (\dot{y}_c - \dot{y}_o)\cos\phi - (\dot{z}_c - \dot{z}_o)\sin\phi \quad \cdots\cdots\cdots (19)$$

Equation (16) indicates that negative pressures are ignored as cavitation condition.

The viscous frictional force (F_{hydro}) acting along the cage's outer diameter surface is expressed by equation (20) as a sum of two equivalent journal bearings. "$R_{co} \times F_{hydro}$" acts as a moment to prevent the cage from rotating on its axis.

$$|F_{hydro}| = \frac{\eta_0 \omega_c R_{co}^2 l_{co}}{R_g - R_{co}} \frac{4\pi}{\sqrt{1-\varepsilon^2}} \quad \cdots\cdots\cdots\cdots (20)$$

where, ε indicates the eccentricity ratio as given in equation (21).

$$\varepsilon = \frac{\sqrt{(y_c - y_o)^2 + (z_c - z_o)^2}}{R_g - R_{co}} \quad \cdots\cdots\cdots\cdots\cdots\cdots (21)$$

4. Cage Behavior Measuring Method

Attach the test bearing to the horizontal type spindle that rotates clockwise about the -X axis, and exert +Z radial load on the outer ring. Gravity is in -Z direction.

Table 1 shows the specifications of the test bearing and running conditions. The cage is made of brass, and is guided by the inner diameter surface of the outer ring's rib as shown in **Fig. 1**. The cage is short in the arc length, but has a cylindrical pocket surface (see **Fig. 2**).

Measurement of cage behavior is carried out using two eddy-current displacement gauges for both Y and Z directions. The reason for using two gauges for the X direction is to check the cage for absence of conical oscillation.

Table 1 Test bearing and operating conditions

Bearing type (**Bore × O. D. × Width, mm**)	**NU2310G1** (**φ 50 × φ 110 × 40**)
Number of rollers	12
Basic static load rating C_{0r}, N	131 000
Cage type	Machined, Outer ring land riding
Radial internal clearance, μm	40, 5
Cage guide clearance, mm	0.445
Lubricant	No-additive turbine oil VG56, Air-oil lubrication
Rotational speed, min^{-1}	1000, 3000, 5000
Radial load F_r, N	980, 4900
Temperature of outer ring at O.D. ˚C	35 ± 3

5. Behavior of Cage Center

5.1 Analysis Results

Fig. 4 shows an example of oscillation occurring at the cage center during analysis. The displacement amount at the cage center shown in **Fig. 4** was made dimensionless using the radius clearance of the cage guide. The initial cage center position was the origin of **Fig. 4**. The cage center moves considerably immediately after the start of calculation, but eventually reaches steady state. The steady state of this cage accompanies minute vibration as shown in **Figs. 4** and **5**.

Fig. 6 shows the result of frequency analysis conducted on the waveform shown in **Fig. 5**, starting from the 0.08-second point following the start of calculation, where the behavior of the cage center has reached the steady state. The amplitude of the motion is large at the cage's self-rotation frequency f_c, its four-fold and N_z-fold frequencies. Since the amplitude at $N_z f_c$ is especially large compared to those at 8f_c and 16f_c, it can be said that the vibration frequency of the cage center is largely influenced by the roller's rotating frequency around the outer ring.

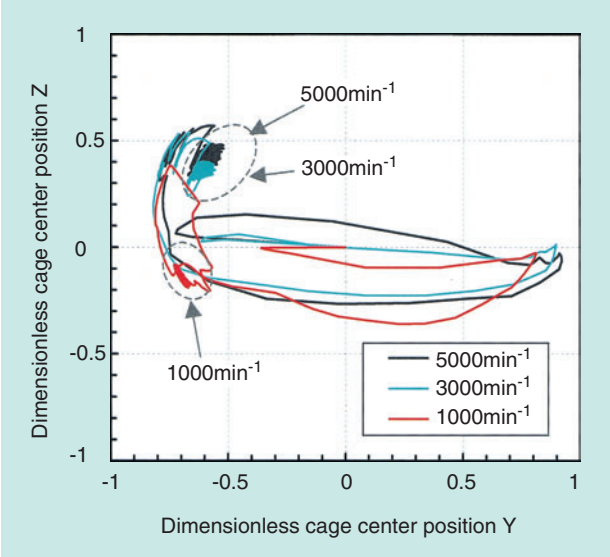

Fig. 4 Numerical results of cage center behavior (F_r : 4900N, Radial clearance: 40 μm)

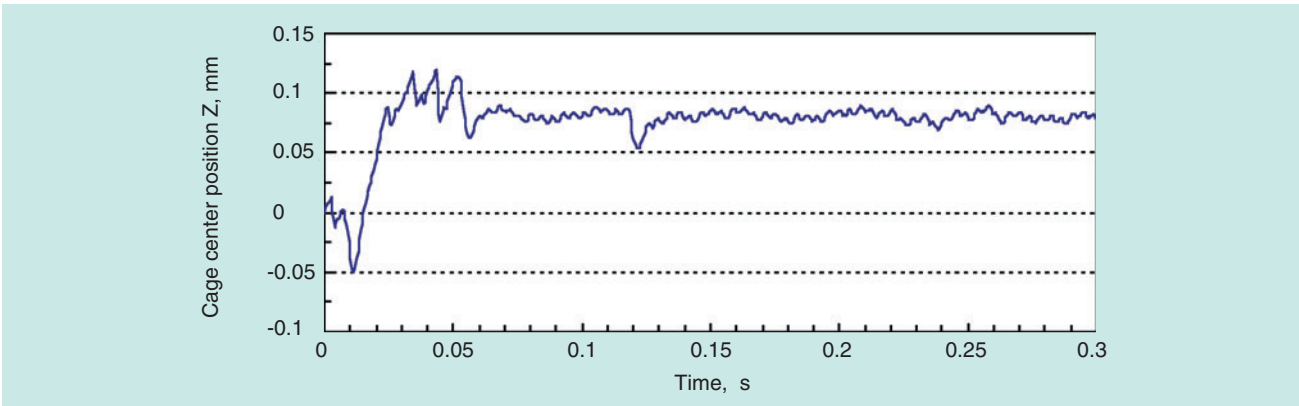

Fig. 5 Numerical result of cage center position along Z axis (F_r : 4900N, radial clearance: 40 μm, 3000min^{-1})

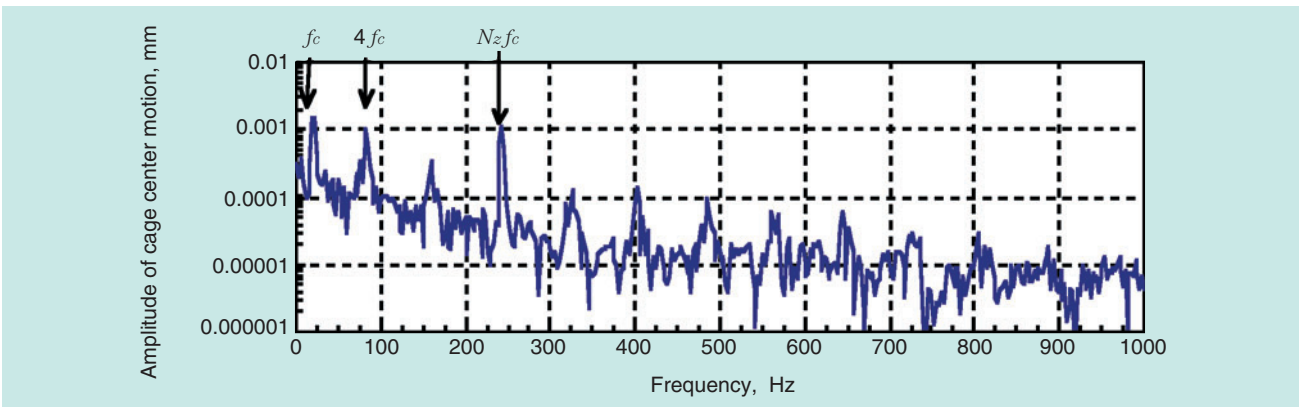

Fig. 6 Frequency analysis of cage vertical steady motion
(F_r : 4900 N, radial clearance: 40 μm, 3000min^{-1}, 841 points, hanning window, f_c : 20Hz, $N_z f_c$: 240Hz)

5.2 Measurement Results

Fig. 7 shows examples of waveforms obtained by the four displacement gauges. Steady motion with minute vibration was observed at the cage center. The signals from the displacement gauge pair for X direction show that there is no phase shift, and no conical oscillation of the cage was found.

Fig. 8 shows the frequency analysis results for the cage center behavior. The bearing running conditions are the same as those for **Fig. 6**. Like **Fig. 6**, the amplitude of motion is large at the cage's self-rotation frequency f_c and $N_z f_c$ (roller's orbital rotating frequency around the outer ring), and the frequency of minute vibration at the steady state is well resembled between analysis and measurement data.

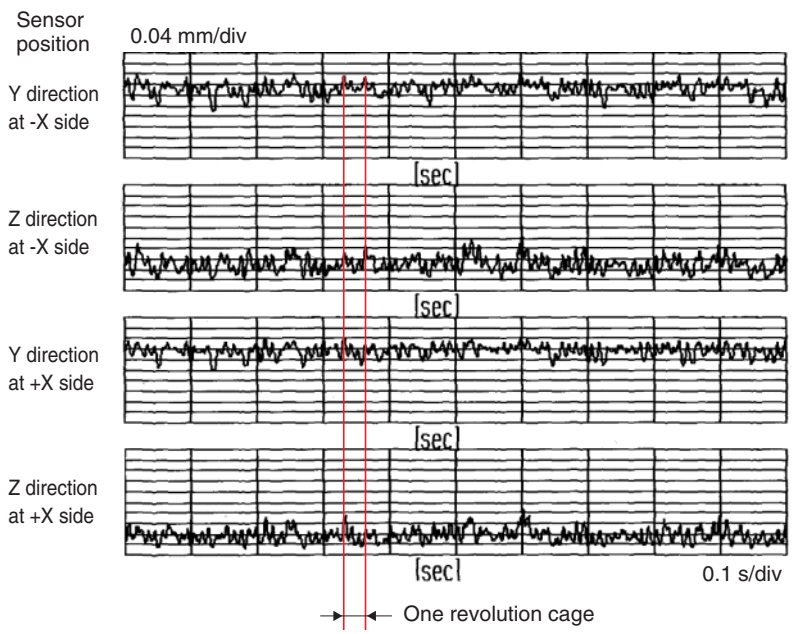

Fig. 7 Experimental results of cage behavior (F_r : 4900 N, radial clearance: 40 μ m, 5000min^{-1})

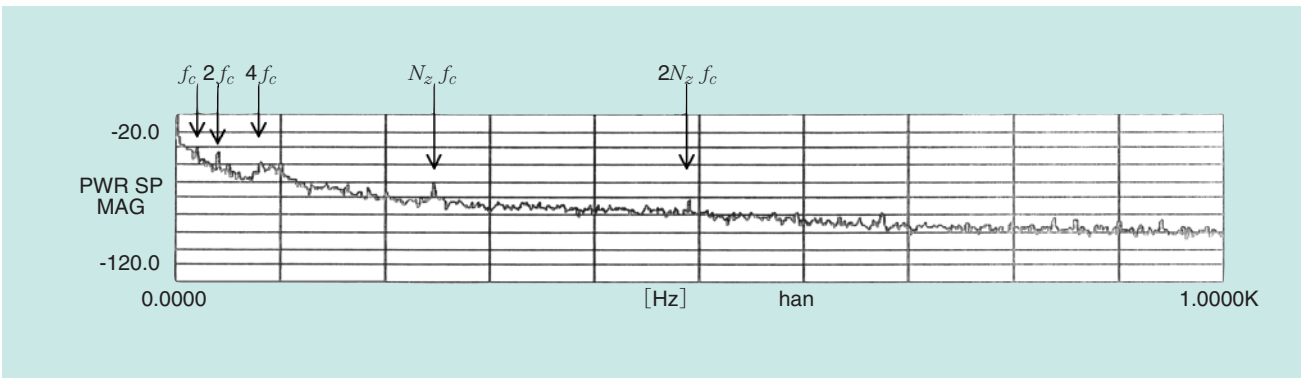

Fig. 8 Frequency analysis of cage vertical motion measured by the top sensor
(F_r : 4900N, radial clearance: 40 μ m, 3000min^{-1}, 2048 words, hanning window, f_c : 20Hz, $N_z f_c$: 240Hz)

5.3 Comparison of Cage Steady Position

Fig. 9 shows a summary of the analysis and experimental results regarding the center position of minute vibration at the cage center during steady state. In **Fig. 9 a**), the angle from the origin to the cage center is slightly different between analysis and experiment results, but the same qualitative trend of rotating speed increase is shown in both results. In **Fig. 9 b**), no experimental results are given in the case of 1000min^{-1}, since the cage did not stabilize. In the case of 4900N load, variation direction of the cage center position for rotational speed rise does not match that of the analysis result, but the center position itself is in close agreement. On the whole, validity of analysis can be confirmed for both trend and position of cage center variation.

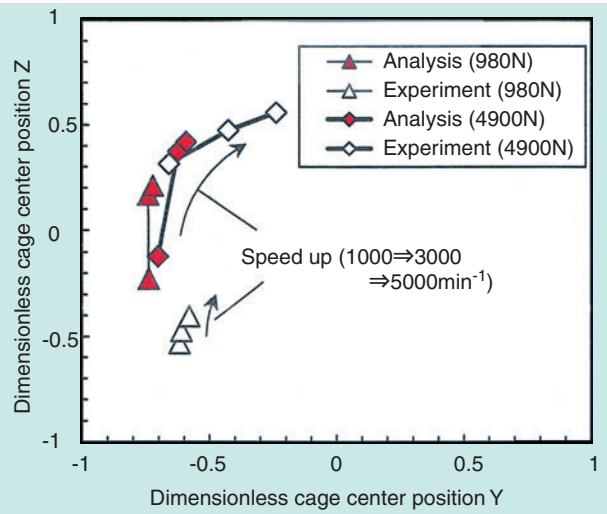

a) Radial clearance : 40 μm

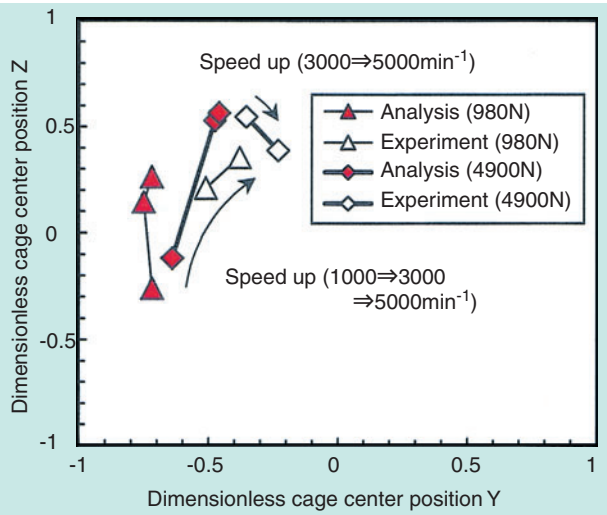

b) Radial clearance : 5 μm

Fig. 9 Comparison of numerical and experimental results for cage center steady position

6. History of Interaction Force between Roller and Cage

Fig. 10 shows an example of variation in roller's self-rotating slip ratio, roller's circumference position inside the pocket, roller's circumferential contact force to the pocket and roller's contact force to the inner ring. Signs (+, -) given to the roller's circumferential contact force to the pocket mean as follows: "+" indicates the direction in which the cage is accelerated, and "-" indicates the direction in which the cage is decelerated. From the variation of the contact force to the inner ring, the time for the roller to pass the load zone can be found. The roller generates a maximum of 22% slippage in the non-load zone and the roller circumferential position is located toward the back of the pocket orbital motion. The roller begins to accelerate rapidly at the entrance of load zone and continues until it reaches the theoretical speed. In the latter half of the load zone, the roller comes into contact with the pocket surface as shown in **Fig. 11**. The reason why the slip ratio is large in the non-load zone is that EHL rolling viscous resistance is also taken into account like it is in the load zone, despite the fact that only centrifugal force, which is relatively small, is exerted at the area contacting with the outer ring raceway. Thus, it appears that the rolling viscous resistance is taken into account more than it should be.

As a result, the force that causes the roller to accelerate the cage in the second half of the load zone is added in the direction shown in **Fig. 11**. Since that force is supported at the cage guide, the cage center position stabilizes at the position shown in **Fig. 9**.

Fig. 9 shows that the motion variation in the analysis result is small, but the cage tends to move in Z direction due to reduction of the radial clearance or increase of load. This is due to the change in roller contact force direction in the second half of load zone caused by extension of the load zone.

Furthermore, the cage moves in Z direction when the rotating speed increases. The reason is given below. First, resisting moment on the cage guide surface increases due to increased rotating speed. The roller contact force to the pocket in the second half of load zone then increases in order to cancel this resisting moment. Since this contact force acts as a translation force for the cage, the force to the upper left corner in **Fig. 9** increases, causing the cage to move in Z direction.

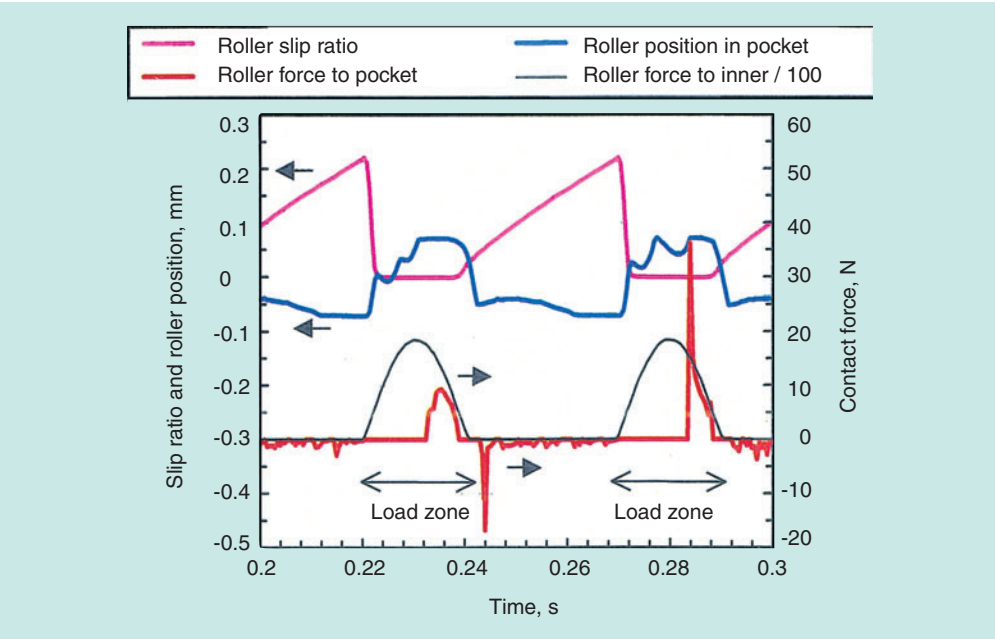

Fig. 10 Numerical results of roller behavior and roller/cage interaction (F_r : 4900N, radial clearance: 5 μ m, 3000min^{-1})

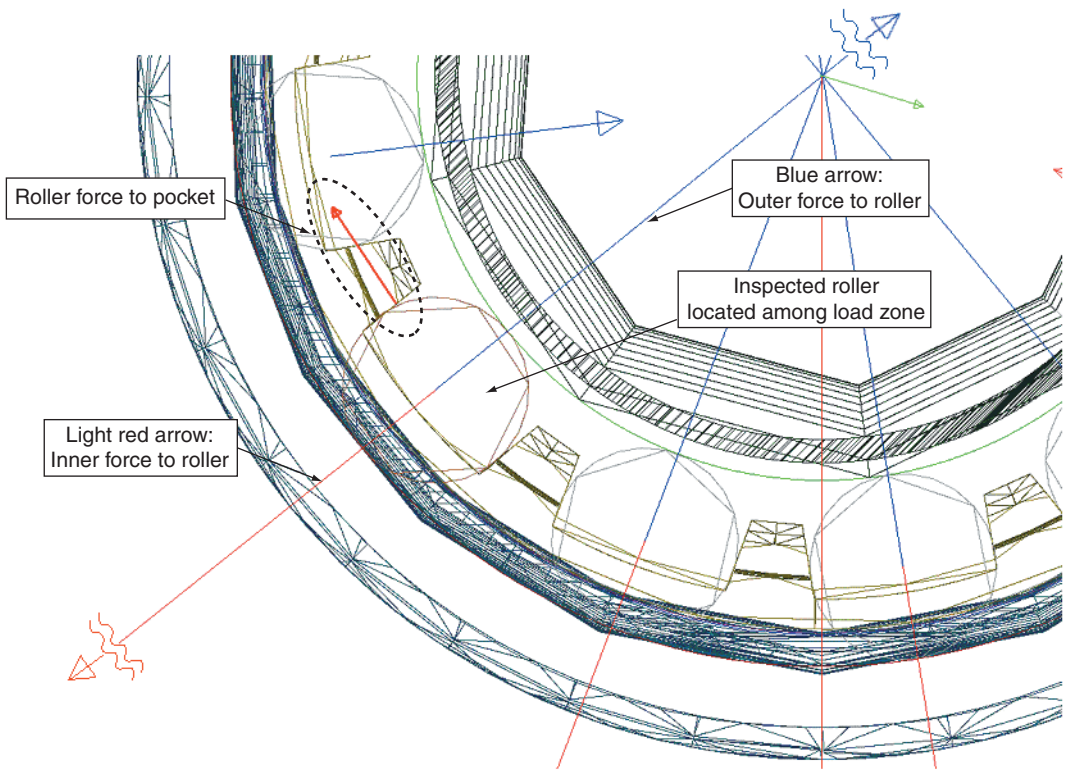

Fig. 11 Graphic example of interaction forces (F_r : 4900N, radial clearance: 5 μ m, 3000min^{-1})

7. Conclusion

Analysis of real-time behavior of a cylindrical roller bearing on a radial plane was carried out using commercial software designed for virtual prototyping of a mechanical system. As a result of verification of the experimental results of the behavior of the cage center, validity was confirmed. It was found that roller contact force in the second half of load zone in the direction in which the cage's self-rotation is accelerated was large and the cage center position is determined by this force.

This report limits to real-time analysis under static load. However, analysis for desired running conditions such as fluctuating load is also possible. With the purpose of drastic improvement in bearing design technology, we plan to develop a code on this software that can simulate the real-time three-dimensional behavior of a cylindrical roller bearing.

References

1) MSC. Software, HP Address：
http://www.adams.co.jp/（2003.5.7）
2) M. Muraki, Y. Kimura: J.JSME, 28,10(1983)753-760.(in Japanese)
3) R. S. Zhou, M. R. Hoeprich: Trans. ASME, J. Trib, 113, 7(1991) 590.
4) P. Pan, B.J. Hamrock: Simple Formulae for Performance Parameters Used in Elastohydrodynamically Line Contacts, Trans. ASME, J. Trib., 111, 2(1989) 246-251.
5) M.K. Ghosh, R.K. Pandey: Thermal Elastohydrodynamic Lubrication of Heavily Loaded Line Contacts-An Efficient Inlet Zone Analysis, Trans. ASME, J. Trib., 120, (1998) 119-125.

Photos of authors

Tomoya SAKAGUCHI

Technical Reserch Dept.
Reserch& Development Center

Kaoru UENO

Industrial Engineering Department,
Industrial Sales Headquarters

Precision Bearings "ULTAGE" Series for Machine Tools

Futoshi KOSUGI*

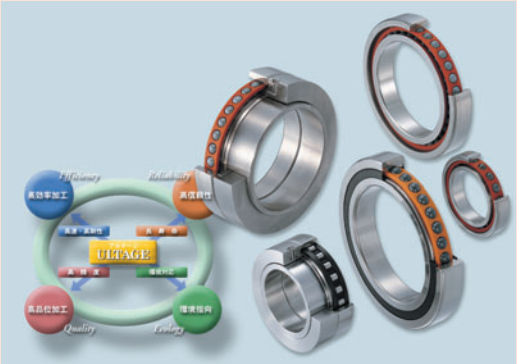

Recently, machine tool manufacturers have placed increasingly demanding performance specifications on the bearings used in their products. Machine Tool Bearings are required for high speed, high efficiency and high precision. In recent years, dry machining technology, which does not use oil in the machining process, is also becoming an important factor in the improvement of working environment.

NTN has been pursuing high d_{mn} values and high precision of bearings for the main spindles of machine tools and concentrating on technology for improvement of working environment. This paper introduces ULTAGE Series for machine tools that have been recently developed not only for high speed and high precision but for harmony with the environment.

1. Introduction

Machine tools, including machining centers, are looking for higher speed, higher efficiency and higher precision. In addition, as the development of dry machining technology that does not use oil during the machining process suggests, more attention is being paid to the working environment.

With regard to bearings designed for the main spindles of machine tools, **NTN** has been pursuing higher d_{mn} values, higher precision and lower NRRO (Non-Repeatable RunOut). We are also paying attention to eco-consciousness.

This paper introduces the "ULTAGE Series", developed as ECO series for machine tools, with the concept of "harmony with the environment" in addition to high speed and high precision features. "ULTAGE" is a combination of the words "ULTIMATE" and "STAGE", to express the **NTN**'s concept of pursuing the ultimate precision rolling bearings for machine tools.

2. ULTAGE Series

The ULTAGE Series offers a total of 10 types of bearings, including angular contact ball bearings and cylindrical roller bearings. (See **Table 1**)

For angular contact ball bearings, a total of eight types are available. They include "70U/79U" type developed from the standard angular contact ball bearings; "HSE" type with improved abrasion resistance and seizure resistance in addition to high speed capability; "HSF" type which achieves higher speed and limited temperature rise; two sealed types (BNS, 70/79AD, CD) designed for grease lubricated applications; the eco-conscious "HSL , HSFL" types designed for air-oil lubricated applications, with reduced noise level and low air/oil consumption; the ball screw support type "2A-BST", and the light contact sealed type "2A-BST LXL".

For cylindrical roller bearings, two types are available; "N10HSR type" featuring high-speed operation under both air-oil and grease lubrication, and the eco-conscious "N10HSL type" designed for

*Industrial Sales Headquarters Industrial Engineering Department

air-oil lubricated applications only, featuring reduced noise level and low air/oil consumption.

In this paper, five types (sealed and eco-conscious types) in the ULTAGE Series are introduced.

Table 1 ULTAGE series

ULTAGE series	Angular contact ball bearing	For spindles	**[Standard]** **70U type , 79U type** (Contact angle 15˚, 25˚, 30˚)	Optimized interior structure and resin cage help positively inhibit temperature rise.
			[High-speed] **5S-2LA-HSE type** (Contact angle 15˚, 20˚, 25˚)	Adoption of special material and surface treatment, with drastically improved abrasion resistance and seizure resistance. Features improved rigidity and reliability in addition to the high speed of the conventional "HSB0CAEX1" ultra high-speed angular contact ball bearing.
			[Super high-speed] **5S-2LA-HSF type** (Contact angle 25˚)	Maintaining the advantages of HSE type, this type has small diameter ceramic balls to achieve higher speed and limited temperature rise.
			[Eco-conscious] **5S-2LA-HSL type** (Contact angle 15˚, 20˚, 25˚) **5S-2LA-HSFL type** (Contact angle 25˚)	Adoption of special material and surface modification, with drastically improved abrasion resistance and seizure resistance. Designed only for air-oil lubrication, with circumferential grooves on the inner ring of the HSE type and eco-conscious nozzle. Features reduced noise and air/oil consumption in addition to the high speed of the HSE type. It is applicable also to HSF type.
			[High-speed] **5S-2LA-BNS type** (Contact angle 15˚, 20˚, 25˚)	Adoption of special material and surface heat treatment , with drastically improved abrasion resistance and seizure resistance. Designed only for grease lubrication, with optimized internal design, grease reservoirs, special grease and non-contact seals.
			[Standard] **70CD type, 79CD type** (Contact angle 15˚) **70AD type, 79AD type** (Contact angle 25˚)	Angular contact ball bearing with optimized internal structure, non-contact rubber seals on both sides, and long-life special grease. Bearing with ceramic balls is also available.
		For ball screw support	**[Open]** **2A-BST type** (Contact angle 60˚)	Open type bearing with longer rolling contact fatigue life by additional surface heat treated rings.
			[Light contact sealed] **2A-BST LXL type** (Contact angle 60˚)	Features longer rolling contact fatigue life by additional surface heat treated rings and drastically reduced fretting wear by employing special grease. Provides improved dust resistance and grease-retaining capability by low-torque and light contact seals.
	Cylindrical roller bearing	For spindles	**N10HSR type**	Features optimized internal structure for high speed capability with low temperature rise. Provides higher limiting speed than the conventional "N10HS" high-speed cylindrical roller bearing.
			N10HSL type	Designed only for air-oil lubricated applications, with circumferential grooves on the inner ring of the N10HSR type and an eco-conscious nozzle. Features reduced noise and low air/oil consumption in addition to the high speed capability of the N10HSR type.

2. 1 Bearings for Main Spindles

2. 1. 1 Grease-lubricated Sealed Angular Contact Ball Bearing (BNS Type)

From the viewpoint of environmental issues, grease is the most suitable lubrication method for bearings used for main spindles. When using bearings under grease lubrication, no external lubrication unit is required, therefore assembly and maintenance are easy. Additionally, because the bearings are pre-lubricated with a suitable amount of grease, the amount of oil mist is very low.

However, when using high-speed angular contact ball bearings, the lubrication life will be a major factor. **NTN** evaluated the long life grease from various viewpoints, and developed "Grease-lubricated Sealed Angular Contact Ball Bearing (BNS Type)" [1] (**Fig. 1**) to be used for high-speed spindles of ϕ50 or larger diameter. Then, **NTN** introduced at JIMTOF2000 (Japan International Machine Tool Fair).

For the BNS type, special material and surface heat treatment are adopted for rings to extend the rolling contact fatigue life. Grease is retained and supplied to the raceway surface by the seals provided on both sides of the bearing. Grease reservoirs set directly adjacent to the outer ring raceway, in order to extend the grease life during high-speed operation.

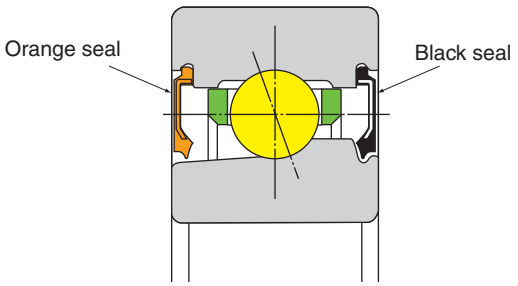

Fig. 1
Grease-lubricated Sealed Angular Contact Ball Bearing

Fig. 2 illustrates the effect of grease reservoirs for bearing life, and **Table 2** shows the results of endurance test

From the test results shown in **Fig. 2**, it was found that the life of the grease-lubricated sealed angular contact ball bearing is 7.4 times longer than the conventional type.

The endurance test was conducted on the BNS type (5S-2LA-BNS020: ϕ100×ϕ150×24) with seals on both sides, and HSE type (5S-2LA-HSE020C without seals: ϕ100×ϕ150×24), with "0N" fixed position

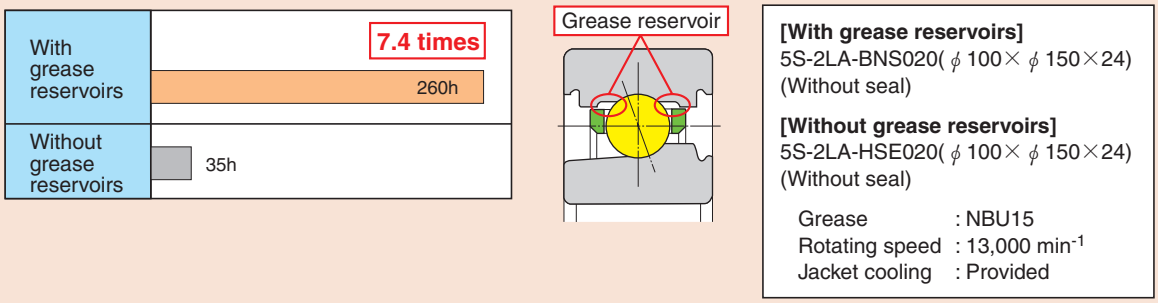

Fig. 2 Effect of grease reservoirs on bearing life

Table 2 Endurance test results

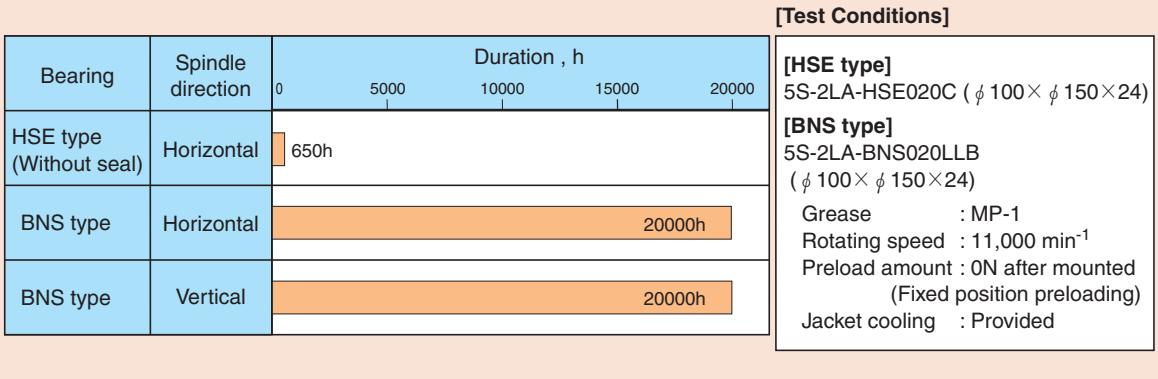

preload (after mounted) and at a rotating speed of 11,000 min^{-1} (d_{mn} value: 1,400,000). The HSE type showed a life of 1,000 hours or shorter, while the BNS type showed a life of 20,000 hours (the test was suspended after 20,000 hours).

This result suggests that air-oil lubricated spindles can be replaced by grease-lubricated spindles in the high-speed range up to 1,400,000 (d_{mn} value).

In addition, since the BNS type is a pre-lubricated sealed type, there is no need to fill grease and to clean the bearings during spindle assembly. This may not only simplify handling procedure and reduce assembly labor, but also improve the working environment (e.g. elimination of cleaning oil disposal).

Furthermore, an improvement was made on the seal after JIMTOF2000. Seal on the back side was replaced by the orange seals (previously, black seals were used on both sides). This facilitates confirmation of bearing direction during assembly work: for DB mounting, the orange seals face each other, and for DF mounting, the black seals face each other.

2. 1. 2 Grease-lubricated Sealed Angular Contact Ball Bearing (70/79 AD, CD Type)

For spindles of ϕ50 or less inner diameter, such as rotating tool spindles and small-size spindles, which are used in low to medium speed ranges, we developed the "Grease-lubricated Sealed Angular Contact Ball Bearing (70/79 AD, CD Type)" (**Fig. 3**) [2] and introduced at JIMTOF2002.

Table 3 Bearing arrangement aided by seal color

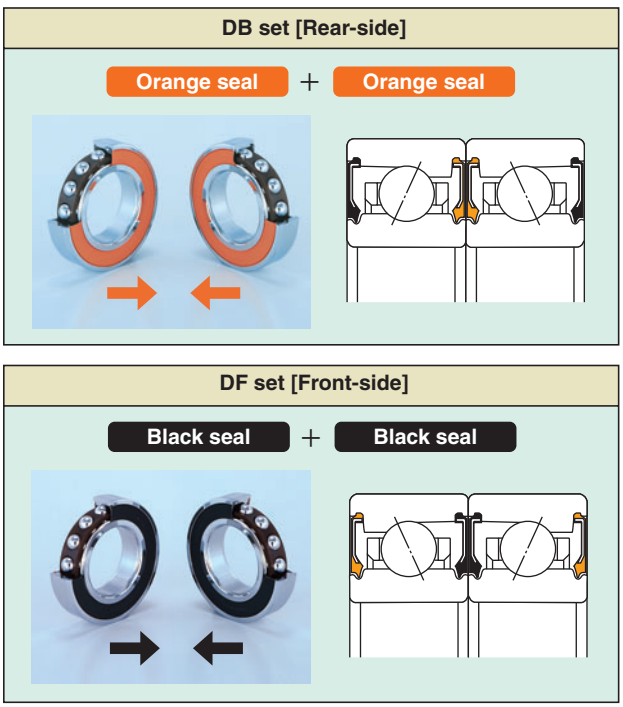

This bearing has a load capacity equal to the standard angular contact ball bearing, and offers two types: CD type (contact angle 15˚) and AD type (contact angle 25˚). It is developed based on the design concept of the BNS type, which features non-contact seals on both sides, long-life special grease and optimized internal structure for reduction of heat generation. Bearing with ceramic balls is also available.

Fig 4 shows the results of high-speed operation test. The test was conducted on the 70CD (7006CD: ϕ30× ϕ55×13) and 70AD type (7006AD: ϕ30× ϕ55×13), with mounted preload of 180N and 250N, respectively. The bearings were mounted with DB arrangement . Both 70CD and 70AD types ran stable at rotating speeds of up to 25,000 min^{-1} (d_{mn} value: 1,100,000).

With 70/79 AD and CD types, black and orange seals were provided at the front and rear sides respectively, like the BNS type, to facilitate confirmation of bearing mounting orientation during assembly work.

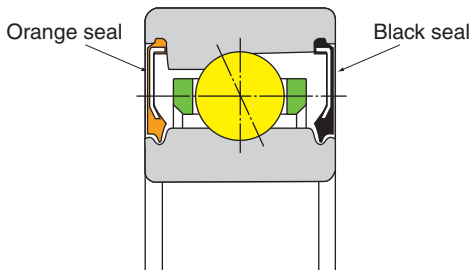

Fig. 3
Grease-lubricated Sealed Angular Contact Ball Bearing

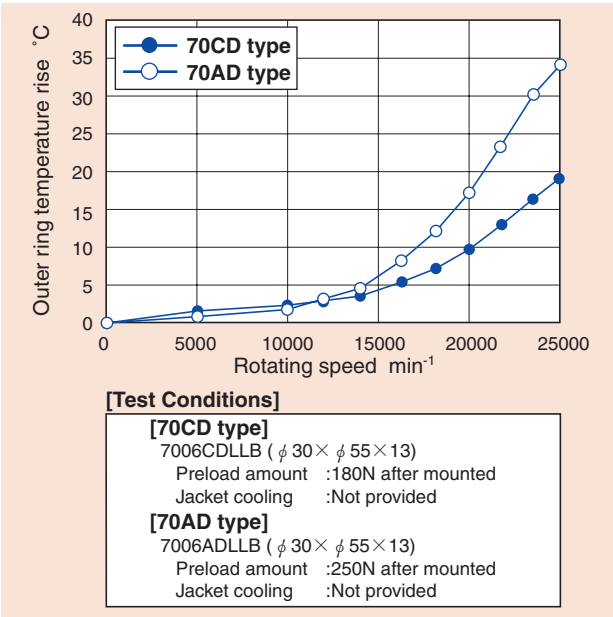

Fig. 4 High-speed test results

2. 1. 3 Eco- conscious Air-Oil Lubricated Angular Contact Ball Bearing (HSL , HSFL Type)

Advantages of grease lubrication with regard to environmental issues were discussed previously. However, sufficient supply of lubricating oil to the raceway is difficult in high-speed operation, thereby, the life of lubricating oil becomes an issue. Because of this, air and oil lubrication is normally used in high-speed applications. However, reduction of air/oil consumption and noise level are constant requirements.

Based on the "Low-Noise Angular Contact Ball Bearing (SF Type)" [1], which was introduced at JIMTOF2000, we continued to make further improvements and have eventually developed the "Eco-conscious Air-Oil Lubricated Angular Contact Ball Bearing (HSL , HSFL Type)" [3], featuring not only high-speed capability and low noise, but also reduced air and oil consumption, which was then introduced at JIMTOF2002.

Even with the SF type (low-noise angular contact ball bearing), oil was supplied efficiently to the inside of the bearing and reduction of air and oil consumption was possible. However, it was found that as the air supply rate is reduced, oil begins to collect in circumferential groove at the exit of the nozzle, and when collected oil enters the inner section of the bearing at once, it causes the bearing temperature to fluctuate. This issue was solved by removing the circumferential groove from the nozzle and instead providing circumferential groove on the outer face of the bearing inner ring. [4) 5)]

Fig. 5 shows the bearing design of HSE(HSF) type , SF type ,and HSL(HSFL) type.

Fig. 6 shows the correlation between air supply rate and outer ring temperature measured for the HSF type, SF type and HSFL type (5S-2LA-HSFL020: ϕ100× ϕ150×24), with a constant spring preload (2.5kN). The test was carried out under fixed conditions: rotating speed of 21,000 min^{-1} (d_{mn} value: 2,650,000) and oil supply rate of 0.03mL/5min.

With the HSF and SF types, the outer ring temperature rose suddenly at an air supply rate of 22.5NL/min and 15NL/min respectively. However, with the HSFL type, operation was still possible at much lower air supply rate of 10NL/min.

Fig. 7 shows change of outer ring temperature at a fixed rotating speed (21,000 min^{-1}) and at different oil supply intervals (oil supply rate: 0.03mL/shot). With the HSFL type, stable operation was possible in the oil supply interval range of 2 to 21 min. With the HSF

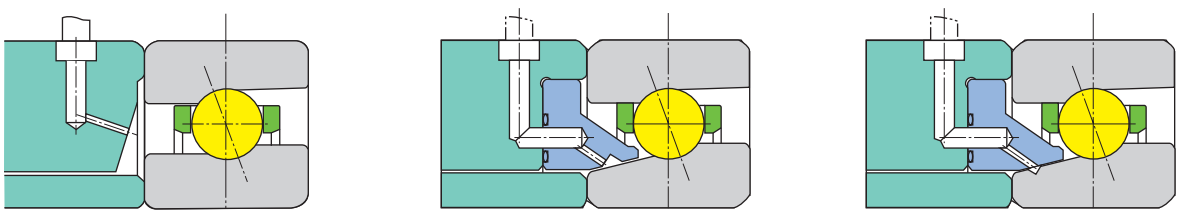

Fig. 5 Bearing design

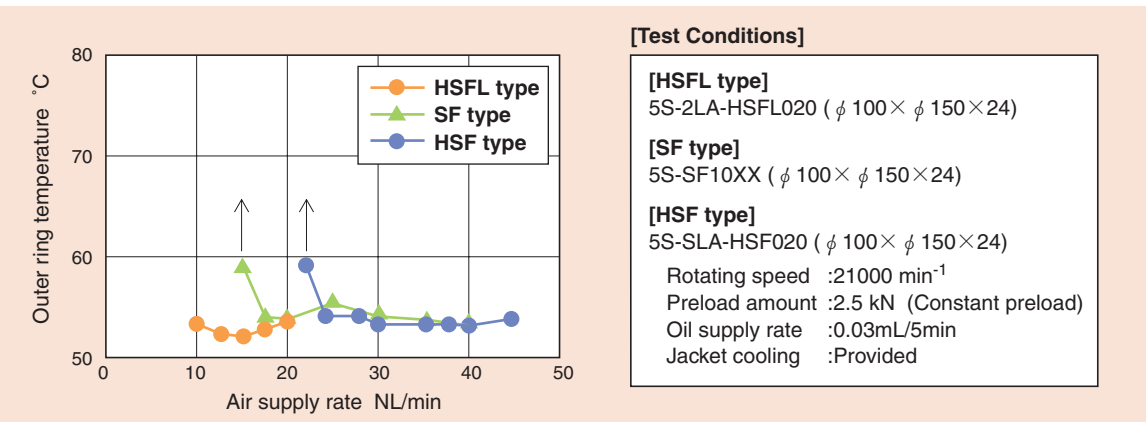

Fig. 6 Air supply rate on outer ring temperature

type, maximum reduction of oil consumption to 1/10 is possible, since an oil supply interval of 2 min is normally recommended for dmn value: 2,650,000.

Fig. 8 shows noise level change at different rotating speeds of up to 20,000 min^{-1}. It is demonstrated that noise level can be reduced by approximately 10dBA.

Fig. 9 shows operation results of the HSL type (5S-2LA-HSL020: ϕ100×ϕ150×24) when operated with a fixed position preload (mounted preload: 0N). With the HSE type, the outer ring temperature becomes unstable when the rotating speed increases over than 16,000 min^{-1}, but the HSL type can achieve stable operation at rotating speeds of up to 19000 min^{-1} (d_{mn} value: 2,400,000), at 10NL/min (air supply rate) and at 0.03mL/10min (oil supply rate).

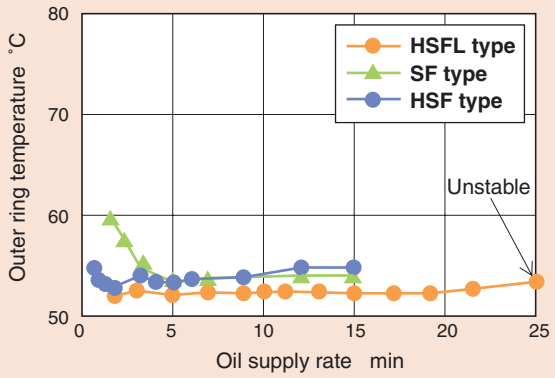

[Test Conditions]

[HSFL type]
5S-2LA-HSFL020 (ϕ100×ϕ150×24)

[SF type]
5S-SF10XX (ϕ100×ϕ150×24)

[HSF type]
5S-2LA-HSF020 (ϕ100×ϕ150×24)

Rotating speed	:21,000 min^{-1}
Preload amount	:2.5 kN (Constant preload)
Oil supply rate	:0.03mL/shot
Air supply rate	:HSFL type: 12.5NL/min
SF type	:25NL/min
HSF type	:30NL/min
Jacket cooling	:Provided

Fig. 7 Effect of oil supply rate on outer ring temperature

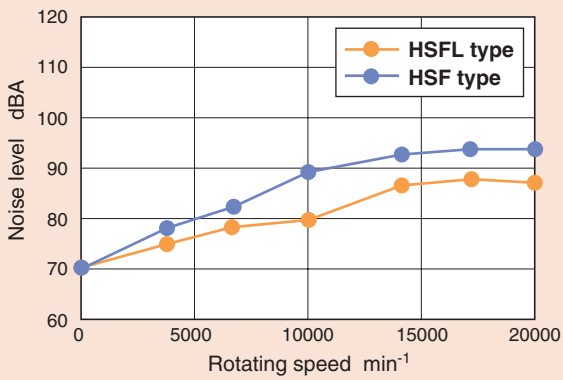

[Test Conditions]

[HSFL type]
5S-2LA-HSFL020 (ϕ100×ϕ150×24)

[HSF type]
5S-2LA-HSF020 (ϕ100×ϕ150×24)

Preload amount	:2.5 kN (Constant preload)
Oil supply rate	:0.03mL/5min
Air supply rate	:30 NL/min
Jacket cooling	:Provided

Fig. 8 Noise level

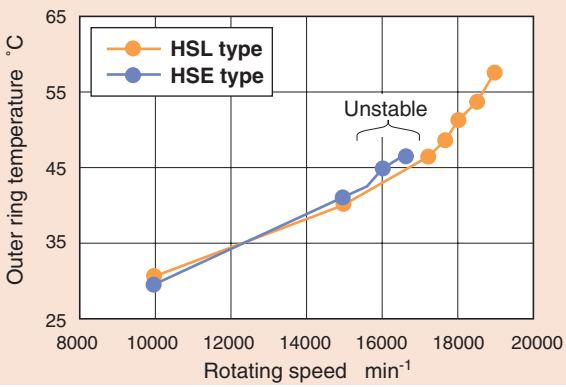

[Test Conditions]

[HSL type]
5S-2LA-HSL020 (ϕ100×ϕ150×24)

[HSE type]
5S-2LA-HSE020 (ϕ100×ϕ150×24)

Preload amount	:0N after assembled (Fixed position preloading)
Oil supply rate	:0.03mL/10min
Air supply rate	:10 NL/min
Jacket cooling	:Provided

Fig. 9 Outer ring temperature rise

2. 1. 4 Eco-conscious Air-Oil Lubricated Cylindrical Roller Bearing (N10HSL Type)

Conventionally, the allowed dmn value of air-oil lubricated cylindrical roller bearings is approximately 1,500,000, therefore, angular contact ball bearings are used for the rear side of spindles that exceed dmn 1,500,000. In this case, a slide mechanism equipped with a ball bushing is used to compensate spindle extension for complicating the spindle structure (**Fig. 10**). To improve this structure , **NTN** developed the "Eco-conscious Air-Oil Lubricated Cylindrical Roller Bearing (N10HSL Type)".

This bearing enables high-speed operation by optimizing the internal structure and using a special resin cage which is lighter than brass cage.

The lubrication system, like the eco-conscious angular contact ball bearing, is constructed in such a way that air cutting noise caused by the rolling elements is reduced and oil is supplied inside of the bearing by supplying air and oil to the tapered portion of the inner ring, not directly to the rolling element. This enables reduction of air and oil supply rates as well as noise level.

Fig. 11 shows the bearing design of standard bearing (N10HS type) and eco-conscious bearing (N10HSL type).

Fig. 12 shows the test results of outer ring temperature rise for the N10HS and N10HSL types.

The N10HS type shows an acute temperature rise of outer ring temperature at 20,000 min^{-1} under conditions of 40NL/min (air supply rate), 0.02mL/5min (oil supply rate) and 0 μm (clearance after mounted).

With the N10HSL type (N1014HSL: ϕ70× ϕ110× 20), operation is possible under conditions of 20NL/min (air supply rate) and 0.02mL/10min (oil supply rate), which are 1/2 of the conventional figures. High-speed operation at 26,000 min^{-1} (d_{mn} value: 2,300,000) is possible. From comparison of the outer

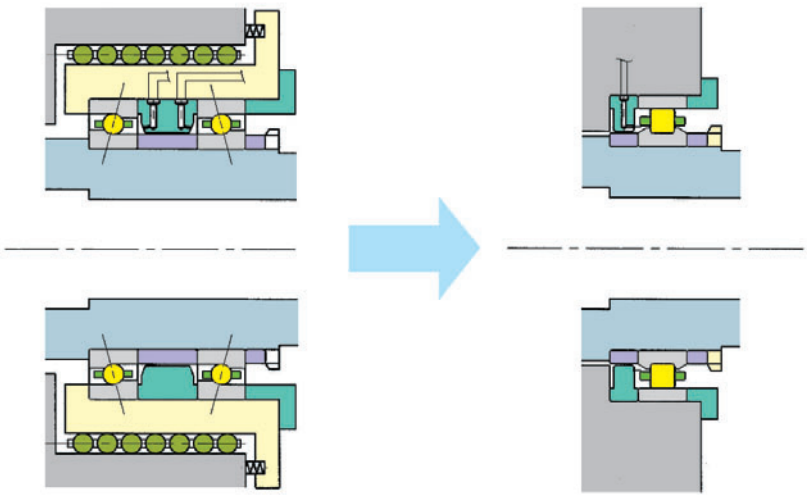

Fig. 10 ULTAGE main spindle rear structure is less complex than current rear structure

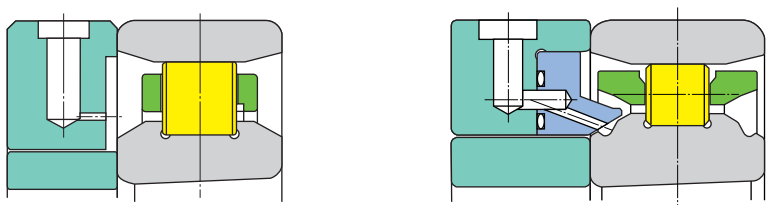

Standard bearing (N10HS type) **Eco-conscious bearing (N10HSL type)**

Fig. 11 Bearing design

ring temperature between N10HS and N10HSL, it is obvious that the N10HSL type has a lower temperature rise, which is because of the low temperature rise effect by smaller rolling elements. A rise of outer ring temperature is shown at low speeds for both types. This caused by the excessive supply of oil which is suitable for the high-speed operation .

Fig. 13 shows the measurement results of noise level. The eco-conscious type shows a lower noise level by approximately 6dBA than the standard type at 15,000 min^{-1}.

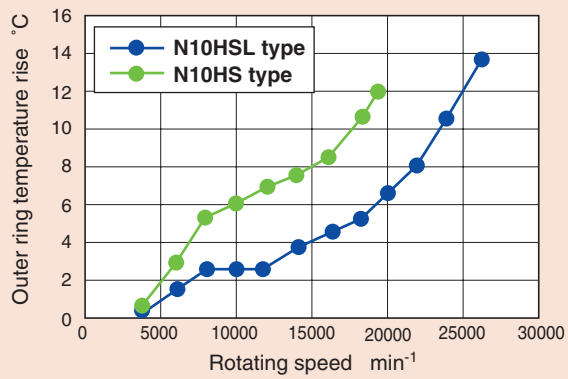

[Test Conditions]

[N10HSL type]
N1014HSL (ϕ 70× ϕ 110×20)

Clearance	:0 μ m after mounted
Oil supply rate	:0.02mL/10min
Air supply rate	:20 NL/min
Jacket cooling	:Provided

[N10HS type]
N1014HS (ϕ 70× ϕ 110×20)

Clearance	:0 μ m after mounted
Oil supply rate	:0.02mL/5min
Air supply rate	:40 NL/min
Jacket cooling	:Provided

Fig. 12 Outer ring temperature rise

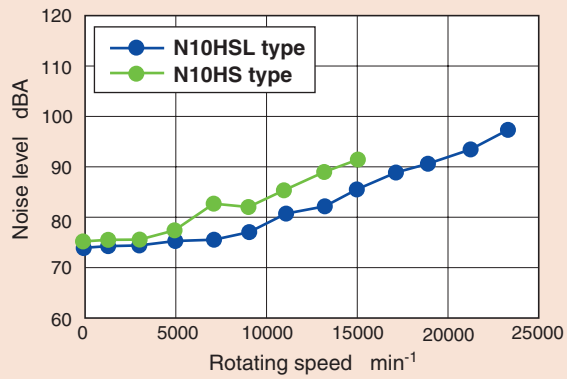

[Test Conditions]

[N10HSL type]
N1014HSL (ϕ 70× ϕ 110×20)

Clearance	:0 μ m after mounted
Oil supply rate	:0.02mL/10min
Air supply rate	:20 NL/min
Jacket cooling	:Provided

[N10HS type]
N1014HS (ϕ 70× ϕ 110×20)

Clearance	:0 μ m after mounted
Oil supply rate	:0.02mL/5min
Air supply rate	:40 NL/min
Jacket cooling	:Provided

Fig. 13 Noise level

2. 2 Ball Screw Support Bearing (2A-BST LXL Type)

To improve efficiency of machine tools, the speed of the feeder also needs to be improved in addition to the main spindle. Ball screw support bearings used for feeders sometimes cause fretting on the raceway due to the oscillation generated by slight feed movement and vibration generated during cutting operation. In addition, deterioration of grease due to entry of cutting oil and shortened life due to entry of contaminants (e.g. ball screw grease, cutting chips) are also present.

The ball screw support thrust angular contact ball bearing (2A-BST LXL type) (**Fig. 14**) has been developed to solve these problems, with the intention of improving resistance to fretting by applying surface heat treatment and pre-lubricating with special grease (the oscillation test results show the improvement in fretting resistance by 10 times). The results are shown in **Fig. 15**.

Unlike the BST type standard bearing (open design), the 2A-BST LXL type that has low-torque, light-contact seals, which not only prevents entry of contaminants but also facilitates assembly work since the greasing process is not required. Furthermore, confirmation of bearing orientation during assembly is also made easier by changing the seal colors between sides, like the sealed angular contact ball bearing developed for main spindles.

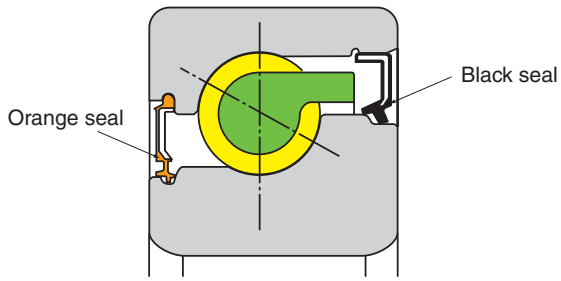

Fig. 14 Thrust angular contact ball bearing for ball screw support

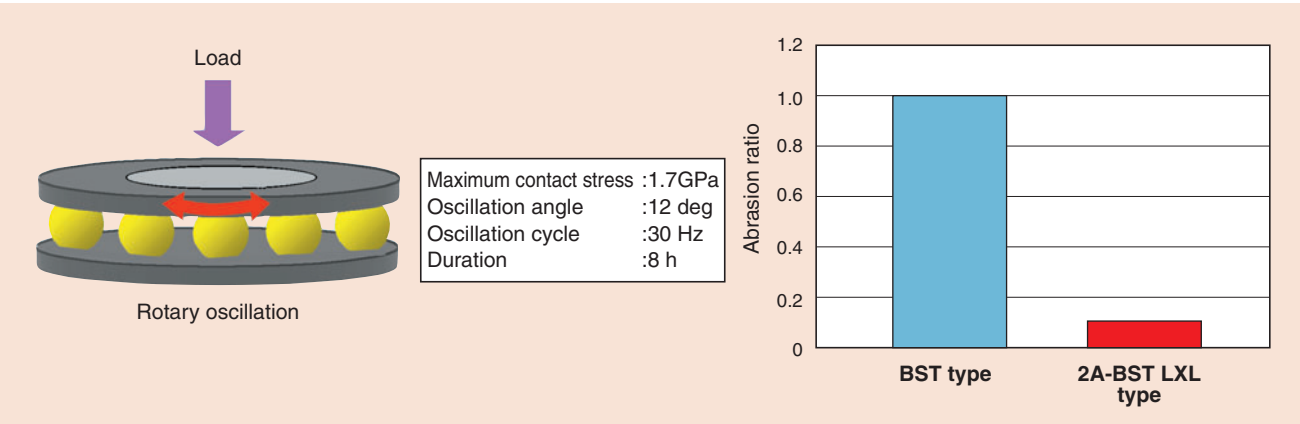

Fig. 15 Oscillation test results

3. Conclusion

Machine tools in the future are expected to feature eco-consciousness in addition to conventional functional requirements such as high speed, high efficiency and high precision. Eco-conscious technologies, including reduction of air/oil consumption, oil mist and noise level with power saving will play more important roles.

For machine tool bearings, including those for spindles and feeders, eco-consciousness will be a key issue in addition to the quest for higher dmn value and lower NRRO.

A wide range of requirements is expected from customers. However, **NTN** will continue to work on improvement and development of ultimate precision bearings keeping its motto "be friendly to the earth and its people" in mind.

References

1) H.Tako , THE TRIBOLOGY NO.164(2001),24 (in Japanese)
2) K.Ueda , THE TRIBOLOGY NO.188(2003),19 (in Japanese)
3) H.Takiuchi , THE TRIBOLOGY NO.174(2002),58 (in Japanese)
4) K.Fujii , M Mori , JSPE Semestrical meeting (autumn)(2001.10) (in Japanese)
5) K.Fujii , JSME Division of Manufacturing and Machine Tools
The 3rd International Conference (2001.11) (in Japanese)

Photo of the author

Futoshi KOSUGI

Industrial Engineering Department
Industrial Sales Headquarters

Bearings for High Speed CT Scanner

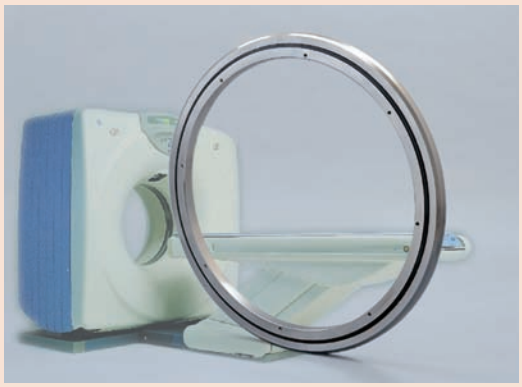

Yosuke OYA*

The Industry of Medical Instruments is steadily growing because of an aging society.

In particular, the CT(Computed Tomography) scanner, which can be an effective tool for medical examination and inspection of patients, has attracted a attention as important imaging equipment.

To ensure smooth rotation of the gantry part of the CT scanner, a super slim large size angular contact ball bearing is used.

This article introduces development of the gantry bearing for higher speed rotation with a lower noise level.

1. Introduction

The medical instrument industry is steadily growing due to an aging society. In particular, the CT (Computed Tomography) scanner has attracted attention as imaging equipment to enable efficient medical examination and inspection of patients. The CT scanner (**Photo 1**) has an inspection section (gantry) that houses an X-ray tube and detector as part of a rotating section to shoot images. A bearing (inner diameter: approx. 1m) is used to support this rotating section. This article introduces the development of rotation support bearings (gantry bearings) that can support improvement of CT scanner performance.

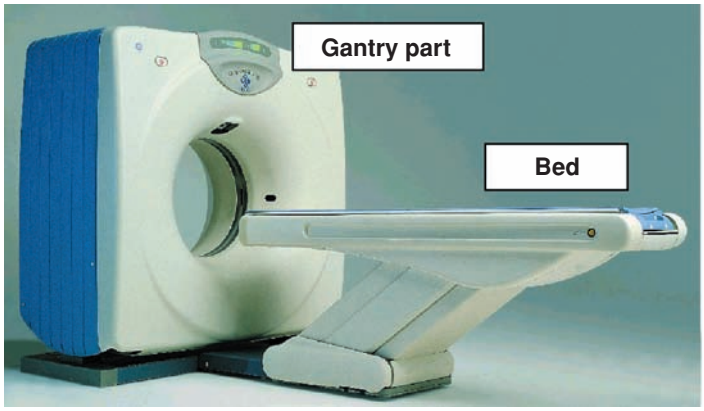

Photo 1 CT scanner

*Industrial Engineering Department Industrial Sales Headquarters

2. Required Functions for Gantry Bearings

Required functions for gantry bearings are explained below.

(1) Higher-speed operation

Improved speed of gantry bearings shortens imaging time, resulting in reduced burden on patients. In other words, the time during which the patient has to stop breathing can be reduced and this reduces the burden placed on patients, especially infants and the elderly. Moreover, reduction of exposure to X-rays is also an important purpose of speed improvement.

Furthermore, higher rotation of the bearing improves imaging speed, enabling high precision imaging of internal organs (e.g. heart), which were difficult to shoot accurately. Furthermore, the number of patients for whom diagnoses can be made per day increases, thereby resulting in a higher operation availability of the CT scanner.

(2) Low noise level

Reducing noise level of gantry bearings can not only ease patients' anxiety during image shooting, but also prevent atrophy of organs.

3. Construction

Fig. 1 shows the construction of a gantry bearing. Since the gantry bearing rotates while supporting the base to which imaging devices (e.g. X-ray tube and detector) are attached, moment load will act on the bearing. In general, single-row type, four-point angular contact ultra-thin ball bearings are used for low- to medium-speed CT scanners because of their compactness. For medium- to high-speed CT scanners, duplex double-row angular contact ball bearings are used to reduce heat build-up inside the bearing and keep rigidity. In particular, duplex double-row angular contact ball bearings, which are used for high-speed CT scanners, have the following features.

(1) Preloading specification

If there is clearance inside the bearing, non-load state will exist while the rolling elements make one turn inside the bearing during rotation. In this non-loaded area, a striking sound will be generated as the rolling elements collide with the ring by their own weight. Since gantry bearings are required to be silent, the bearing we have developed is the preloaded type that prevents generation of such striking noise.

Fig. 2 shows the state in which clearance is existent inside the bearing when moment load is exerted on the bearing, and the state in which an appropriate preload is exerted on the entire bearing. The horizontal axis of the graphs indicates the positions of rolling elements (e.g. 110 balls) located along the entire inner circumference of the bearing, and the vertical axis indicates the contact stress on the rolling elements and rings. Setting an appropriate preload eliminates non-load state on the rolling elements across the entire inner circumference of the bearing. In addition, exertion of appropriate preload keeps required bearing rigidity and improves imaging accuracy.

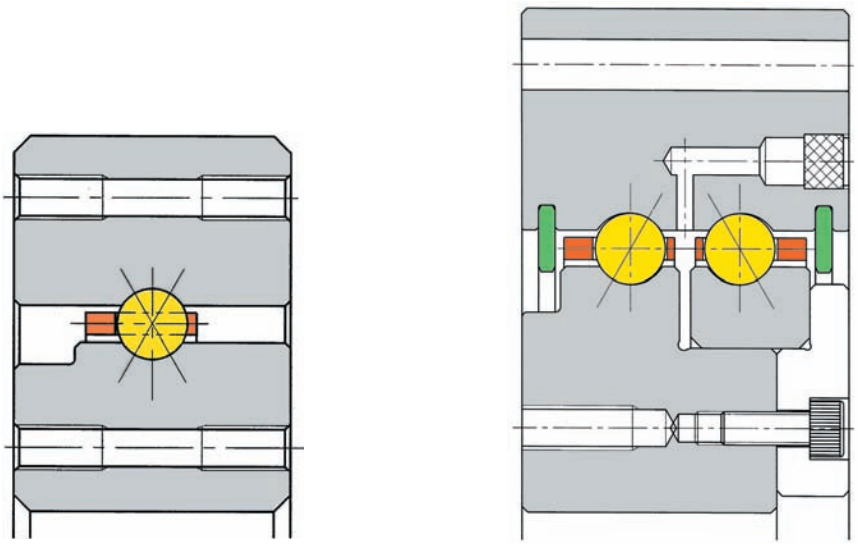

Single-row type　　Double-row type

Fig. 1 Schematic of CT scanner bearing

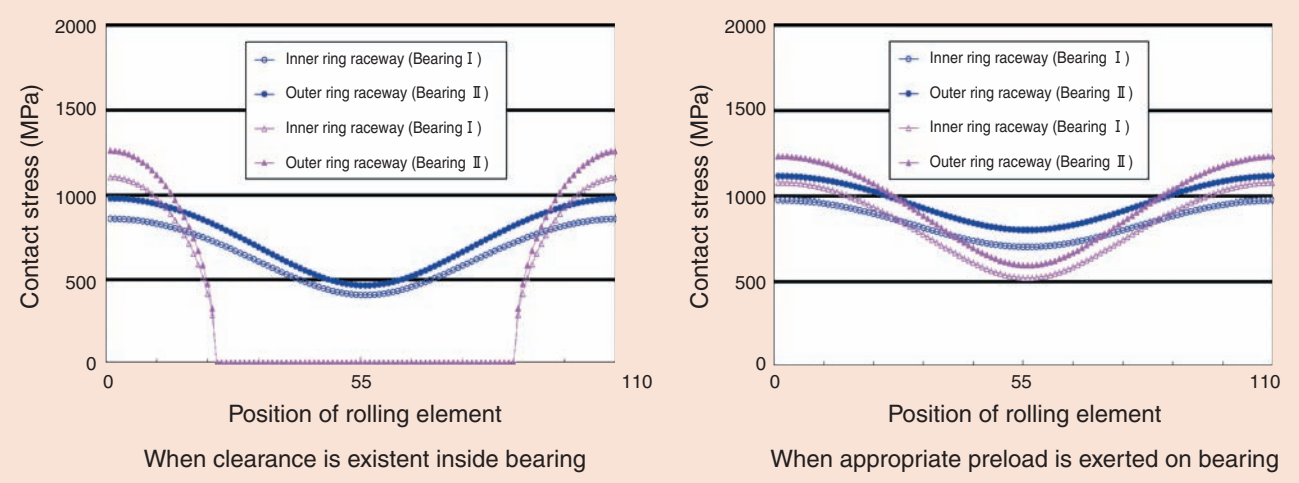

Fig. 2 Relationship of contact stress between each ball position and inner/outer ring

(2) Development of low-noise cage (Table 1, Fig. 3)

An especially important factor in noise reduction is optimization of cage design. In particular, large, thin cages, like those used for gantry bearings, are the link type and made of resin.

Conventionally, PA material was used as the resin, but it caused dimensional changes due to absorption of water, resulting in interference with the outer/inner rings and generation of stress on the cage itself. Therefore, a free area (opening) was provided, instead of connecting the entire circumference of the cage.

However, since this opening was not constrained inside the bearing, collision sounds (striking noise) between the inner and outer rings during rotation was generated, resulting in being one of the causes of unpleasant jarring sound on the ear.

The cage we developed has no such opening and has its entire circumference connected to eliminate such striking noise, and employs a mechanism that guides the cage by means of rolling elements to prevent interference between the cage and inner- outer-ring during rotation. Furthermore, the rigidity of the cage has been improved by employing a PPS resin cage instead of the conventional PA resin cage and improving GF to 30%. The elimination of the opening was the result realized by consideration given to the characteristic of the PPS resin so that it does not cause dimensional change through water absorption.

Table 1 Comparison of cage type

	Conventional cage	**Developed cage**
Opening	Provided	Not provided
Material	PA66+GF10%	PPS+GF30%
Pocket form	Cylindrical and square (alternately)	Special spherical
Guide type	—	Rolling element guide
Sound	Aural judgment: × (NG) × Striking sound from openings × Striking sound between cage and rings (× Dropping sound of rolling elements)	Aural judgment: ○ (OK) ○ No striking sound from openings ○ No striking sound between cage and rings (○ No dropping sound of rolling elements)

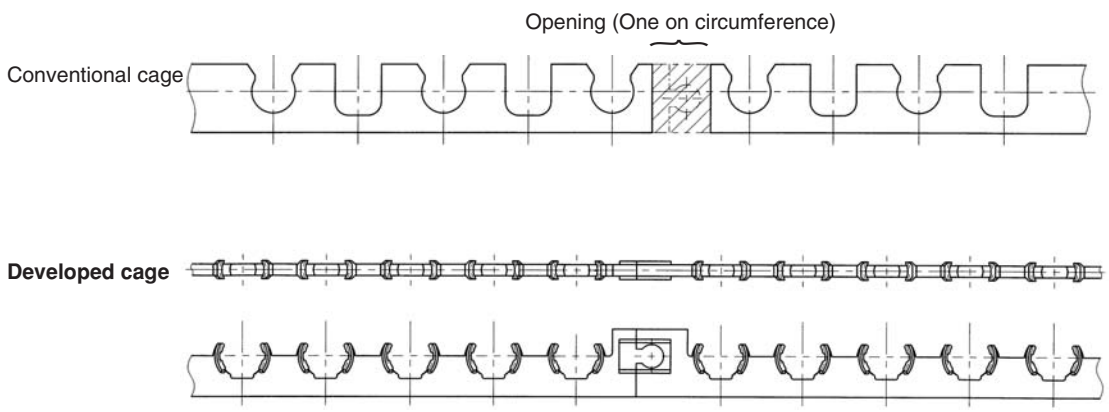

Fig. 3 Cage forms

4. Confirmation Test Results for Required Functions

The results of each test conducted on the required functions of gantry bearings are explained below.

(1) Higher-speed operation

(Test Contents)

A double-row angular contact ball bearing (approx. ID800 ×OD1000×Width 60 mm) was attached to the back plate of the test equipment shown in **Photo 2**. A weight was placed approximately 150 mm away from the center of the bearing, and test was conducted with radial load of 8000N. Evaluation was made at three bearing tilt angles : 0˚ (upright) and ±30˚ (tilted to front and rear), which are normally used for CT scanners.

(Test Results)

Fig. 4 shows the relationship between bearing rotating speed and outer ring temperature rise. With current high-speed CT scanners, the bearing rotating speed varies from 120 to 180 min^{-1}, depending on the bore diameter of the gantry. It was confirmed by this test that no abnormal outer ring temperature rise occurred even at 300 min^{-1} (d_{mn}=270,000) and operation was stable at high speeds twice those of current speed.

Photo 2 Test equipment

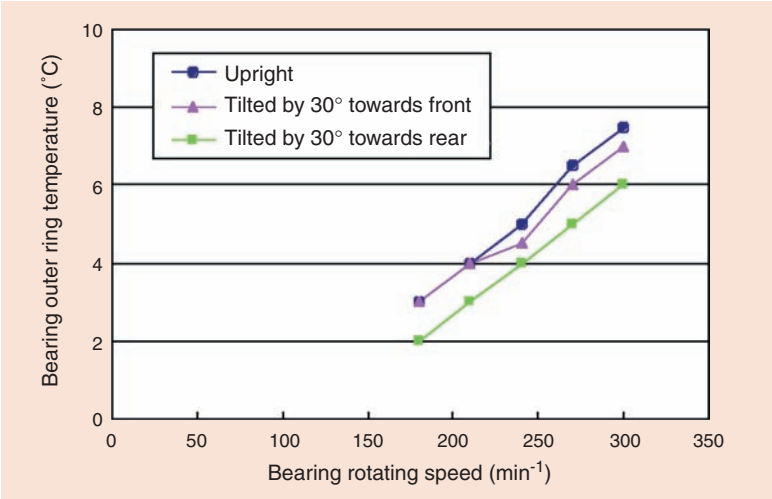

Fig. 4 High speed rotation test results

(2) Low noise level

(Test Contents)

A double-row angular contact ball bearing (approx. ID1000×OD1200×Width 80 mm) was attached to the back plate of the noise level test equipment shown in **Photo 3**. A microphone was placed approximately 1m away from the center of the bearing, and test was conducted.

(Test Results)

As shown in **Fig. 5**, the noise level increases proportionally to the bearing rotating speed. However, with the bearing equipped with the developed cage, the noise level is 3dBA lower, even at 180 min^{-1}, than that of the bearing equipped with the conventional cage, whose noise level is 72dBA at 60 min^{-1}. Furthermore, unpleasant sounds on the ears, which are typically heard in the case of cages that operate in synchronization with the bearing, were not heard.

Fig. 6 shows the waveform of noise obtained when the test was conducted at 120 min^{-1}. In the case of the bearing equipped with the conventional cage, the noise waveform shows clear peaks synchronized with rotation, and at that time peaks in the range of 1000 to 1500 Hz in particular were heard as noise. On the contrary, with the bearing equipped with the newly developed cage, no peaks synchronizing with rotation were observed, and it was confirmed that noise level was low on the whole.

Photo 3 Test equipment

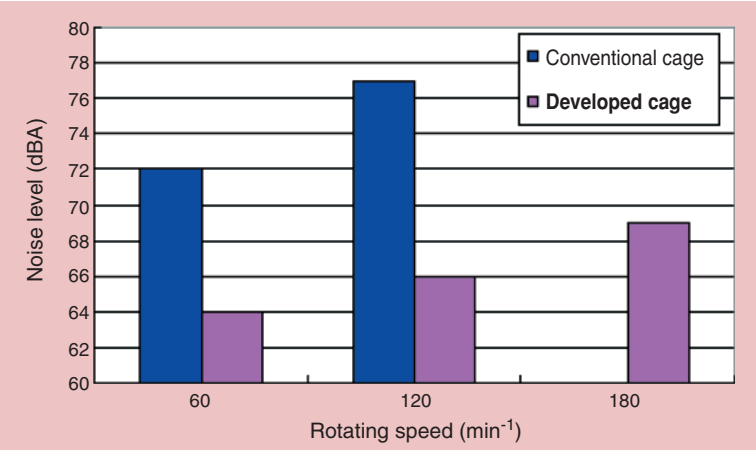

Fig. 5 Noise level test rsesults

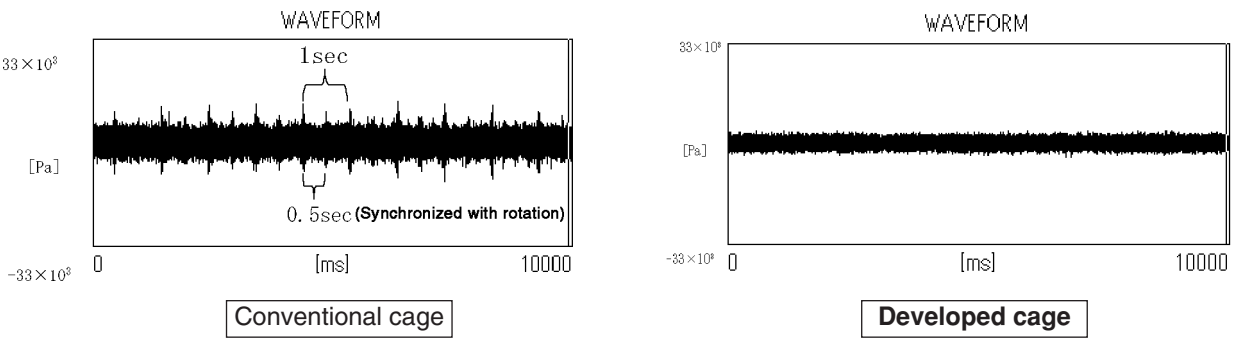

Fig. 6 Wave form of noise (120min^{-1})

5. Conclusion

In response to improved speed of gantry bearings, we were able to develop bearings that not only enable high-speed operation but also provide low noise level, by setting an appropriate preload and employing a cage of appropriate material and form in double-row angular contact ball bearings. Development of this bearing will surely help in improving the speed and reducing the noise level of CT scanners. From now on, we will also continue to develop bearings that will contribute to the entire medical instrument industry.

Photo of the author

Yosuke OYA

Industrial Engineering Department
Industrial Sales Headquarters

Integrated Sensor Bearing Unit for Axleboxes

Masanori UENO*

Constant monitoring of axlebox bearings , which are some of the most important components of rail vehicles, contributes to the reliability and safety of railways. In addition, railway companies today desire to reduce components and to simplify maintenance procedure for reduction of maintenance cost.

To meet this demand , we have developed a sealed double row tapered roller bearing with an integrated sensor. This sensor is incorporated into plastic housing which is attached to the oil seal case on the shaft end side. This sensor can detect temperature , rotating speed and rotating direction.

This report introduces laboratory test results for performance of the temperature sensor and impact- and vibration-resistance of the speed sensor.

1. Introduction

Railroad vehicle axle bearings are very important. Damage to them will hinder proper operation of the railroad vehicle and may even result in serious accidents. Due to recent extensions of maintenance intervals and increases in vehicle speed, a higher level of reliability is required of these bearings.

Railroad axle bearing operating parameters are currently monitored through constant observation of temperature using sensors attached to the axle box or by periodic inspection of the thermo-label affixed to the axle box/axle end. In addition, detection of axle rotating speed and associated wheel sliding during braking has been conducted using a gear attached to the axle end and a speed sensor attached to the axle box. However, this method requires many large components requiring maintenance adjustments of the gap between the sensor and gear.

Since the demands for reduction of maintenance costs are high for railroad vehicles, simplification of axle bearing and reduction in the number of components are desired. The development of an integrated sensor-bearing unit that enables detection of both temperature and rotating speed of bearings is also desired. **NTN** has developed an axle bearing with a sensor function, consisting of a sealed double row tapered roller bearing that is widely used for railroad vehicles. This paper introduces this new axle bearing together with various evaluation tests that were performed.

*Industrial Sales Headquarters Industrial Engineering Department

2. Structure of Sensor Axle Bearing Unit

The bearing unit developed by **NTN** consists of a sealed, double row, tapered roller bearing with an inner diameter of 120mm and outer diameter of 220mm and a sensor unit. The sensor unit is attached to the oil seal case on the axle end side, and designed to detect temperature and rotating speed/direction of the inner ring (see **Fig. 1)**.

To maintain compatibility with conventional axle bearings, the external dimensions of the unit are kept the same as those of conventional axle bearings. Specially shaped oil seal lips have been designed to that offer sufficient installation space of the sensor unit. The sensor unit is bolted to the seat on the oil seal case. Since axle bearings for railroad vehicles are exposed to operational impact and vibration from rail tracks, specially designed jam washers are used to prevent loosening of bolts.

In addition, the magnetic ring used for detection of rotating speed is fit onto the rib of the inner ring on the axle end side as shown in **Fig. 1**. The magnetic ring can also be attached to the seal wear ring depending on the structure of the bearing.

3. Specifications of Sensor Unit

Photo 1 shows an external view of the sensor unit, while **Table 1** shows the main specifications.

The sensor unit comes in a resin housing containing a temperature thermistor (thermally sensitive resistors) to measure the bearing temperature. Two magnetic sensor elements (Hall IC) are used to detect the axle rotating speed.

The magnetic ring consists of N and S poles magnetized alternately in the circumferential direction. This causes the magnetic field to pass through the Hall ICs according to the axle rotation. The speed sensors convert the change in the magnetic field to voltage pulses. Two Hall ICs are placed so that the phase difference of the output pulses is 90 degrees. By detecting the frequency and phase difference of the pulses, the rotating speed and direction of the axle can be found.

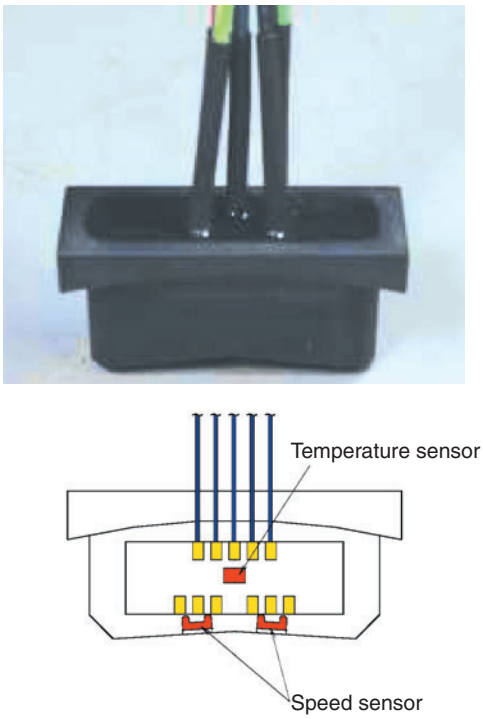

Photo 1 Sensor unit

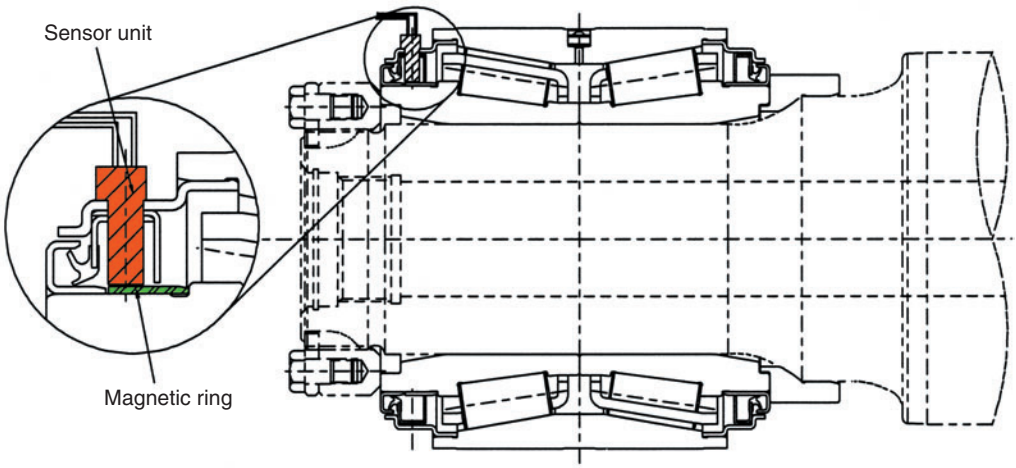

Fig. 1 Axlebox bearing unit with integrated sensor

Table 1 Specification of sensor unit

Operating temperature range		-40 to 125˚C
Impact resistance		100 G
Vibration resistance		35 G
Frequency response of speed sensor		0 to 8kHz
Resolution of speed sensor (Fig. 2)	Adjacent pitch error	5% or less
	Duty ratio	50±15%
	Phase difference between A & B signals	90±45 degrees

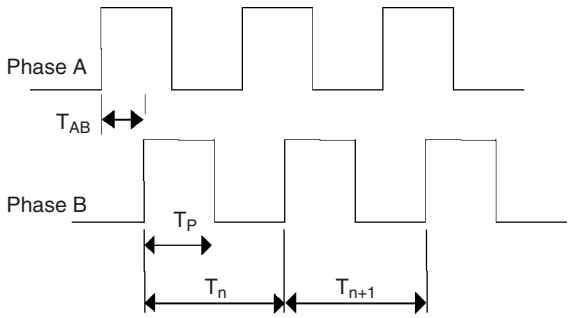

①Adjacent pitch error (%)=|(T_n−T_{n+1})| T_n×100

②Duty ratio (%)=T_P/T_n×100

③Phase difference between A & B signals (degree) =T_{AB}/T_n×360

Fig. 2 Resolution of speed sensors

4. Evaluation Test

4. 1. Bearing Temperature Detection Test

The axle bearing test rig shown in **Fig. 3** was used to test the axle bearing sensor unit. The output temperature of the temperature sensors was compared with the bearing temperature measured by a thermocouple attached to the bearing.

In this test, four sensor units were attached to the oil seal case, one at every 90 degrees in the circumferential direction, to check the difference in the output temperatures due to different sensor unit positions.

(Test Results)

Fig. 4 shows the outputs from the temperature sensors and the results measured by the thermocouplers.

- The outputs from the temperature sensors are approximately 10˚C lower at maximum than the temperature measured on the outside surface of the outer ring by the thermocouple. However, they can monitor temperature change on the outer ring,while the temperature sensor is available for actual use.
- Comparison of the sensor outputs with each position indicates that the output from the top sensor (in the bearing load range) is approximately 5˚C higher at maximum than the others. There is almost no difference among the other outputs.

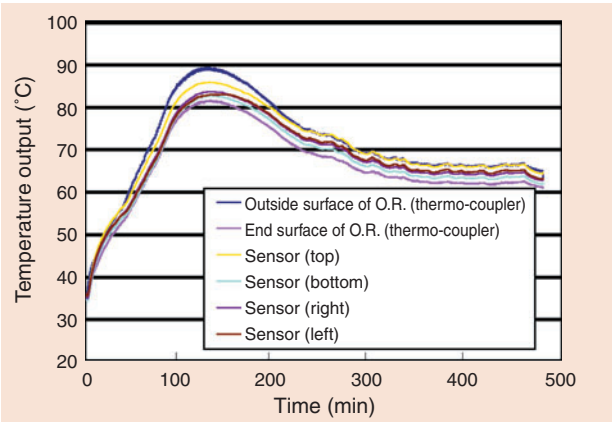

Fig. 4 Relationship between bearing temp. and output of temp. sensor

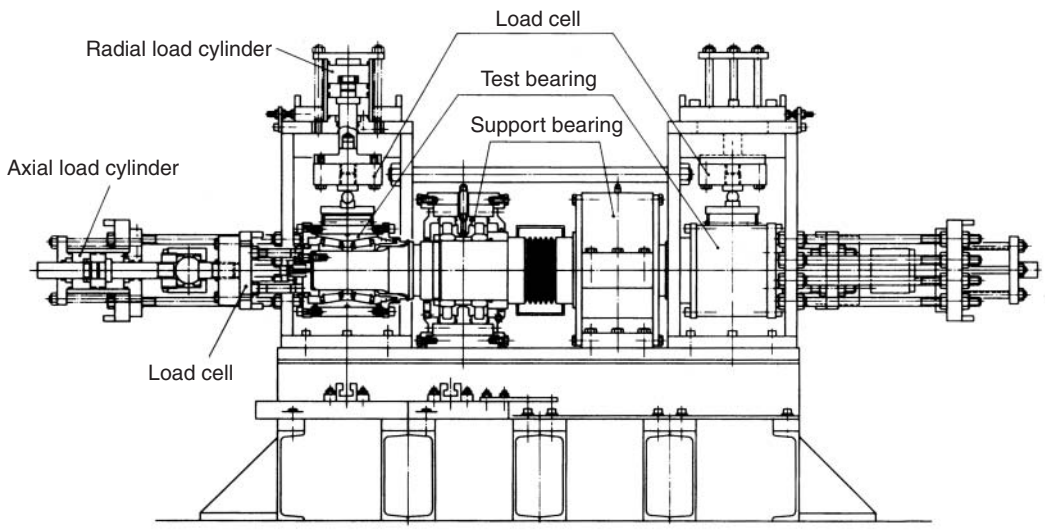

Fig. 3 Test rig for axle bearings

4. 2. Vibration Test

The sensor units were exposed to continuous vibration. The test confirmed the resolution of the speed sensors shown in **Table 1** was maintained.

(Test Conditions)

- Vibration acceleration : ±35G
- Vibration direction : Vertical, crosswise, lengthwise
- Frequency : 60Hz
- Vibration cycle : 10^7 cycles for each direction
- Specimen : 3 specimens

(Test Results)

Figs. 5 to **7** show the measured adjacent pitch error, duty ratio and phase difference between A & B signals, respectively. The designed resolution of the speed sensors was verified even at the end of the test, demonstrating that the sensors have sufficient vibration resistance required for railroad applications.

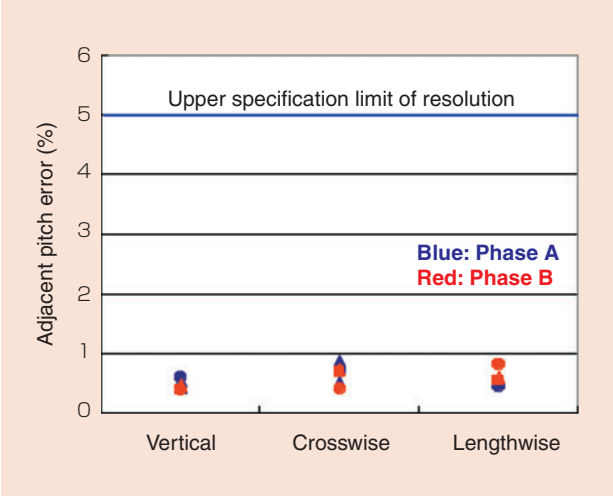

Fig. 5 Adjacent pitch error

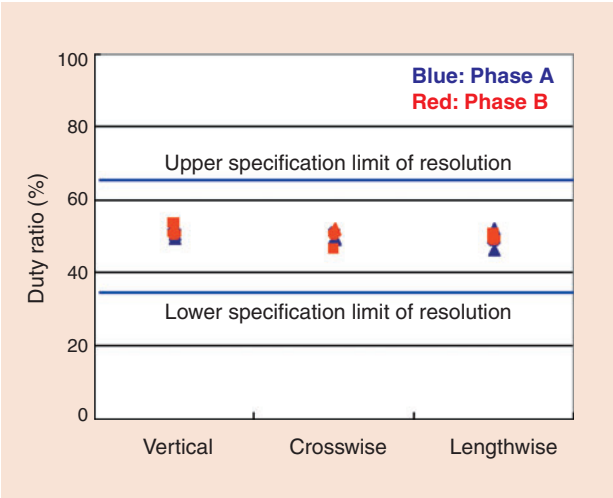

Fig. 6 Duty ratio

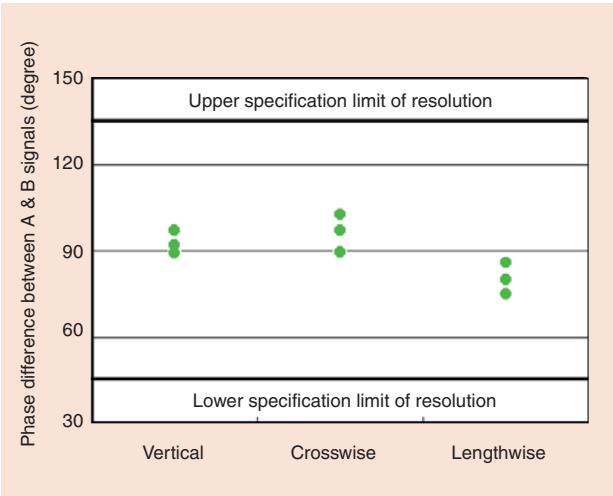

Fig. 7 Phase difference between A & B signals

4. 3. Impact Test

The sensor units were exposed to impact. The test confirmed the resolution of the speed sensors shown in **Table 1** was maintained.

(Test Conditions)

- Impact : 100G
- Impact direction : Vertical, crosswise, lengthwise
- Vibration cycle : 4000 cycles for each direction
- Specimen : 2 specimens

(Test Results)

Figs. 8 to **10** show the measured adjacent pitch error, duty ratio and phase difference between A & B signals, respectively. The designed resolution of the speed sensors was verified even at the end of the test, demonstrating that the sensors have sufficient impact resistance required for railroad applications.

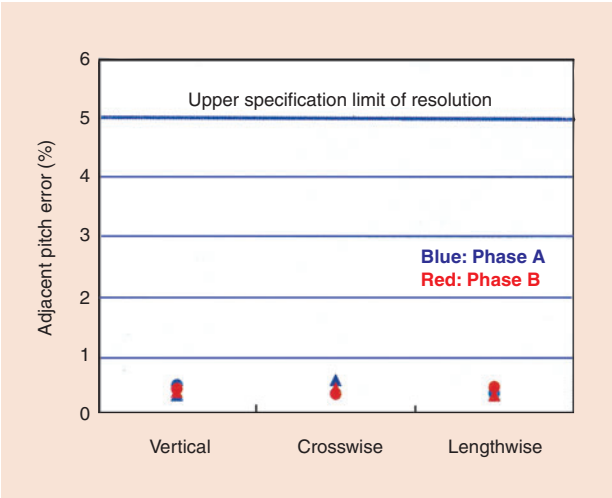

Fig. 8 Adjacent pitch error

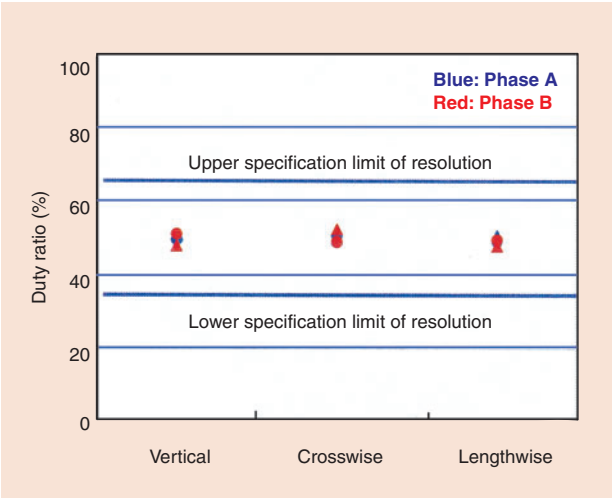

Fig. 9 Duty ratio

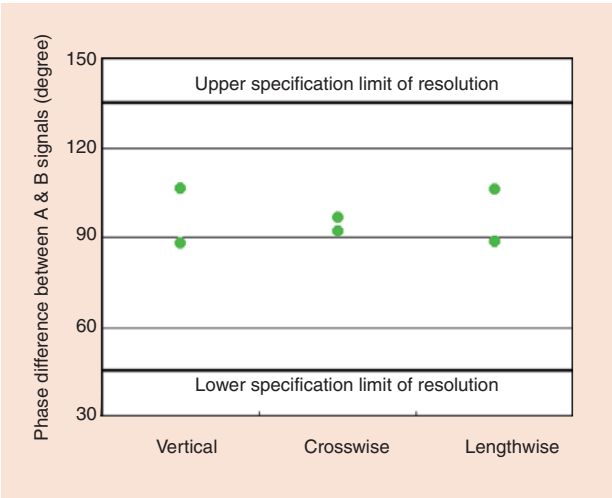

Fig. 10 Phase difference between A & B signals

5- Conclusion

This overview of the integrated sensor-bearing unit designed for axle boxes with associated test results has been presented in response to an expected increase in demand for improvement in safety and reliability of railroad vehicles. Additionally, railway companies are likely to seek reduction of vehicle maintenance costs. Reliability of railroad axle bearings is critical. **NTN** is confident the integrated sensor-bearing unit introduced in this paper will be an effective means of addressing this attribute while helping to reduce the size and maintenance cost of the bearings.

Photo of the author

Masanori UENO

Industrial Engineering Department
Industrial Sales Headquarters

Bearings for Wind Turbine

Souichi YAGI*

In 2002, worldwide electricity production was about 31,000MW. This is a 27% increase over the previous year.

In the past few years, the wind turbine generating system, which emits no carbon dioxide, has gained widespread acceptance as the cleanest and most environmentally friendly energy. The technical trend for wind turbines is to increase reliability and efficiency while reducing the cost of operation. The bearings, which are one of the most important components for wind turbines, require designs that optimize reliability and economic efficiency while considering the characteristics of this applications.

This report introduces special characteristics for wind turbine bearings and a method to optimize wind turbine bearing design.

1. Introduction

Worldwide electricity production reached about 31,000MW by the end of 2002. This is a 27% increase over the previous year. In the past few years wind power generation, which emits no carbon dioxide, has gained widespread acceptance as the cleanest and most environmentally friendly form of energy. Technical issues remaining in the development of wind power generation include increasing reliability of the system while reducing the cost of operation. Bearings are one of the most important components of wind turbines and require designs that optimize reliability and economic efficiency while taking into account the characteristics of the applications. This report introduces a method to optimize wind turbine bearing design and the features of bearings developed for wind turbines.

2. Structure of Wind Turbines and Bearings

Fig. 1 shows the nacelle of 1 to 2MW wind turbines. Bearings are used in various places of the nacelle: rotor shaft, gearbox (step-up gear), generator, yaw gearbox (reduction), yaw slewing table, blade pitch revolving seat and hydraulic pump.

3. Bearing Operating Conditions

The rotor shaft bearing supports the blades and rotor and transmits torque to the gearbox. The bearing loads and rotating speeds vary considerably due to constantly changing winds.

At wind speeds below the cut-in wind speed (i.e. the minimum wind speed required for power generation), the rotor shaft will idle resulting in low-speed, low-load operation. At wind speeds above the cut-in speed, the

*Industrial Sales Headquarters

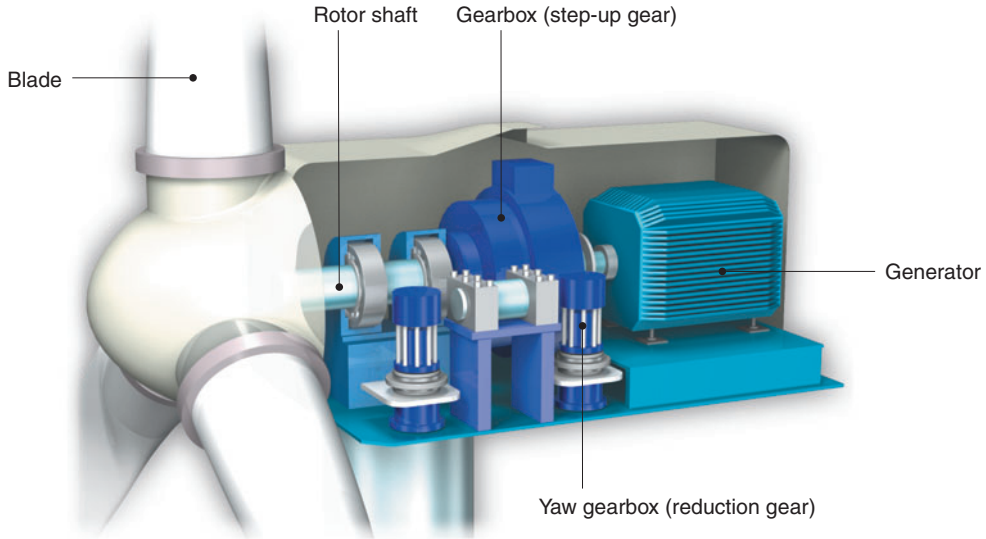

Fig. 1 Nacelle

rotating speed increases above the rated speed, resulting in average loads. In the case of wind gusts, the blades and rotor will exert large loads on the rotor shaft bearing. **Fig. 2** shows the load and moment exerted on the rotor shaft bearing.

Such changes in the load, moment and rotating speed also affect the gearbox bearing. One of the features of wind turbine bearings is that they operate in a wide range of loads from light to heavy load (when exposed to gusts). **Fig. 3** shows examples of measured rotor load and moment over one minute when a 700-kW wind turbine is operated at wind speeds of 23 to 24m/s.

Rotor shaft bearings repeat start, acceleration, deceleration and stop operations irregularly as they are exposed to fluctuation of load. Therefore, the optimal specifications for various parameters, including bearing type, clearance, number of bearing rollers, crowning and cage must be examined for each condition (minimum load, average load, maximum load).

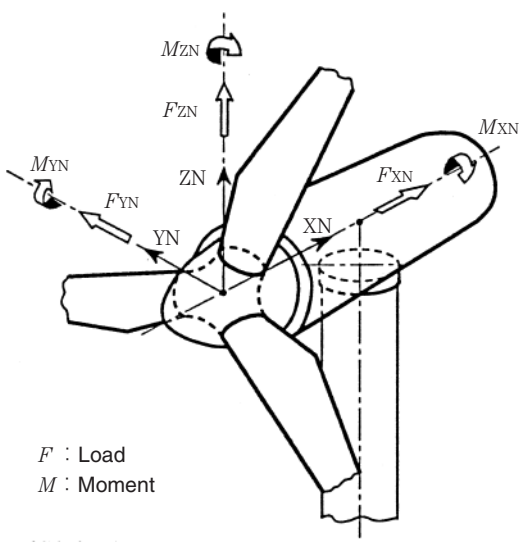

Fig. 2 Rotor load schematic

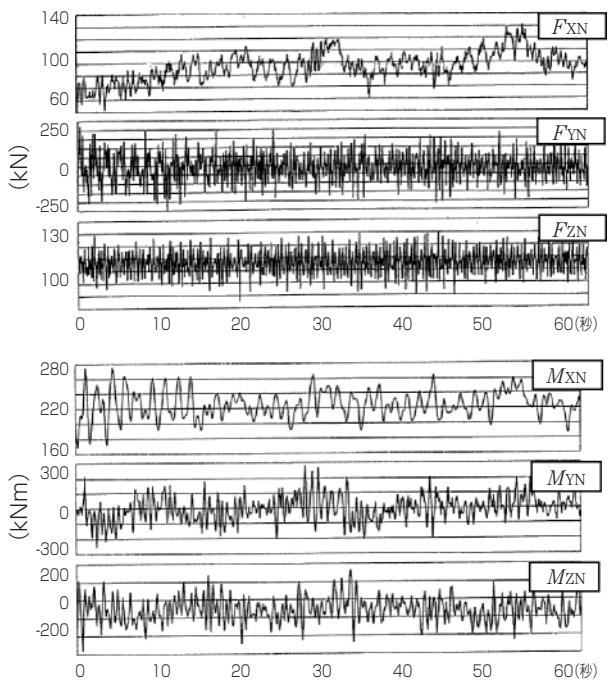

Fig. 3 Measurements of rotor load and moment

4. Rotor Shaft Bearings

Table 1 shows the structures of the shafts that use a gearbox to increase blade speed to the rated speed of the induction generator. Bearings suitable for each rotor shaft type are also shown. Table 2 shows the structures of the shaft of synchronous generators not equipped with a gearbox.

Table 1 Wind turbine rotor shaft bearing assembly (with gearbox)

Structure	Blade-side bearing	Generator-side bearing	Features
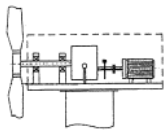	SRB SRB SRB	SRB CRB DTRB	● Two bearings are used. ● The gearbox is supported on the rotor shaft.
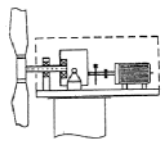	SRB	CRB	● The generator-side bearing is also used as the gearbox's input bearing.
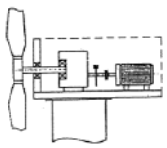	SRB	CRB	● The generator-side bearing is also used as the gearbox's input bearing. ● The load on the blade-side bearing is supported by the nacelle.
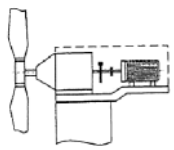	TRRB DTRB	—	● No rotor bearing is used and the rotor load is borne by the gearbox bearing.

SRB : Spherical roller bearing　CRB : Cylindrical roller bearing
DTRB : Double-row tapered roller bearing　TRRB : Triple-row cylindrical roller bearing

Table 2 Wind turbine rotor shaft bearing assembly (without gearbox)

Structure	Blade-side bearing	Generator-side bearing	Features
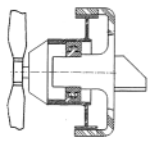	TRRB DTRB	CRB	● Direct drive ● Outer ring rotation
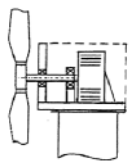	SRB DTRB	CRB CRB	● The load on the blade-side bearing is supported by the nacelle. ● Inner ring rotation

When designing the bearing, first calculate the bearing life for the maximum required strength of the housing and the average deformation of the housing. Then design a slim housing and choose a shaft bearing that meets the required calculated life.

With deformation of the housing and outer ring raceway taken into account, calculate the load on each rolling element to obtain the life of the rotating and stationary rings.

$$Q_R = \left[\frac{1}{Z} \sum_{J=1}^{Z} (Q_{RJ})^{wi} \right]^{1/wi}$$

$$Q_S = \left[\frac{1}{Z} \sum_{J=1}^{Z} (Q_{SJ})^{we} \right]^{1/we}$$

Q_R, Q_s : Average load on rotating and stationary rings
Z : Number of rolling elements
wi, we : Constant
$L_R = (C_n / Q_R)^p$: Life of rotating ring
$L_S = (C_n / Q_s)^p$: Life of stationary ring
$L = (L_R^{-e} + L_S^{-e})^{-1/e}$: Life of bearing
C_n : Dynamic rated load on contact point
p : For ball bearing 3
For roller bearing 10/3
e : For ball bearing 10/9
For roller bearing 9/8

Spherical roller and tapered roller bearings are mainly used. However, spherical roller bearings, that feature low misalignment rates, are widely used. Normally, misalignment of ±0.5° needs to be taken into account.

With B type spherical roller bearings, the rollers are guided by the inner ring's center rib. This enables operation with stable torque, low skew and low heat generation in a wide load range from the minimum to the maximum load. **Fig. 4** shows the structure of **NTN**'s spherical roller bearings (both B and C types).

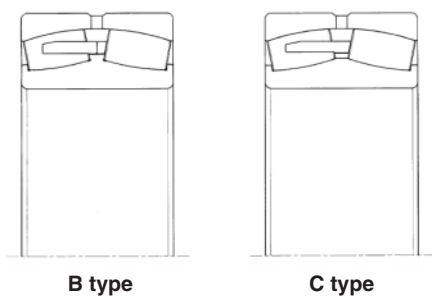

Fig. 4 Spherical roller bearing, B type and C type

Since rotor shaft bearings are exposed to vibration of blades and gearbox, fretting corrosion may occur. Therefore, selection of appropriate bearings and grease, as well as optimization of clearance and fitting are important factors.

Photo 1 shows an external view of a bearing at the end of vibration test.

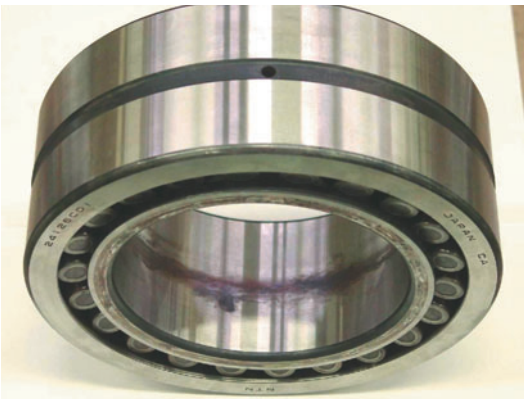

(1) Fretting on inner ring bore

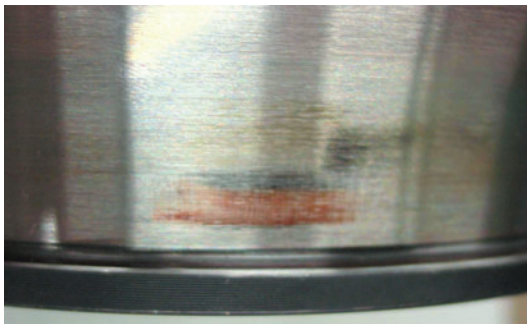

(2) Fretting on inner ring raceway

《Vibration test》

Bearing：24126CL1
Vibration acceleration：9G
Vibration cycles：10 million cycles
Maximum surface pressure：1080MPa

Photo 1 Vibration test results

Fig. 5 shows an example of the deformation of a rotor shaft bearing outer ring and housing. The bearing and housing are optimized by calculating the bearing life, including housing deformation and bearing clearance and also confirming the housing strength based on a stress analysis. In this example, a bearing for 1.5-MW wind turbines was used, and the maximum deformation in the axial direction was 0.07mm. The difference in the bearing life calculated with this deformation and bearing clearance taken into account and the one calculated with the housing and outer ring considered to be non-deformed was within 5%, which is not problematic in actual use. If this difference is excessively large and the life is short, the design of the housing needs to be changed to improve rigidity.

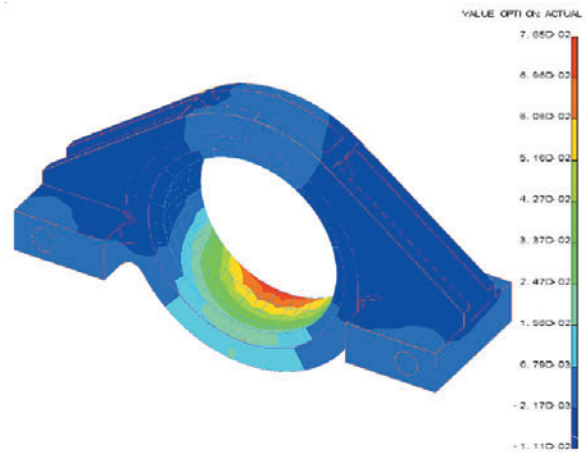

Fig. 5 Bearing outer ring and Pillow Block deformation

5. Planet Bearings for Gearbox

A gearbox consists of an input shaft, planet gear, low-speed shaft, intermediate shaft and high-speed shaft. Fig. 6 shows the structure of a gearbox, and **Photo 2** shows an external view of a full complement cylindrical roller bearing, that is used for input and low-speed shafts.

Fig. 7 shows an example of planet gear mechanism.

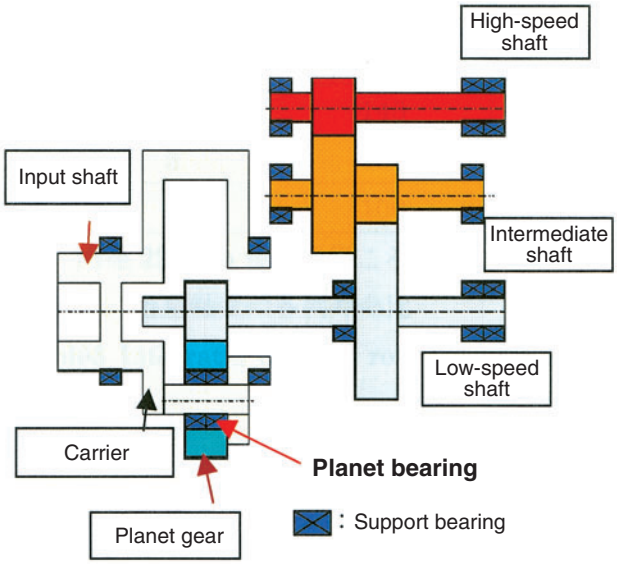

Fig. 6 Gearbox for wind turbine

Photo 2 NTN Full complement cylindrical roller bearing

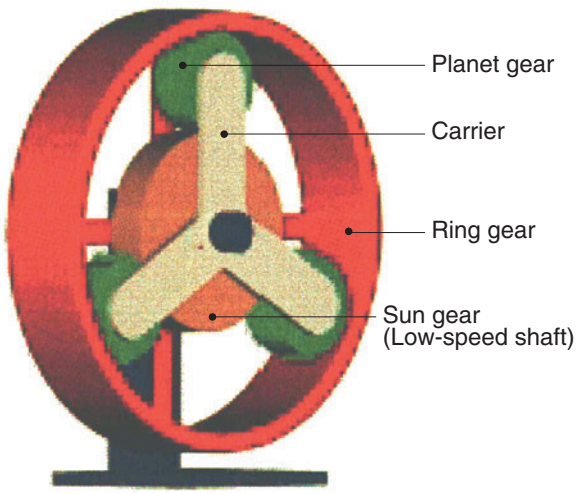

Fig. 7 Planetary gear model

Spherical roller bearings or full complement cylindrical roller bearings are used as planet bearings. An analysis model of the planet bearing is used to calculate the life of bearing with deformation of the outer ring taken into account. When calculating, make sure that the load on the bearing is considered to be the one exerted on rolling elements and the gear engagement point between the ring gear and sun gear is fixed.

Fig. 8 shows an example of deflection analysis results of a planet bearing used for 1.5-MW gearbox. The planet bearing used for analysis consists of two double-row cylindrical roller bearings with four rows of rolling elements, and the maximum deflection was 0.21mm.

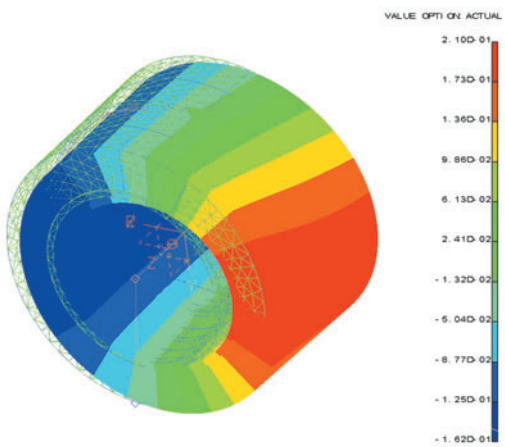

Fig. 8 Deflection of planet bearing

The life, calculated from the analysis results with elastic deformation of the rings taken into account, varies by a maximum of 58% among rows. The carrier-side rows have higher load ratio than the others, resulting in shorter calculated life. **Fig. 9** illustrates the arrangement of bearings, and **Table 3** shows the calculated results.

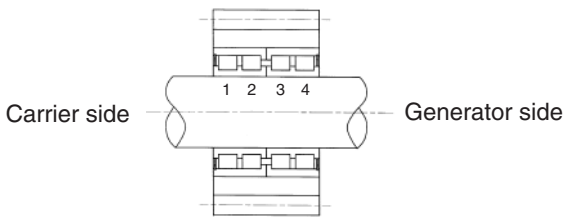

Fig. 9 Arrangement of bearings

Table 3 Life ratio of each row for planet bearing

Row No.	Life ratio
1	85
2	143
3	133
4	100

Inner diameter ϕ 220mm
Double-row cylindrical roller bearing

The maximum contact surface pressure (P_{max}) for gearbox bearings is calculated based on point contact for spherical roller bearings, and line contact for cylindrical roller bearings. In most cases misalignment is taken into account when specifying the maximum contact surface pressure.

$P_{max} = K_{\ell c}\, K_m\, P_{line}$ (Cylindrical roller bearing)

$K_{\ell c}$: Crowning correction factor

K_m : Misalignment factor

P_{line} : Maximum line contact surface pressure

In the case of spherical roller bearings, if the maximum contact surface pressure exceeds the limit, the bearing size needs to increase. This will increase the calculated life and reduce the maximum contact surface pressure. However, in the case of light loads the rolling elements may not roll properly on the raceway and will begin to slide. This sliding may cause damage to the raceway. Because of this, **NTN** recommends the minimum load be at least 4% of the basic static load rating.

Concerning lubrication, some measures need to be implemented to prevent a situation in which the planet bearing is exposed to insufficient lubrication when it begins to move.

The problems concerning the planet bearings can be summarized into the following three points.

- Influences by plastic deformation of gears and bearing
- Influences by misalignment of planet bearing caused by twisting of carrier
- Influences by dry start up (insufficient lubricating oil)

The specifications for the optimal bearing must be take into account these properties. **NTN** has been working on the design of ribs that have high load capacity and that provide sufficient resistance against sliding and scuffing under light loads, as well optimal axial clearance. In addition, **NTN** has also been working to prolong the life of bearings by employing special heat treatment.

Furthermore, **NTN** has introduced the special test machines shown in **Figs. 10** and **11**, to promote the development of next generation planet bearings.

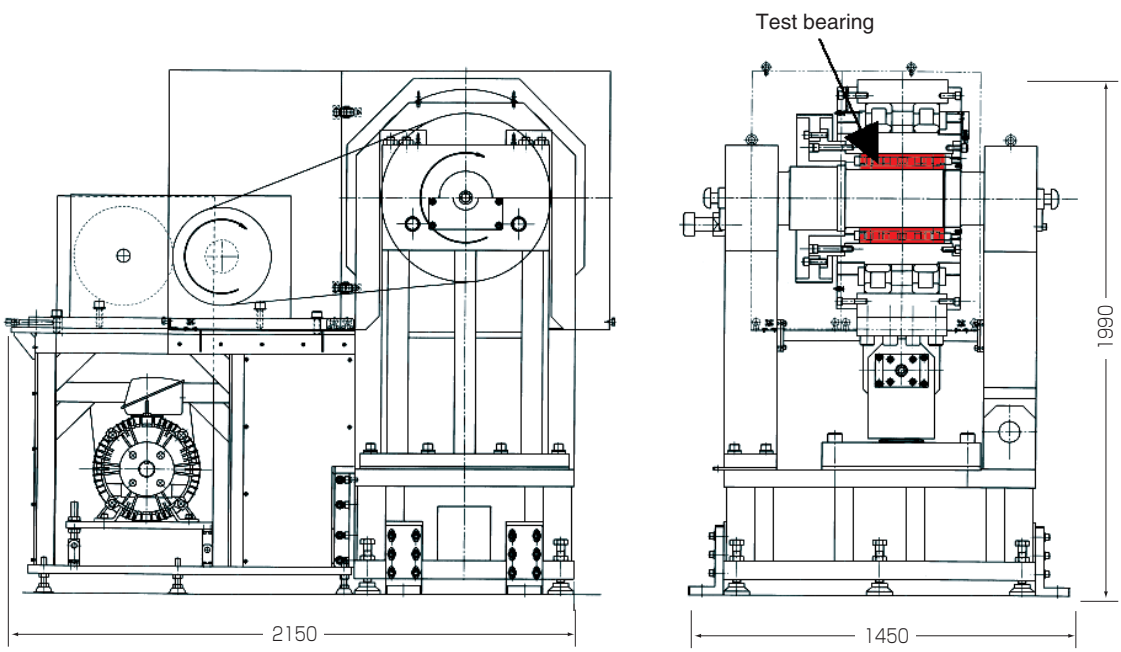

Fig. 10 **NTN** outer ring rotating test machine

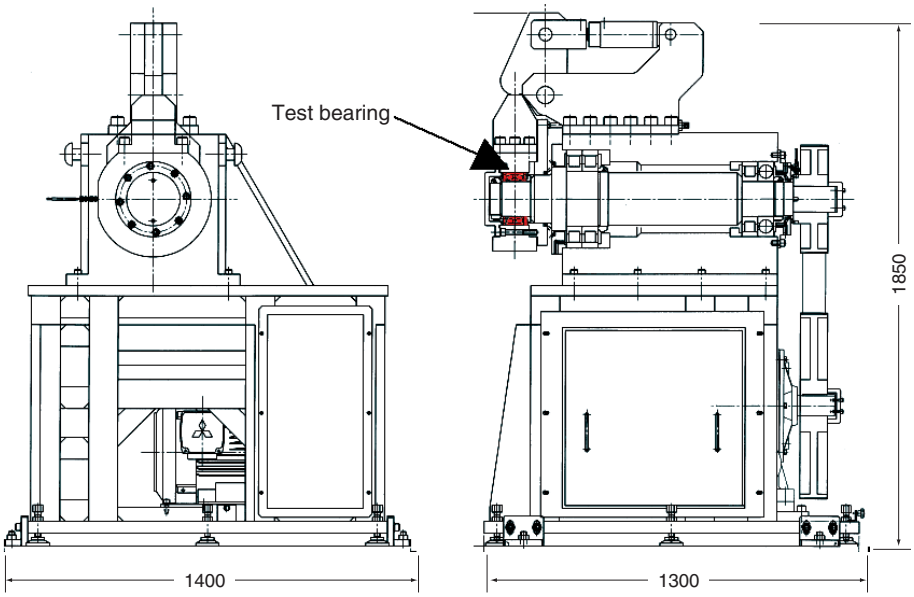

Fig. 11 **NTN** inner ring rotating test machine

6. Insulated Bearings for Generator

To improve the reliability of bearings used in generators, it is necessary to prevent sparks (galvanic corrosion) caused by electric current passing through the bearings. **NTN** has produced a new single-layer bearing having sufficient insulation capability and reliability by adopting special ceramics and improving the spray-coating method.

This bearing provides insulation resistance of 100MΩ or higher and dielectric breakdown voltage of 2kV or higher, meeting the insulation performance required for wind turbines.

Photo. 3 shows an external view of this insulated bearing.

For details, refer to "Insulated Bearing "MEGAOHM" Series" in this book.

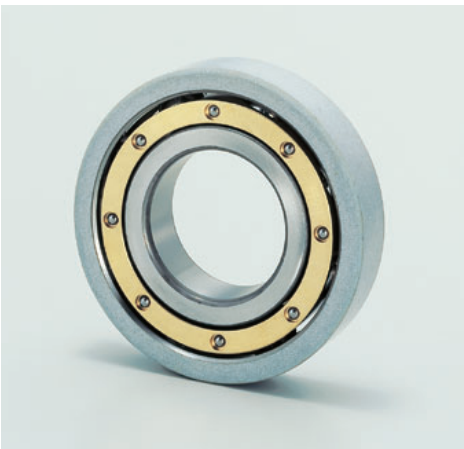

Photo 3 Insulated Bearing

7. Bearings for Yaw Gearbox

Since yaw gearboxes need to be small and capable of conveying large torque, the bearings to be used for them must be compact and have high load capacity. Because of this, angular contact ball bearings with thin inner/outer rings and tapered roller bearings are often used.

With angular contact ball bearings, which are exposed to large axial load, the resistance to axial load has been improved by increasing the groove depth on the inner and outer rings. **Fig. 12** shows the cross-sectional view of the standard bearing and that of special design bearings for yaw gearboxes. The special design bearing has a high axial load resistance, approximately 9 times higher than the standard bearing.

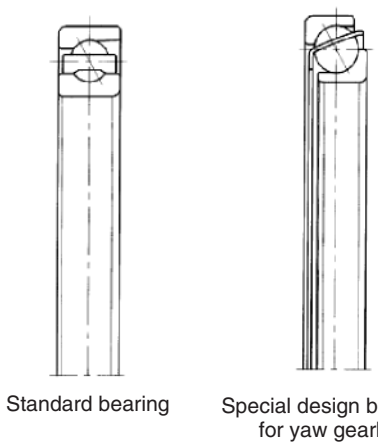

Fig. 12 Special design angular contact ball bearings

For tapered roller bearings, carbonitrided ETA bearings are used to provide longer life.

ETA bearings are long-life bearings with high thermal stability gained by optimizing distribution of retained austenite and carbide present on the surface through special heat treatment. They feature high resistance to contaminants contained in lubricating oil and high peeling resistance. **Table 4** shows the life test conditions and **Fig. 13** shows the results.

Such implementation has enabled **NTN** to provide compact, highly reliable bearings.

Table 4 Test conditions (30206, ETA30206)

	Normal lubricating oil	Contaminated lubricating oil (Reference)
Radial load (kN)	17.64	
Rotating speed (min^{-1})	2000	
Lubricating oil	Turbine oil 56	Turbine oil 56 + **NTN**'s standard contaminants

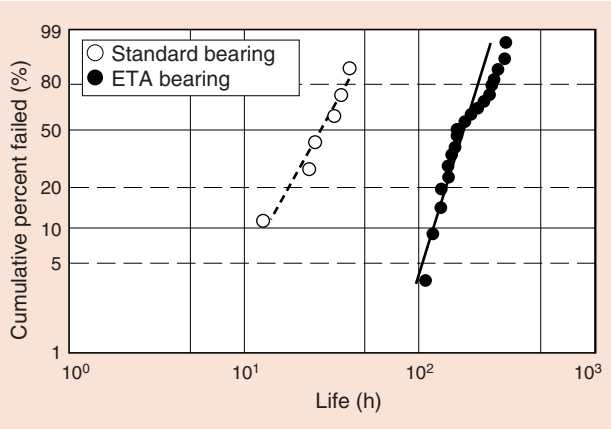

Fig. 13 Comparison of life of ETA tapered roller bearing and standard bearing (with contamination)

8. Conclusion

Compared with Europe and North America, where the use of wind turbines is widespread, Japan often suffers from considerable atmospheric turbulence, severe tropical storms and lightening (winter). Thus, wind turbines that are reliable and suit Japan's climatic conditions are desired. **NTN** has been working on improving the reliability of bearings designed for wind turbines. By choosing optimal bearing specifications that satisfy wind turbine manufacturers and users and supplying high-quality products, **NTN** will contribute to the development of an eco-friendly wind power generation.

References

1) Germanischer Lloyd
Regulations for the Certification of Wind Energy Conversion Systems

2) B.Schlecht
Moderne Simulationstechniken zur dynamischen Auslegung von Triebstraengen in Multi- Megawatt-Windenergieanlagen

3) B.Schlecht et al
"MULTIBODY-SYSTEM-SIMULATION OF DRIVE TRAINS OF WIND TURBINES"

4) B.Niederstucke et al
LOAD DATA ANALYSIS FOR WIND TURBINE GEARBOXES

Photo of the author

Souichi YAGI

Industrial Sales Headquarters

Insulated bearing "MEGAOHM" series

Hideji ITO*

NTN has developed a new ceramic-coated, insulated bearing that uses a single-layer, spray-coated ceramic.

Applications for this bearing include electrical wind turbine generators, general purpose motors, and traction motors for trains.

NTN recently established the MEGAOHM series of insulated bearings. The MEGAOHM series, includes multi-layer, spray-coated ceramic, insulated bearings, the new single-layer type, and the PPS resin-coated type.

The new single-layer, ceramic-coated, insulated bearing is introduced below.

1. Introduction

Traction motors for trains use bearings that are insulated to prevent electric corrosion by coating the outer diameters with ceramic or injection-molded resin (glass fiber contained).

Conventionally, bearings were coated with ceramic in multi layers (3-layer, 2-layer). The new bearing developed by **NTN** (**Fig. 1)** is a low-cost, single-layer, ceramic-coated, insulated bearing and is designed for use in wind turbine generators, general-purpose motors and traction motors for trains. This paper explains the bearing features and evaluation test results.

In addition to the conventional, multi-layer, ceramic-coated, insulated bearings and special, resin-coated, insulated bearings, the bearings developed this time are named "**MEGAOHM Series**", featuring high insulation performance.

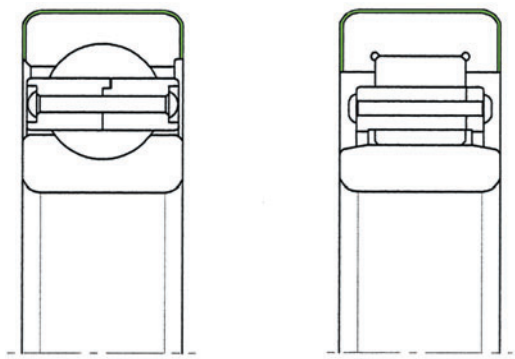

Fig. 1 Single-layer, ceramic-coated, insulated bearings

*Industrial Sales Headquarters Industrial Engineering Department

2. Features of Single-Layer, Ceramic-Coated, Insulated Bearings

1. Available as a drop-in replacement for standard bearing sizes
2. Applicable bearing types include deep groove ball bearings and cylindrical roller bearings
3. Insulation performance
   Insulation resistance: ≧100MΩ
   (500V forced, at 20˚C)
   Dielectric breakdown voltage: ≧2kV (AC60Hz)

3. Evaluation Tests for Single-Layer, Ceramic-Coated, Insulated Bearings

3. 1 Drop Test

A drop test was conducted to determine the effect of an impact load on the insulated surfaces.

(Test Method)

A 6316 bearing was dropped from a height of 50 mm as shown in **Fig. 2**, and then immersed in hot water (80˚C for one hour). If cracks are present, water passes through , resulting in decreased insulation resistance. The insulation resistance was measured using the equipment shown in **Fig. 3**.

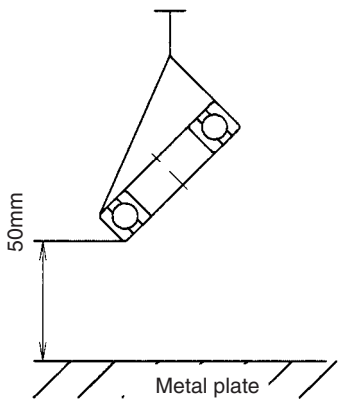

Fig. 2 Schematic of drop test

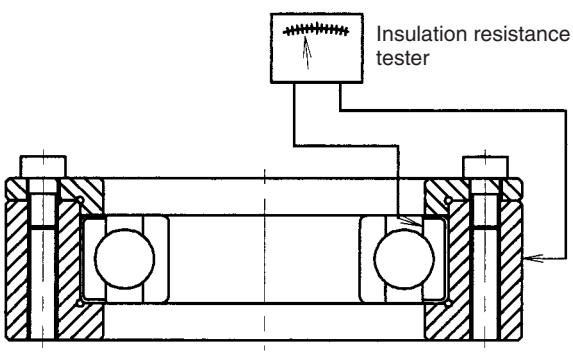

Fig. 3 Measurement of insulation resistance

(Test Results)

A slight indentation or mark was observed in the area exposed to impact, but the insulation resistance after immersion in hot water remained 1000 MΩ or higher.

3. 2 Mounting and Dismounting Test

In some applications, the bearings need to be dismounted and re-mounted repeatedly for periodic inspection. A mount/dismount test was conducted to check whether damage (if any) to the ceramic-coating would result in deteriorated performance.

(Test Method)

The equipment shown in **Fig. 4** was used to dismount and re-mount the bearing five times. Then, the bearing was immersed in hot water, and the change in insulation resistance was measured to check for the presence of abnormalities in the plasma-coated ceramic layer. In an actual application, the ceramic surface should be coated with used grease. However, this test was conducted under a severe condition with no grease coating.

The fit between the outer diameter of the outer ring and inner diameter of the equipment is ϕ 170 (36 μm tight fit).

(Test Results)

After the test, no abnormalities were found on the ceramic-coated surfaces. In addition, it was confirmed that the insulation resistance after immersion in hot water was again 1000 MΩ or higher and the ceramic-coated layers were not damaged.

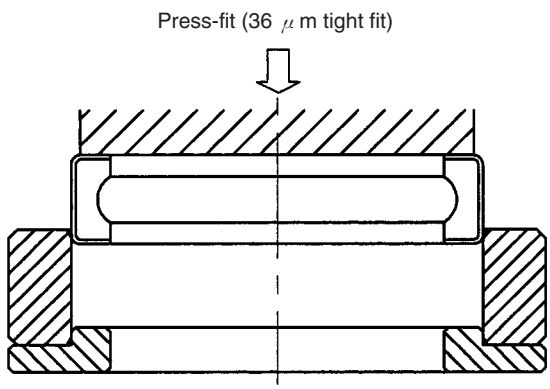

Fig. 4 Mounting and dismounting test

3. 3 Humidity Test

A test was conducted to check the effects of temperature and humidity on the insulation performance. Typical environmental conditions were used during this test.

(Test Method)

The bearings were placed inside the temperature/humidity-controlled chamber and exposed to the following conditions for 10 cycles.

Temperature 40˚C, humidity 85%: 2 hours
↓
Temperature 25˚C, humidity 50%: 0.5 hours
1 cycle

Four bearings were tested.

(Test Results)

The insulation resistance was measured immediately after the 10-cycle test. This test revealed that the bearings, which had an insulation resistance of 1000 MΩ or higher before the test, provided a minimum of 180 MΩ resistance. After the bearings were left to stand, the insulation resistance was measured again. At this time, all the bearings showed 1000 MΩ or higher. This indicates that the ceramic-coated layers developed condensation when exposed to high humidity. So, when handling bearings, care must be taken to avoid humid environments.

3. 4 Heat Deterioration Test

A test was conducted to consider the effects of rapid temperature change on the insulation performance. Temperatures were based on typical operating conditions.

(Test Method)

Condition 1: The bearings were placed inside the thermal shock chamber and exposed to the following conditions for 20 cycles.

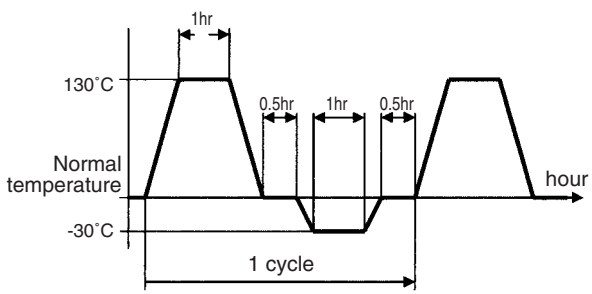

Condition 2: The bearings were placed inside the temperature-controlled chamber and left at 160C˚ for 2,200 hours.

(Test Results)

After the test, no abnormalities were found on the ceramic-coated surface . In addition, it was confirmed that the insulation resistance after immersion in hot water was 1000MΩ or higher and the ceramic-coated layers were not damaged.

3. 5 Rotation Performance Test

Since the ceramic-coated surfaces have a lower thermal conductivity than bearing steels, the heat radiation property was checked while rotating the bearings.

(Test Method)

Condition 1: Test bearing part no.: 6316
Test equipment: See **Fig 5**.
Radial load: 3920N
Rotating speed: 1000, 2000, 3000, 4000, 5000 min^{-1}
Grease: Unimax R No.2
Grease Fill: 30% of free space

Condition 2: Rotating speed 4000 min^{-1} (endurance test)

* All other conditions are the same as in Condition 1 above.

(Test Results)

Table 1 shows the temperatures measured at each of the rotating speeds defined in Condition 1.

Table 2 shows the temperatures measured after operating for 2,200 hours as defined in Condition 2.

Table 1 Temperature rise test (˚C)

Rotating speed (min^{-1})	1000	2000	3000	4000	5000
Surface temperature of outer ring (bearing steel) (1)	31.9	33.8	37.2	39.6	43.5
Surface temperature of ceramic layers (2)	31.6	33.5	37.0	39.4	43.3
(1) - (2)	0.3	0.3	0.2	0.2	0.2
Inner ring temperature	31.3	36.5	41.3	44.8	49.7

* The temperatures shown at each rotating speed were those when the difference in surface temperature between outer ring (bearing steel) and ceramic layers was the largest.

Table 2 Bearing endurance test (˚C)

Test time (hr)	2200
Surface temperature of outer ring (bearing steel) (1)	39.2
Surface temperature of ceramic layers (2)	39.2
(1) - (2)	0
Inner ring temperature	43.9

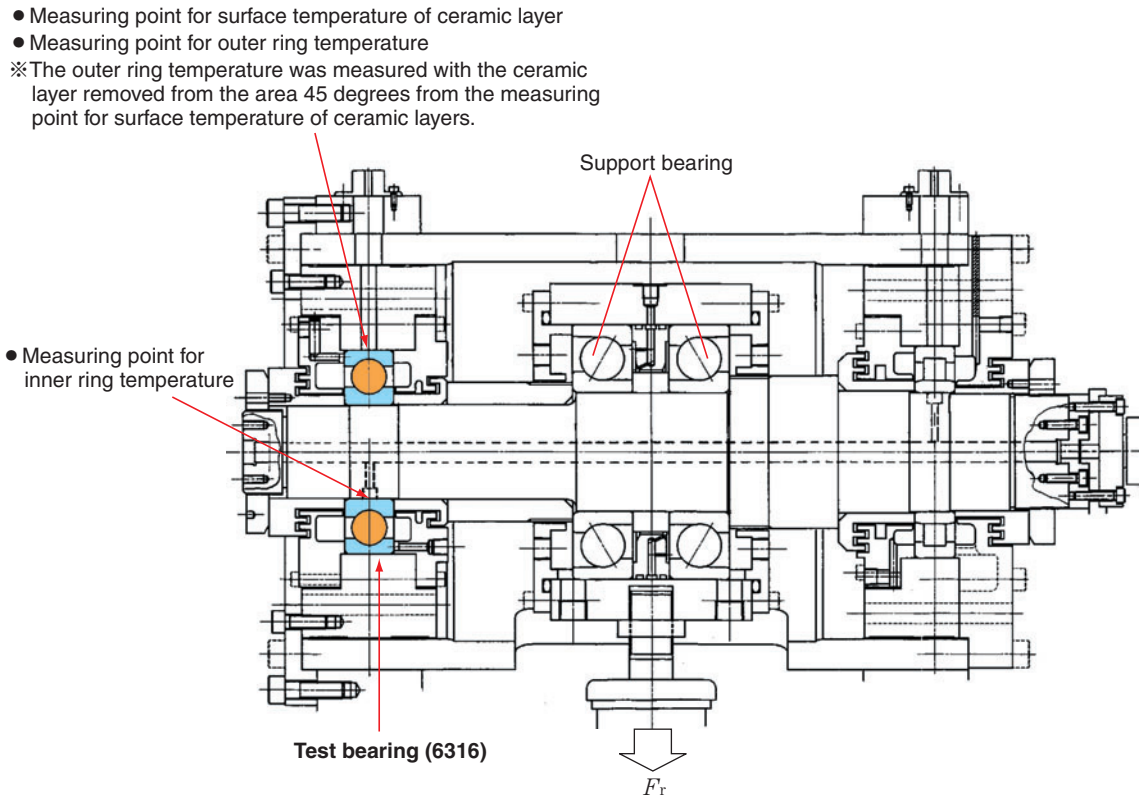

Fig. 5 Test rig

4. Conclusion

This paper introduced single-layer, ceramic-coated, insulated bearings that can be used for wind turbine generators. Tests conducted under various operating conditions showed high insulation levels of ceramic layers. The rotation test also showed only a small temperature difference of 1˚C or less between the outer ring material and ceramic surface, indicating that thermal conduction was sufficient and rotation performance was satisfactory. This newly developed bearing will provide sufficient prevention of electric corrosion in most applications that currently experience such problems.

Photo of the author

Hideji ITO

Industrial Engineering Department
Industrial Sales Headquarters

New High-Capacity HWTJ Type Pressed Cage and Needle Roller Assemblies

Katsufumi ABE*

Needle roller bearings offer compact size, large basic load ratings, and high rigidity compared to ball bearings. Because of these properties, the use of cage and needle roller assemblies assists our customers with size and weight reduction of their products.

In recent years, customers have called for bearings that have ever-increasing capacity. In response, **NTN** created a new high-capacity pressed cage and needle roller assembly as the HWTJ Type. Compared to the standard design, the number of rollers was increased by 20 to 30% and basic load rating by 20 to 35%. This bearing series satisfies the requirements of large basic load rating, long life under severe operating conditions, and high rigidity.

This report introduces the structure and the performance of the new high-capacity HWTJ Type pressed cage and needle roller assembly.

1. Introduction

Compared to ball bearings, needle bearings not only require smaller space but also offer larger load capacity and higher rigidity. Cage and needle roller assemblies are composed of only a cage and a set of rollers. They do not have inner or outer rings and use the shaft and housing as the raceway surfaces. Because of this, they enable the smallest and lightest-weight design among the needle bearings, making it possible to reduce the size of some machines in which they are used.

Cage and needle roller assemblies are used as bearings in the track planetary reduction gears of construction machines, swing arm planetary reduction gears of hydraulic excavators and in the arm joints of industrial robots. Recently, as a result of the drastic reduction in machine size and advancement of functions, a bearing with a larger load capacity (size reduction) is required. Currently, in these applications, M-shaped cages (PK type) are often used. (See **Fig. 1** and **Photo 1**.)

NTN has developed a new high-capacity pressed cage and needle roller assembly (HWTJ type) for this market, featuring a larger number of rollers when compared to the M-shaped cage. (See **Fig. 2** and **Photo 2**.)

This bearing series also offers a drastically improved basic load rating, as well as longer life and higher rigidity under severe operating conditions without sacrificing necessary bearing features (i.e. smooth rotational movement, durability).

*Needle Roller Bearing Engineering Department Automotive Sales Headquarters

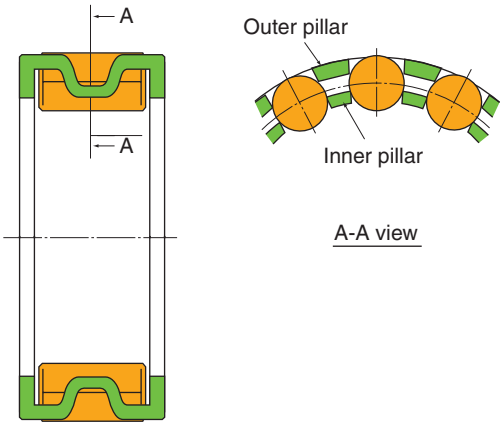

Fig. 1 PK type

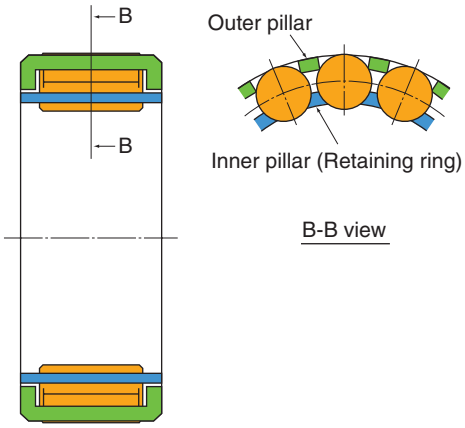

Fig. 2 HWTJ type

Photo 1 PK type

Photo 2 HWTJ type

2. Features of New High-Capacity (HWTJ) Type Pressed Cage and Needle Roller Assemblies

The only way to achieve higher load capacity for cage and needle roller assemblies that consist of only two components (cage and roller) is to increase the number of rollers. With the conventional M-shaped cage (**Fig. 1**), pillars are located at the inner diameter side to prevent the rollers from dropping out. This requires the cage to pass through the bearing PCD, thereby limiting the number of rollers that can be inserted in a given bearing size.

To solve the conflicting issues of "higher load capacity" and "roller drop-out prevention", the high-capacity pressed cage and needle roller assembly consists of three components (a cage, rollers, and a resin retaining ring). The form of the cage was also changed and the method of retaining the rollers was modified to include a resin retaining ring, thus eliminating cage pillars at the bearing PCD. This made it possible to increase the number of rollers by 20 to 30% when compared to the conventional product (M-shaped cage).

This has not only increased the load capacity (basic static load rating) by 20 to 35%, but also improved bearing rigidity and life drastically. **Table 1** shows a comparison of the bearing specifications between the new roller assembly and the conventional type (PK type), and **Table 2** shows the comparison of their general performance.

Table 1 Comparison of bearing specifications (Size :ID46×OD66×Width 22.8 mm)

	Developed product (HWTJ type)	Conventional product (PK type)
Number of rollers	16	12
Roller length (mm)	18	18
Basic dynamic load rating (kN)	84.0	67.5
Basic static load rating (kN)	98.5	73.5

Table 2 Comparison of general performance

Item	Compared to conventional type
① Number of rollers	Increased by 20 to 30%
② Static load rating (impact load)	Increased by 20 to 35%
③ Dynamic load rating	Increased by 15 to 25%
④ Calculated bearing life	1.5 to 2 times
⑤ Rigidity	Increased by 15 to 25%

3. Main Features of New Technological Development

Items to note about the design of this bearing are summarized in the following two points.

① **Roller Retention**

Resin retaining rings are provided on the inner side of the cage to prevent rollers from dropping out inwards.

② **High load capacity (increased number of rollers)**

The positions of the roller retaining pillars were moved closer to the inner and outer diameter of the bearing to eliminate the pillars near the PCD that were limiting the number of rollers that could be used.

4. Performance Evaluation

In order to evaluate the performance of the bearings, a life test and a strength test for the cage and retaining rings were conducted. Some of these evaluation results are introduced below.

4. 1 Bearing Life Test

A 2 to 4-ton radial load test machine shown in **Fig. 3** was used to conduct the bearing life test.

4. 1. 1 Bearing Specifications

Bearing size :ID46×OD66×Width 22.8 mm
Roller size :OD10×length 18 mm
Number of rollers : 16

4. 1. 2 Test Conditions

Radial load: 37.7kN : (45% of dynamic load rating C_r)
Rotating speed : 1,560 rpm
Lubrication : Grease
Calculated L_{10} life : 152 hours
(Reference : The same size PK type bearing had a life of 59.8 hours)

4. 1. 3 Test Results

Fig. 4 shows the results of the bearing life test. The major damage observed was flaking of the shaft. The bearing life was 178 hours, which exceeded the calculated L_{10} life of 152 hours.

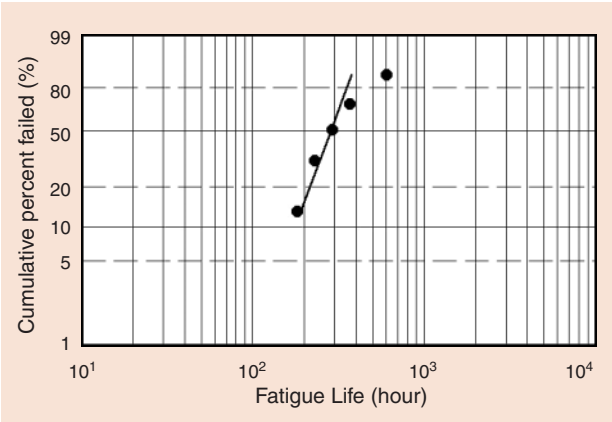

Fig. 4 Rolling contact fatigue life of bearing

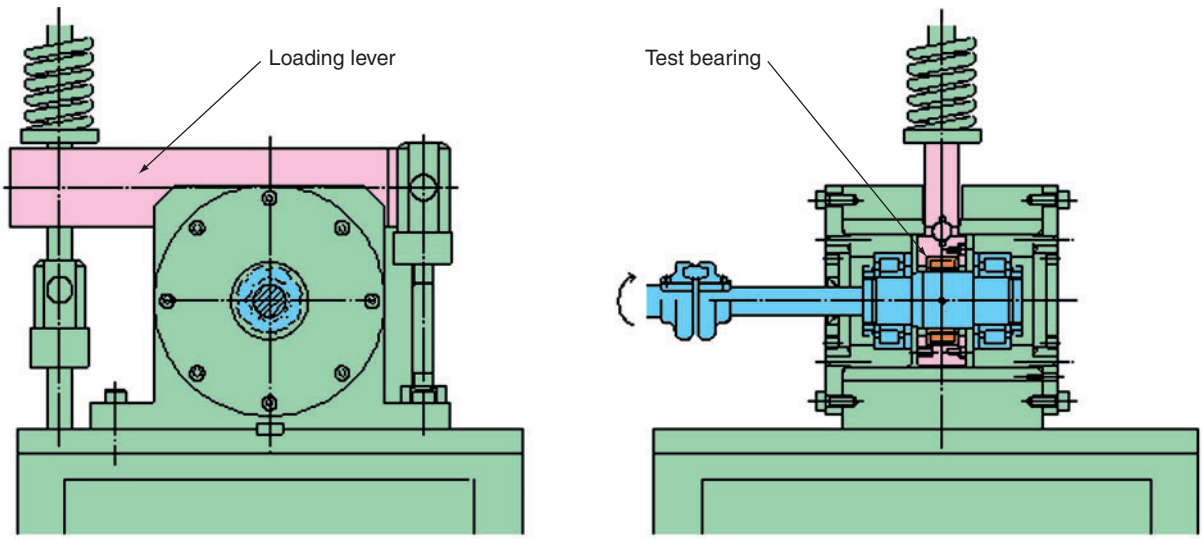

Fig. 3 2 to 4-ton radial load test machine

4. 2 Confirming Roller Interaction with Cage and Retaining Rings

One of the applications for which this bearing can be used is a planetary reduction gear used in construction machines. In these machines, the bearing rotates with oscillating motion. Unlike the M-shaped cage that has pillars near PCD to guide the rollers, this bearing has cage pillars near the bearing's outer diameter and retaining ring pillars near the bearing's inner diameter. To ensure that the rollers do not run onto the pillars during changes in rotation direction, a test was performed under the oscillation conditions listed in 4.2.1. For this test, a bearing having the same specifications as the life test was used in a cross-joint endurance test machine. The structure of the bearing mating components in this machine is the same as the 2 to 4-ton radial load test machine shown in **Fig. 3**.

4. 2. 1 Test Conditions

Radial load: 37.7kN : (45% of dynamic load rating C_r)
Oscillation angle: ±720˚
Oscillation cycle speed: 48 cpm
Lubrication: Grease
Test duration: 1 million cycles

4. 2. 2 Test results

Table 3 shows the test results. This data shows that the bearing operated more than one million cycles, which is the **NTN** test standard, without any issues with the rollers running onto the cage pillars or retaining ring pillars.

Table 3 Test results

	Number of cycles	Appearance after test	
		Cage/retaining ring	Roller/shaft/outer ring
No.1	1 million suspend	No problem found with these components	No Problem.
No.2	1.72 million cycles	No problem found with these components	Flaking on outer ring No problem found with rollers and shaft

4. 3 Bearing Rigidity

This new bearing can have 20 to 30% more rollers than the conventional bearing, without any modification of the major envelope dimensions. This has enabled the use of the HWTJ type bearing in applications where the conventional bearing was not adequate. In addition, since the HWTJ bearing is more rigid than the conventional bearing, under the same load products using the HWTJ bearing can have higher precision.

To compare bearing rigidity with the conventional bearing, a **NTN** technical computing program was used.

4. 3. 1 Calculation Conditions

Bearing size :ID46×OD66×Width 22.8 mm
Roller size: OD10×length 18 mm
Number of rollers : Developed bearing: 16,
Conventional bearing: 12
Load: 1, 5, 10, 50, 100 kN

4. 3. 2 Calculation Results

Fig. 5 shows the calculated rigidity comparison. The rigidity of the developed bearing (HWTJ type) is approx. 20% higher than that of the conventional bearing's rigidity.

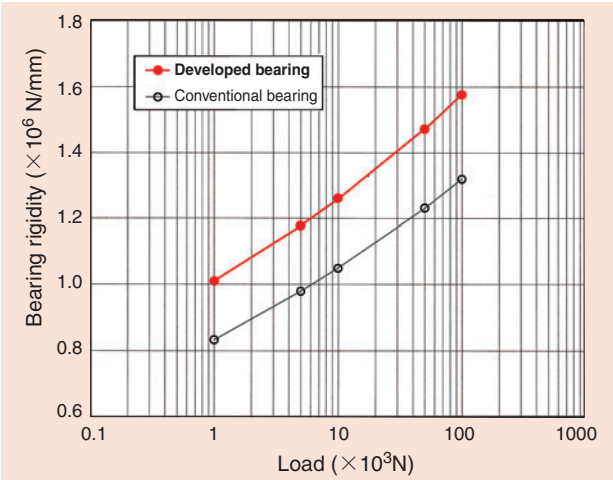

Fig. 5 Comparison of rigidity

5. Conclusion

By designing and building a bearing using three components (cage, rollers and resin retaining ring) and adopting a cage drawn from a thick plate, we have succeeded in the development of "New High-Capacity Pressed Cage and Needle Roller Assemblies" featuring a high load carrying capacity and compact size.

We will continue to work on the development of products such as this that offer larger load capacities and a more compact design.

Photo of the author

Katsufumi ABE

Needle Roller Bearing Engineering Department
Automotive Sales Headquarters

HK-F type drawn cup needle roller bearings

Hideki AKAMATSU*

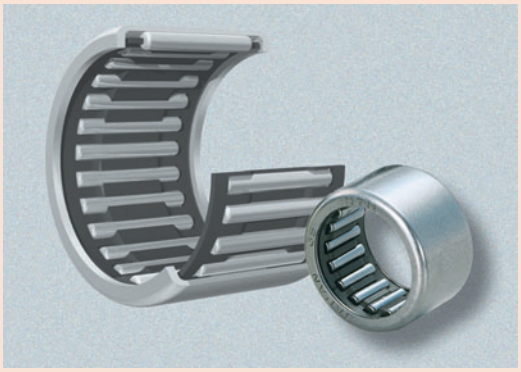

The drawn cup needle roller bearing has an outer ring which is precisely drawn from a thin steel plate. Of all bearings with outer rings, drawn cup needle roller bearings have the smallest section height, which enables space and cost saving.

NTN has applied this technology to many applications.

NTN's next generation "HK-F Series" are standard drawn cup needle roller bearings to which **NTN** has applied new technology.

1. Introduction

Since needle roller bearings have a small section height and provide larger load capacity and rigidity than the other type bearings in spite of small space, they are used in many applications including the automotive field. In particular, drawn cup needle roller bearings (hereafter called drawn cup NRBs) have an outer ring that is drawn from a steel plate. In addition to having the lowest section height of any needle roller bearings with outer rings, they have excellent cost performance. Furthermore, because they use a press-fitted housing, they do not need a snap ring or other device to fix them in the axial direction. This expands the range of applications to include those of conventional machined-ring needle roller bearings.

Special specifications have been employed to the standard type bearings in response to the increasing demand for longer life, reduced fuel cost, and greater power particularly in the automotive field.

Some of these special specifications have been employed as standard specifications in order to respond to worldwide needs. This has enabled **NTN** to offer its standard drawn cup bearings "HK-F Series", featuring longer life, improved load resistance, and easier assembly.

Now, I will introduce its features, design concept, and evaluate test results.

*Needle Roller Bearing Engineering Department　Automotive Sales Headquarters

2. Features

The features of the HK-F type drawn cup NRB are given below (**Fig. 1**)).

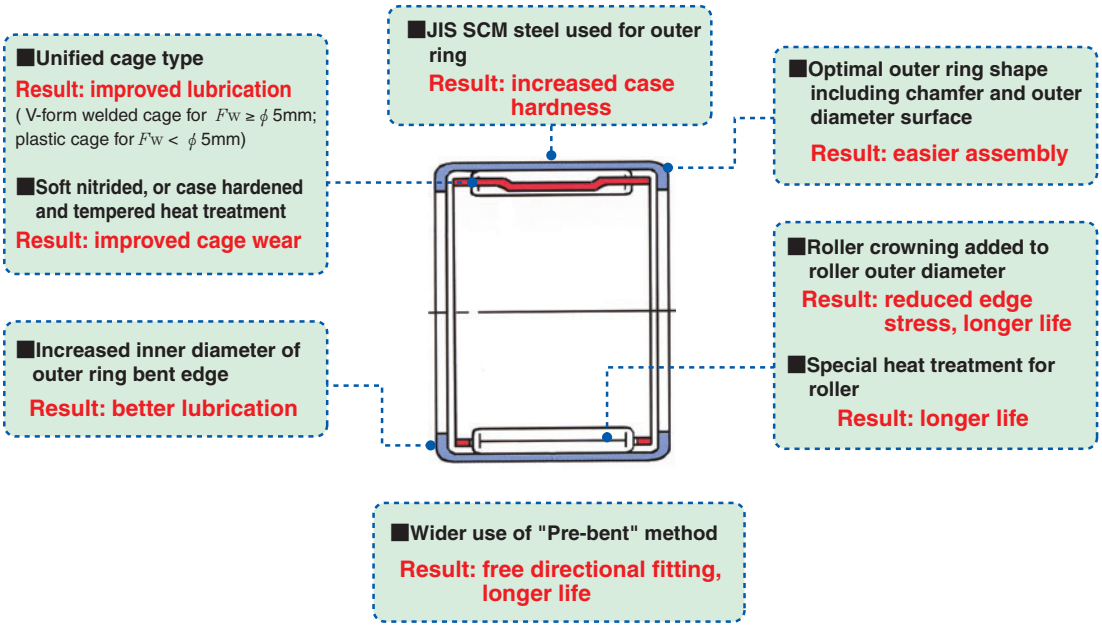

Fig. 1 Specification of HK-F type drawn cup NRB

2. 1 Long Life

HK-F type drawn cup NRB has a longer life as a result of the following improvements.

① **Adoption of crowning as a standard feature**
Stress concentration (edge load) at the roller ends caused by assembly misalignment and heavy load is reduced, enabling use of the standard type under a wider range of conditions. **Fig. 2** shows the calculation results of contact surface pressure between the current standard type and HK-F type.

② **Adoption of a special heat treatment on rollers as the standard feature**
Special carbonitriding improves resistance to softening that occurs as a result of tempering and increases the amount of residual austenite, which eases stress concentration.
This has enabled HK-F type to have a three times longer life than the current standard type when used under clean lubrication conditions (**Figs. 3, 4**)).

③ **Adoption of "Pre-bent" method (Only for some HK-F type drawn cup NRBs)**
Bearings manufactured by "Pre-bent" method (patent obtained, explained later) provide even longer life as a result of optimization of heat treatment conditions.

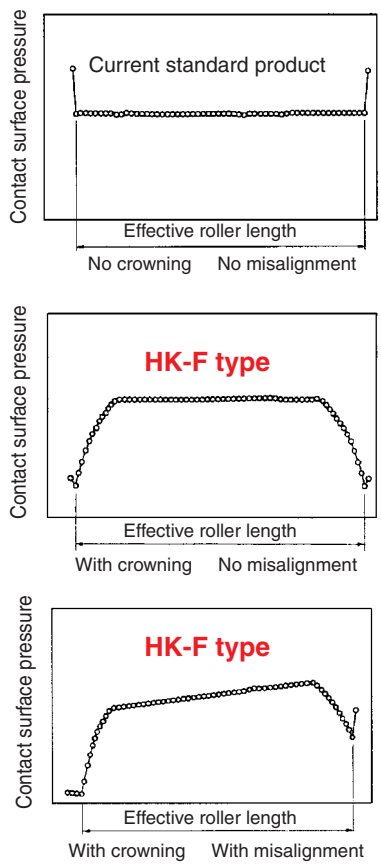

Fig. 2 Calculation result of contact surface pressure

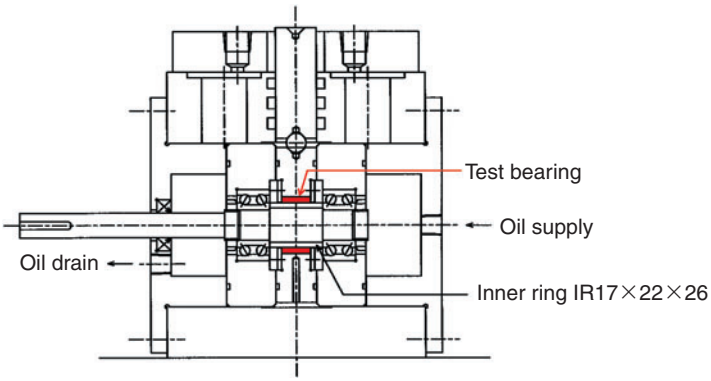

Fig. 3 Bearing life test rig

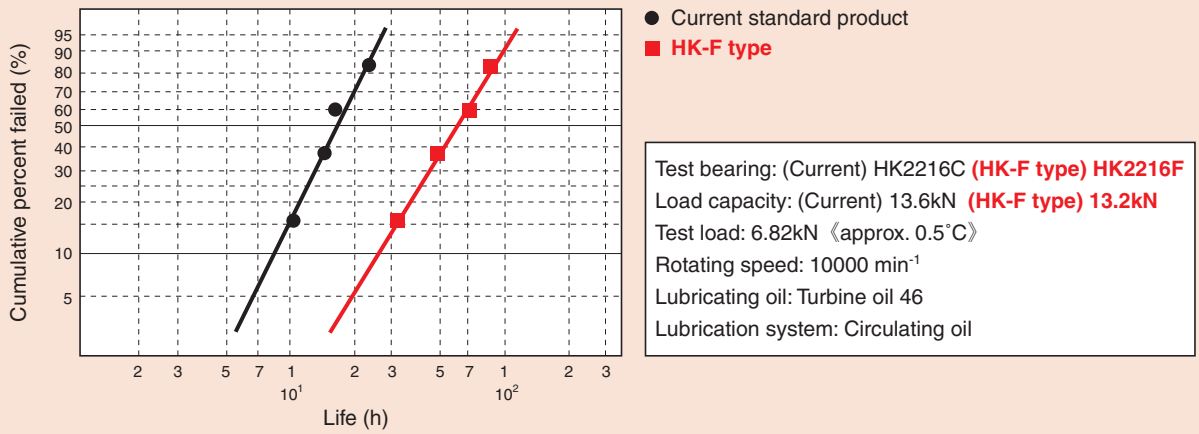

Fig. 4 Bearing life test results

④ **Adoption of V-form welded cage (Only for some HK-F type drawn cup NRBs)**

Adoption of the V-form welded cage design allows use of roller guide closer to the roller center than the conventional U-form cage, as a result movement of roller during rotation is smooth. Furthermore, the cage rib can be shaped so as to prevent flow-in/-out of lubricating oil, resulting in better lubrication and better effect on the sliding surface.

Fig. 5 shows a cross-sectional view of the current and HK-F type drawn cup NRB cages.

For heat treatment of cage, soft nitriding (carburization for "Pre-bent" type) has been adopted as the standard feature to improve wear resistance and strength.

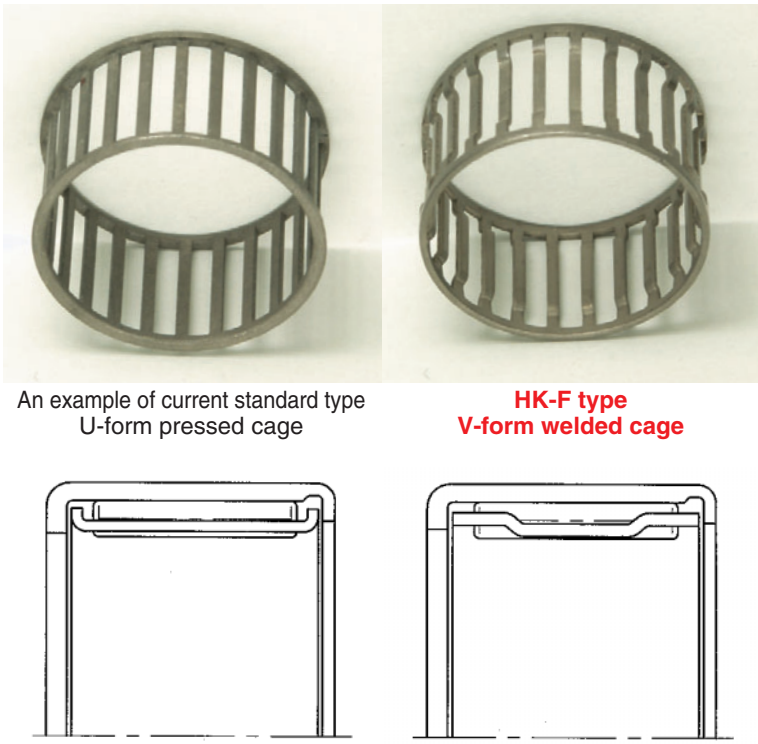

Fig. 5 Cross section of current and HK-F type drawn cup NRB cages

2. 2 Improvement of Allowable Static Load

Chrome molybdenum steel (JIS SCM steel) has been adopted as the material for the drawn cup.

This has increased inner hardness of the drawn cup, widening the usage range for heavy-load applications.

Fig. 6 shows the method of static load test conducted to compare HK-F type with the current standard type, and the results are shown in **Fig. 7**.

Since HK-F type drawn cup NRBs do not develop permanent deformation even at loads of $S_0 \geqq 2$ (up to 50% of static rated load) while the current standard bearings can be used at $S_0 \geqq 3$.

Note) S_0 (safety factor) = Static rated load / Radial load

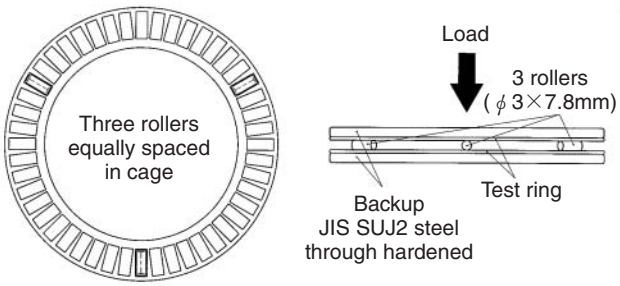

Fig. 6 Static load test condition

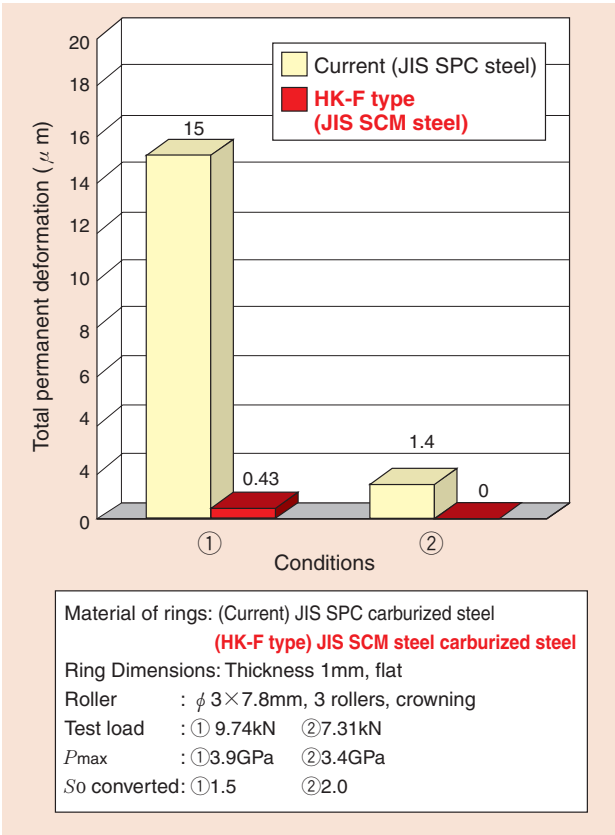

Fig. 7 Comparison of static load test results

2. 3 Reduction of Initial Mounting Force and Stabilization of Mounting Force

① Improved assembly

Drawn cup NRBs are press-fitted into the housing.

With HK-F type drawn cup NRB, outer diameter chamfer shape is optimized to reduce the initial mounting force and stabilize the mounting force.

Fig. 8 shows the results of the fit test.

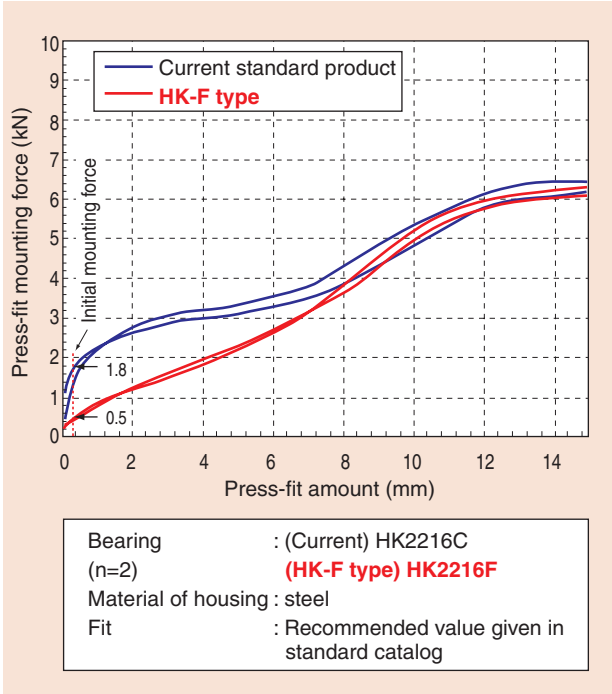

Fig. 8 Fit test result

② Free Direction Fitting ("Pre-bent" method)

In the manufacturing process of conventional drawn cup bearings, the rib of the heat-treated outer ring (at the bent edge side) is annealed first, and then the rollers and cage are assembled into the outer ring. Finally, the rib is bent to prevent separation. (**Fig. 9**) As a result, the hardness of the rib (bent edge side) is low, therefore, press-fitting the bearing into the housing by pushing on the bent edge rib is not desirable in terms of strength.

With drawn cup NRBs of "Pre-bent" method, the rollers and cage are assembled into the outer ring first, and then the bent edge rib is bent prior to heat treatment. This gives the rib (at the bent edge side) the same hardness as that of the other areas. As a result, the hardness of the rib (at the bent edge side) increases compared with conventional cup bearings, enabling free directional fitting into the housing.

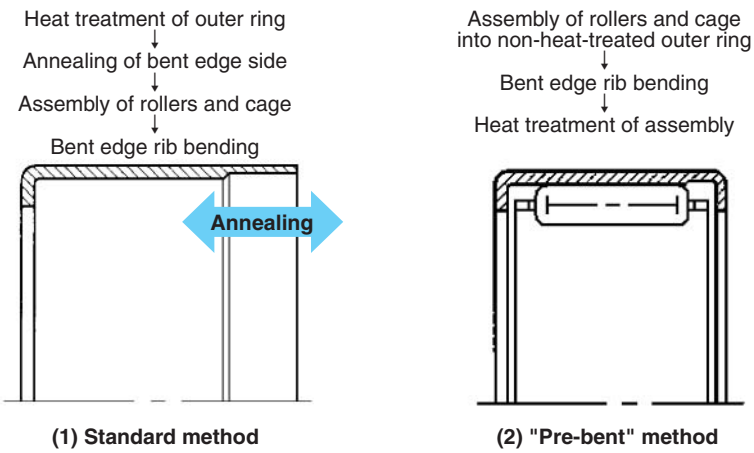

Fig. 9 Process of bent edge rib bending

Table 1 **NTN** HK-F type drawn cup NRBs products

Boundary dimensions (mm)			Bearing numbers		
Inscribed circle diameter F_w	Outer diameter D	Width B	Current catalog part number	**HK-F type part number**	
3	6.5	6	HK0306T2	**HK0306FT2**	Polyamide Resin cage
4	8	8	HK0408T2	**HK0408FT2**	Polyamide Resin cage
5	9	9	HK0509T2	**HK0509FM**	"Pre-bent" method
6	10	9	HK0609T2	**HK0609FM**	"Pre-bent" method
7	11	9	HK0709	**HK0709FM**	"Pre-bent" method
8	12	10	HK0810C	**HK0810FM**	"Pre-bent" method
9	13	10	HK0910	**HK0910FM**	"Pre-bent" method
	13	12	HK0912	**HK0912F**	
10	14	10	HK1010	**HK1010FM**	"Pre-bent" method
	14	12	HK1012	**HK1012F**	
	14	15	HK1015	**HK1015F**	
12	16	10	HK1210	**HK1210FM**	"Pre-bent" method
	18	12	HK1212	**HK1212FM**	"Pre-bent" method
13	19	12	HK1312	**HK1312FM**	"Pre-bent" method
14	20	12	HK1412	**HK1412FM**	"Pre-bent" method
	20	16	HK1416	**HK1416F**	
15	21	12	HK1512	**HK1512FM**	"Pre-bent" method
	21	16	HK1516	**HK1516F**	
	21	22	HK1522ZWD	**HK1522ZWFD**	
16	22	12	HK1612	**HK1612FM**	"Pre-bent" method
	22	16	HK1616	**HK1616F**	
	22	22	HK1622ZWD	**HK1622ZWFD**	
17	23	12	HK1712	**HK1712FM**	"Pre-bent" method
18	24	12	HK1812	**HK1812FM**	"Pre-bent" method
	24	16	HK1816	**HK1816F**	
20	26	12	HK2012C	**HK2012FM**	"Pre-bent" method
	26	16	HK2016	**HK2016F**	
	26	20	HK2020C	**HK2020F**	
	26	30	HK2030ZWD	**HK2030ZWFD**	
22	28	12	HK2212	**HK2212FM**	"Pre-bent" method
	28	16	HK2216C	**HK2216F**	
	28	20	HK2220C	**HK2220F**	

3. Conclusion

The HK-F type drawn cup NRBs have a longer life and improved functionality compared with the current standard type, which enables its use in applications where special specifications are required.

Currently, a total of 32 HK series models, ranging from ϕ3mm to ϕ22mm in inscribed circle diameter are available (see **table 1**). The application range of this specification will be expanded in the future.

Photo of the author

Hideki AKAMATSU

Needle Roller Bearing Engineering Department
Automotive Sales Headquarters

Hydrodynamic BEARPHITE Unit for HDD

Kiyotaka KUSUNOKI*

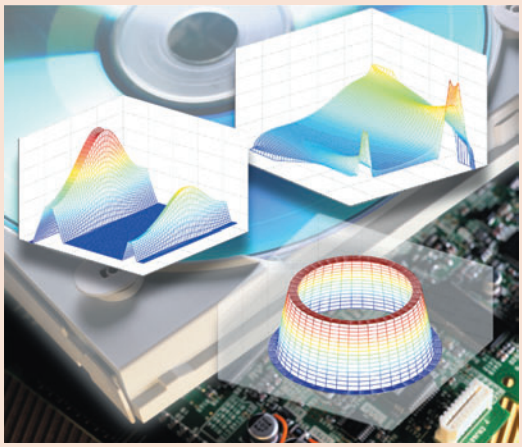

Hard disk drives are used mainly as storage systems in personal computers, and it is expected that consumer usage will continue to grow in the near future. In order to increase the storage capacity on hard disk drives, the Non-repetitive Run Out (NRRO) needs to be decreased. In addition, requirements for shock endurance and low noise have led to the rapidly increasing use of hydrodynamic bearings for hard disk drive spindles.
Hydrodynamic bearings are suitable because of their compact size and rotational accuracy.

NTN has long been working on the hydrodynamic bearings to solve these HDD problems, and mass production of the BEARPHITE unit began last year. The details of this bearing are explained below.

1. Introduction

The surface recording density of hard disk drives (HDD) is doubling every year, and an HDD with a surface recording density of 80GB per disk has been released to the market. Among the many storage disk alternatives, HDD has established itself as the leader because of its low cost per storage capacity unit and high data transfer speed. Conventionally, HDD were used primarily in personal computers and servers. However, use in consumer products (recorders, car GPS navigators, video game consoles, etc.) has already begun and this market is expected to continue to grow.

For HDD spindles, rolling bearings have typically been used. However, in order to improve the Non-repetitive Runout (NRRO) and meet requirements for high shock endurance and low noise, the use of hydrodynamic bearings for HDD spindles has been rapidly increasing over the last two years.

NTN has worked on the development of hydrodynamic bearings for many years and solved several technical problems. **NTN** has begun mass production of hydrodynamic BEARPHITE units equipped with porous oil retaining bearings. An overview of the hydrodynamic BEARPHITE unit is given below.

*Fluid Dynamic Bearing Unit Division

2. Classification and Features of Bearings

2. 1 HDD and Bearing Characteristics

Rolling bearings that are designed solely for improvement of NRRO have been used in HDD spindles because of their price, easy handling and reliability.

Hydrodynamic bearings retain oil between the shaft and bearing in special grooves. These grooves produce a high oil film pressure, which enables the bearing to be supported without being in contact with the shaft. Because of the oil film, imperfections in the shaft surface condition (roundness, surface roughness) and bearing are diminished, providing high rotational accuracy (NRRO). Therefore, hydrodynamic bearings have been determined to be more suitable for HDD than roller bearings due to the compactness and high rotational accuracy required. In order to use hydrodynamic bearings in HDD, electric-appliance and bearing manufacturers have spent much time on the development of these bearings. Since hydrodynamic bearings require better component precision and precise machining of the hydrodynamic grooves, they are more expensive than ball bearings and suffer from reliability problems due to an abrupt seizure known as sudden death. Because of these reasons, they are not very common.

Over the past decade, the track pitch of HDD units has been reduced to increase the storage capacity and now can be measured in tens of nanometers. The head can respond to low-frequency repetitive runout (RRO) but cannot follow irregular-frequency non-repetitive runout (NRRO). Therefore, there is a strong demand for HDD spindles with improved NRRO. Manufacturers are switching from ball bearings to hydrodynamic bearings since quietness and shock resistance are required for the application. Rolling bearings are at a disadvantage because their rolling elements contact the raceway, thereby placing a limit on the size of the track pitch even if the raceway is machined very precisely.

Table 1 shows a summary of requirements for HDD and the characteristics of various types of bearings. From a functionality comparison, hydrodynamic bearings (including hydrodynamic BEARPHITE unit) are better for NRRO, high-speed rotation, noise level and shock resistance, but worse for rigidity and reliability. Both bearings showed about the same torque. Porous bearing sleeves are another advantage of hydrodynamic BEARPHITE units, because lubricating oil is retained inside the sleeves and is supplied to the bearing continuously. This prevents bearing seizure, thereby allowing their reliability to exceed that of standard solid metal hydrodynamic bearings.

2. 2 Lubricating Oil

Lubricating oil plays an important role in hydrodynamic bearings since the function equivalent to rolling bearings is required. The lubricating oil requires the following characteristics for long life and high performance. Recently, ester-based lubricating oil has been used in hydrodynamic bearings.

① **Excellent lubricating performance**: Improved contact condition between shaft and bearing at start and stop.

② **Sealing performance**: Prevent leakage from the bearing due to higher surface tension and lower specific gravity.

③ **High temperature-viscosity characteristic**: Reduce the changes in torque and rigidity caused by temperature change.

④ **Low evaporation**: Prevent the reduction of lubricating oil amount even if used for long periods of time.

⑤ **Low torque**: Low viscosity with acceptable bearing stiffness

Table 1 Requirements and characteristics

◎ : Very good ○ : Good △ : Fair

Requirements for HDD	Requirements for bearing	Roller bearing	Hydrodynamic bearing *	Hydrodynamic BEARPHITE unit *	Typical applications
Large storage capacity	NRRO	△	○	○	Personal computer, server
	High-speed rotation	△	○	○	Server
Low noise level	Low noise level	○	◎	◎	Consumer
Low current consumption	Low torque	○	○	○	Mobile
Impact resistance	Impact resistance	○	◎		Mobile
Reliability	Seizure resistance	◎	△	○	General
Rigidity	Rigidity	◎	△	△	Server

* The hydrodynamic bearing is made of solid metal and the hydrodynamic BEARPHITE unit is made of porous material.

Table 2 Bearing specifications

Item	Current spec.→Required spec.	Remarks
Radial NRRO	0.05μm → 0.03μm	Storage capacity 40→80→120GB
High-speed rotation	10,000min^{-1} → 15,000min^{-1}	20,000min^{-1} (for server)
Low noise level	30dB → 20dB	
Low torque	5mN·m → 3.5mN·m (-10°C)	Notebook computers, mobile devices with 2.5-in. or smaller hard disk
Impact resistance	300G → 1,000G	Notebook computers, mobile devices with 2.5-in. or smaller hard disk
Seizure resistance	Designed life: 7 years, Start/stop: 100,000 times	

2. 3 Required Specifications

Table 2 shows an example of the required specifications of HDD spindle bearings.

3. Structure

3. 1 Structure of Bearing Unit

Fig. 1 shows the structure of a hydrodynamic BEARPHITE unit designed for HDD spindles. The unit consists of four components: a shaft, a hydrodynamic BEARPHITE bearing sleeve (hereafter called bearing sleeve), a housing and a thrust bushing.

The shaft has two cylindrical sections that are designed to support radial loads from the bearing cylindrical components. Hydrodynamic herringbone-shaped grooves are located at these same two points on the bearing sleeve bore. The radial clearance between the shaft and the cylindrical bearing components is on the order of microns. To prevent negative pressure from being generated inside the bearing, the width of the herringbone grooves is closely controlled.

The bearing's components are made so that the flange on the end of the shaft is sandwiched between the cylindrical sleeve and the thrust bushing. The thrust bushing has spiral-shaped thrust hydrodynamic grooves. The flange, cylindrical sleeve and thrust bushing are separated by clearances of just microns.

A seal is located at the point where the unit's shaft extends from the housing to protect contamination from entering the unit. The shaft outer diameter surface and housing inner diameter surface are tapered on the inboard side of the seal. When the bearing is not rotating, the lubricating oil is retained by surface tension in order to prevent leakage. When the bearing is rotating, the lubricating oil is drawn towards the bearing by centrifugal force to prevent splashing.

As the shaft rotates, the hydrodynamic slots pump the lubricating oil and a high-pressure oil film develops (see **Fig. 2**), causing the shaft to float. Since the shaft is rotating, when radial load is applied to the shaft, the minimum clearance between the shaft and the cylindrical bearing is off-set from the centerline of the force.

3. 2 Structure of HDD

Fig. 3 shows the structure of a HDD. A rotor magnet is attached to a hub and the hub assembly is press-fit onto the shaft of a hydrodynamic BEARPHITE unit. The HD spindle is formed when a housing outer diameter surface is connected to a bracket where a stator coil and control PCB are attached. The actuator (pivot bearing with voice coil motor) supporting the head is attached to the base, and it writes/reads signals while detecting recording positions on the hard disk.

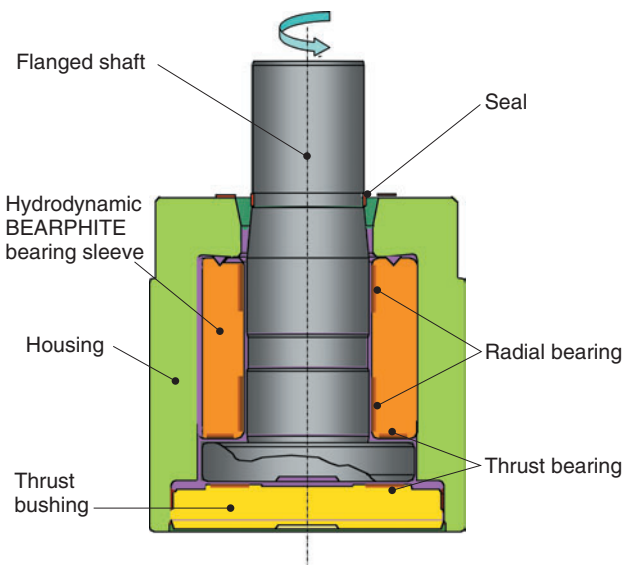

Fig. 1 Structure of hydrodynamic BEARPHITE unit (longitudinal cross section)

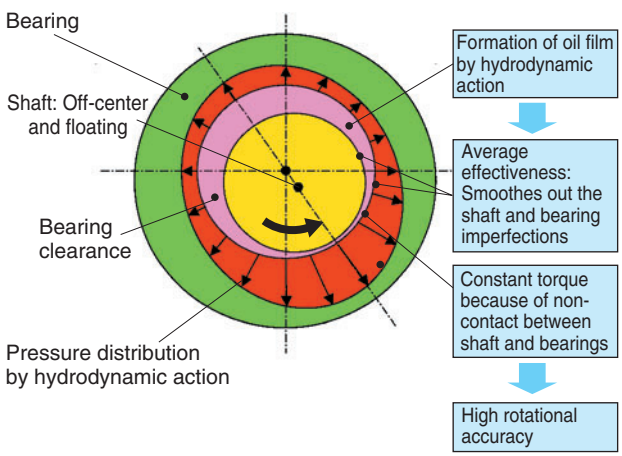

Fig. 2 Structure of hydrodynamic BEARPHITE unit (radial cross section)

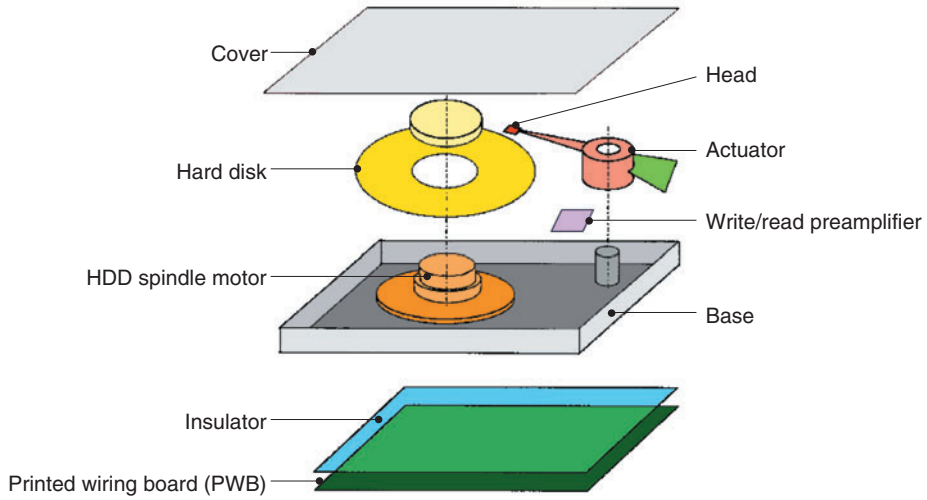

Fig. 3 Structure of HDD

4. Theory and Measured Values]

4. 1 Theoretical Calculation

With the porosity of the BEARPHITE sleeve and the lubricating oil between the radial and thrust bearings taken into account, a program was created utilizing the narrow groove theory to analyze the performance of the hydrodynamic BEARPHITE unit. This program calculates the bearing pressure distribution and determines bearing stiffness, load capacity, torque and attenuation factors. Use of this program helps optimize HDD spindle rigidity, load capacity and critical speed. Examples of bearing pressure distribution calculations are shown in **Fig. 4**.

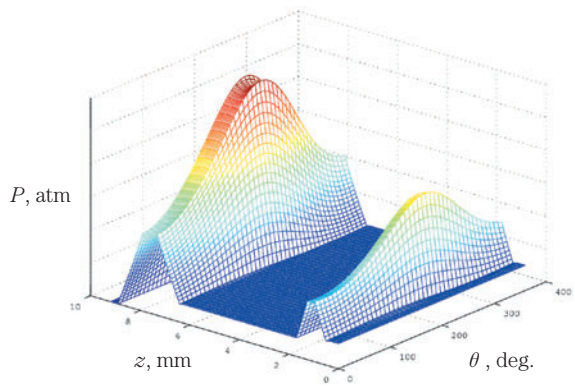

Fig. 4-2 Bearing pressure distribution (radial clearance)

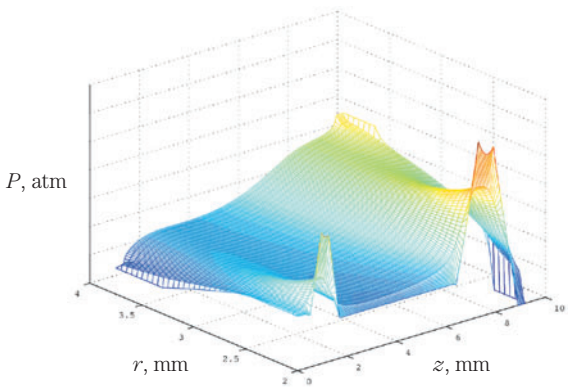

Fig. 4-1 Bearing pressure distribution (sleeve)

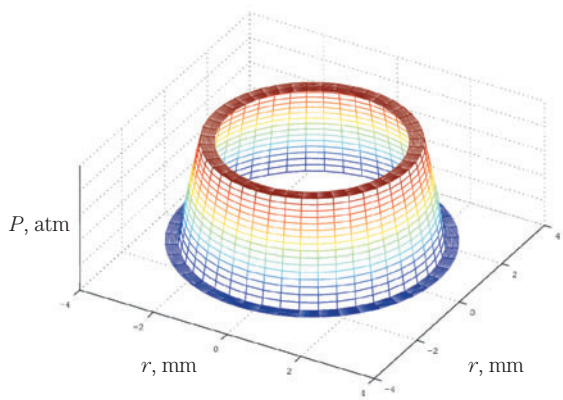

Fig. 4-3 Bearing pressure distribution (axial clearance)

4. 2 Measurement Results

(1) Radial stiffness

Fig. 5 shows the test equipment used to measure the radial stiffness of hydrodynamic BEARPHITE units. A disk with weight (inertia) equivalent to the actual machine was placed on the shaft and driven by an air turbine. A magnet, calibrated for distance and draw-in load, was placed close to the magnetic ring on the disk outer face. A radial load was exerted without any contact between the two objects. The change in inertia was measured by two non-contact electrostatic capacitance displacement gauges positioned at a 90-degree phase (load/change amount). The bearing stiffness value of the specimen was measured to be 9.47×10^6 N/m.

(2) Torque

A disk with weight (inertia) equivalent to the actual machine was placed on the shaft of the hydrodynamic BEARPHITE unit. The housing was secured to the top of the static air bearing (see Figure 6). To drive the disk, a turbine blew air onto the disk outer diameter. A strain gauge measured the tangential force of the string attached to the pulley. The tangential force was converted into a torque by multiplying it by the pulley radius. **Fig. 7** shows the torque result of 1.2 to 1.4 mN·m.

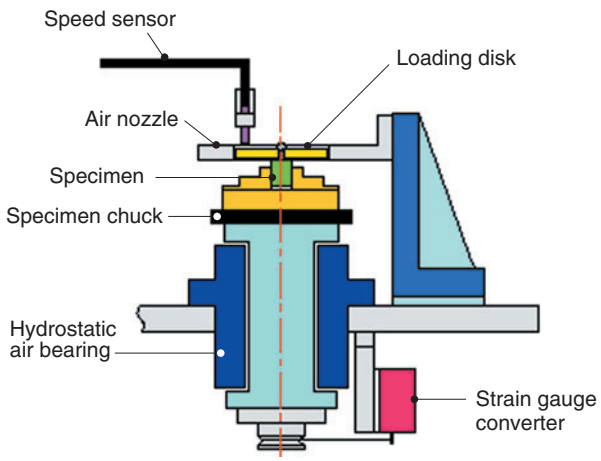

Fig. 6 Torque measurement test equipment

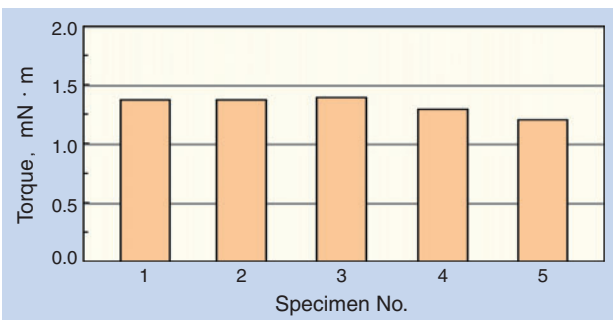

Fig. 7 Torque measurement test results

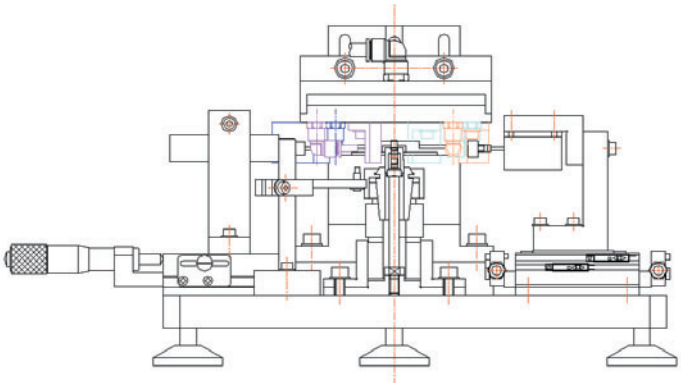

Fig. 5 Radial stiffness measurement equipment

(3) NRRO (Non-repetitive Run Out)

Fig. 8 shows the test equipment used to measure the NRRO of hydrodynamic BEARPHITE units. The hydrodynamic BEARPHITE unit was placed on a motor and an aluminum disk with weight (inertia) equivalent to the hard disk was attached to the unit. Next the motor was turned on to drive the unit. Run-out in both radial and axial directions was measured using a non-contact electrostatic capacitance displacement gauge and was analyzed by FFT to obtain NRRO. The NRRO measurement results are shown in **Fig. 9**. It shows that radial NRRO was 0.010 to 0.015 μm at room temperature and 0.013 to 0.024 μm at 60˚C. Both of these measurements satisfy

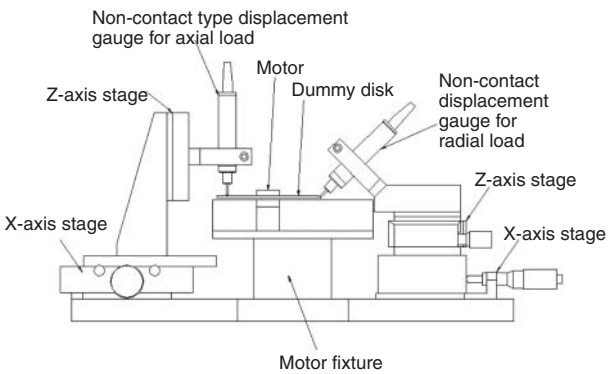

Fig. 8 NRRO measurement equipment

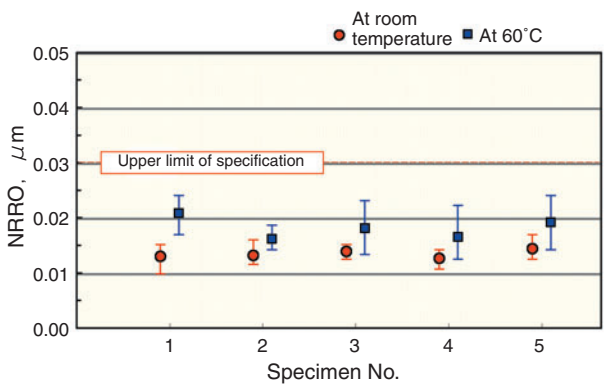

Fig. 9 NRRO measurement results

NTN's requirements.

Theoretically, the hydrodynamic bearing run-out has a repeatable component and a non-repeatable (NRRO) with each rotation. The causes of the bearing NRRO could be air flow near the measuring points, unsteady lubricating oil flow, motor vibration, centrifugal force caused by fluctuation of rotating speed, change of hydrodynamic effect or component precision not dampened by oil film.

(4) Low Noise Level

The noise measuring method for HDD is stipulated by both JIS and ISO standards. With rolling bearings, noise is generated from rolling contact between the rolling elements and raceways as well as sliding contact between the cage and the other components. To the contrary, no noise is generated by hydrodynamic bearings, since their shaft and bearings do not contact. Most of noise is produced by the electro-magnetic sound from the motor and the hard disk wind noise. **Fig. 10** shows a comparison of test results from a roller bearing and a hydrodynamic bearing. The noise level of the hydrodynamic BEARPHITE unit was 22 dBA, which was 8 dBA lower than the roller bearing, showing that the hydrodynamic BEARPHITE unit operates more quietly.

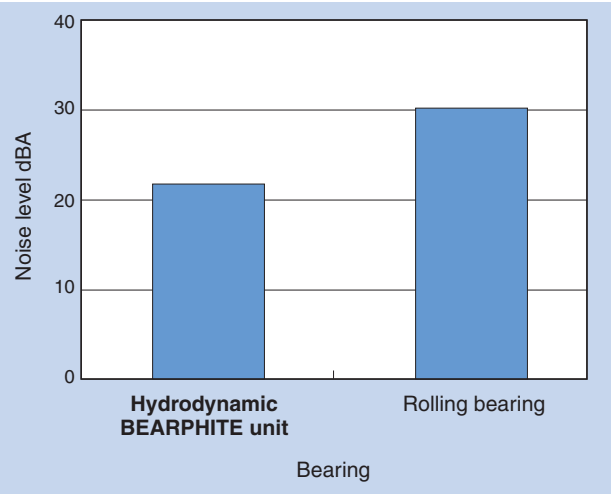

Fig. 10 Noise test results

(5) Durability

A HDD can quickly become obsolete in terms of its functionality due to frequent model changes. However, it is essential to provide the designed durability during the warranty period (7 to 10 years). In addition, it is very important that they do not stop during use, since critical data is saved in personal computers and servers via HDD's.

Figs 11-1 and **11-2** show endurance test results taken while a HDD bearing was started and stopped frequently by a motor running at a high temperature (60˚C). It shows that there was no change in the NRRO or the motor's current during the test and no decrease in functionality of the HDD.

For home use, this sound level is lower than the background noise.

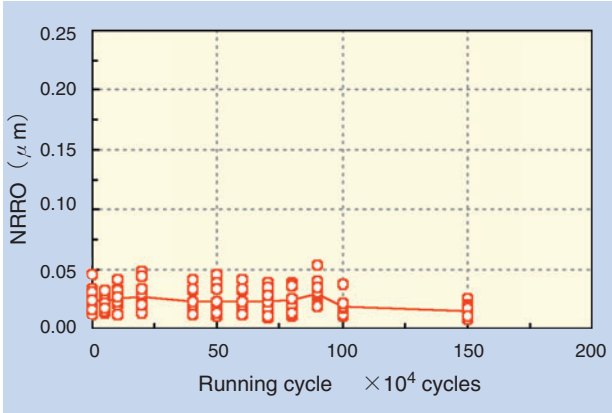

Fig. 11-1 Endurance test (radial NRRO)

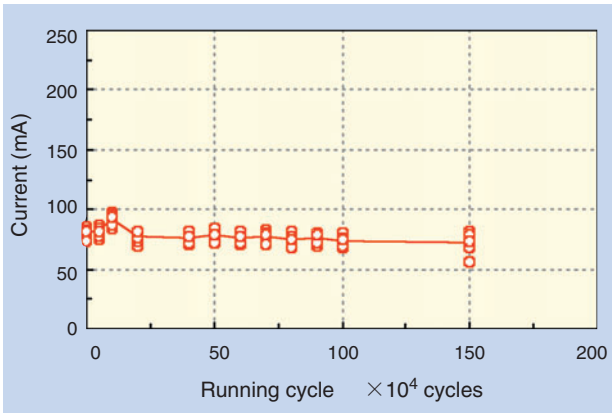

Fig. 11-2 Endurance test (motor current)

(6) Impact resistance

When using HDD's in mobile devices such as notebook computers, it is important that there is no drop in the HDD's functionality. An impact test was conducted on the bearing unit and its functionality was evaluated. **Tables 3-1** and **3-2** show the test conditions and **Figs. 12-1** and **12-2** show the test results. The figures show there was no change in either torque or NRRO. Although it is known that the surface pressure generated between the shaft and bearing is lower than bearings using steel balls, this test confirms that the unit is resistant to impact.

Table 3-1 Impact test conditions

Ambient temperature	Room temperature (approx. 23 to 24˚C)
Unit direction	Upright, horizontal, upside down
Disk weight load	5 g
Impact load	1200 G
	(0.2 msec)
Impact cycle	3 cycles continuously for each direction
Specimen	3 specimens

Table 3-2 Impact test conditions

Measuring apparatus	NRRO, torque tester
Rotating speed	4000, 7000 min^{-1}
Ambient temperature	Room temperature (approx. 23 to 24˚C)
Unit direction	Upright
Loading disk weight	5 g
Measurement interval	Approx. 4 min. (2 min. for each rotating speed)
Measurement properties	Radial NRRO, torque

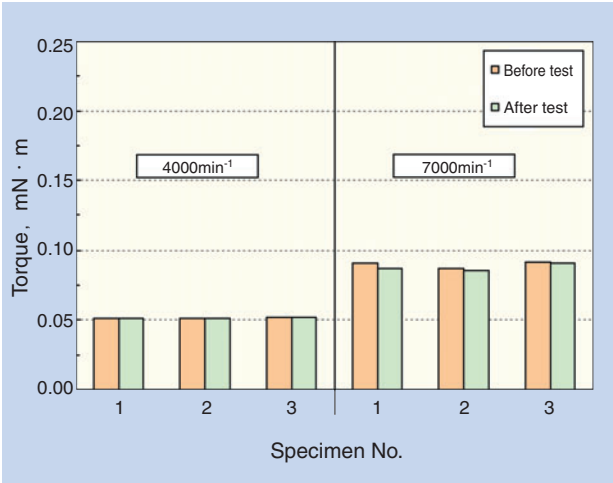

Fig. 12-1 Torque comparison before and after impact test

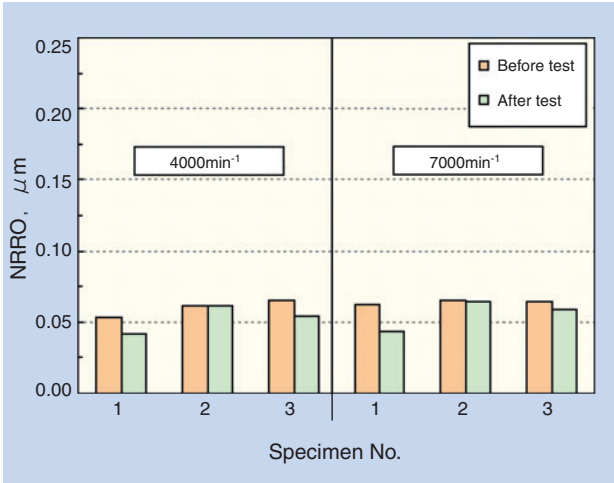

Fig. 12-2 NRRO comparison before and after impact test

5. Future Developments

It is expected that sales of HDD's will continue to grow due to the popularity of personal computers. However, it is also expected to spread to the consumer product field, including HDD recorders, mobile storage devices, digital video cameras and mobile phones. One more area of potential in the near future is home servers. Currently, 3.5-inch HDD's are 80% of total sales, but 2.5-inch and 1-inch HDD are expected to expand in the future with new applications.

One of the technological innovations expected to appear soon is the perpendicular magnetic recording method. If it goes into mass-production, the storage capacity will increase further. As a major trend, the requirements for the bearing's rotational accuracy (such as RRO) will become more severe. When classifying requirements by application, home products will require low noise level, mobile products will require low torque to reduce power consumption and higher impact resistance, and navigation systems will require a wider operating temperature range since they are used in cars. On the other hand, there will still be a need for low-cost products even though their storage capacity is limited.

NTN will continue to improve functionality and promote product development to respond to these needs. Since hydrodynamic BEARPHITE units employ press-formed hydrodynamic grooves and need to be price-competitive, design will work closely with manufacturing from the early stages of development to produce low-cost bearing units. This paper has only introduced the hydrodynamic BEARPHITE unit that was developed for HDD. However, it can also be used in optical disk drives such as DVD, polygon scanners and fan motors.

The hydrodynamic BEARPHITE unit is a product **NTN** has been working on for many years and contains various bearing technologies. **NTN** is using a business model where technological development and design are performed in Japan and the products are manufactured in factories overseas.

NTN will continue to promote the advantages of hydrodynamic BEARPHITE units to our customers in order to increase their sales. **NTN** expects these units to become one of the mainstream bearings products in the future. **NTN** will actively follow our customer's ever-changing requirements to make the hydrodynamic BEARPHITE unit acceptable worldwide for HDD devices and strive for a high-quality reputation in the marketplace. **NTN** expects that the hydrodynamic BEARPHITE unit will become widespread in various fields.

Photo of the author

Kiyotaka KUSUNOKI

Fluid Dynamic Bearing Unit Division

High Angle Active Link

Keisuke SONE*
Hiroshi ISOBE*
Koji YAMADA*

NTN has developed a High Angle Active Link that can control movement with two degrees of freedom. This equipment consists of a constant velocity joint(CVJ) with a power unit. This system is expected to be used for robotic joints and as an optical platform.

This paper introduces the advantages that the constant velocity joint has over a parallel link mechanism and some considerations on its link positions obtained by analytical study of ADAMS(a dynamic modeling software package).

1. Introduction

NTN is looking to improve joints with a link mechanism, for example a constant velocity joint with high bend angle. Such a joint is composed of links whose connection can rotate with one degree of freedom. We have located actuators in the link connector as an improvement to these joints. As a result, we developed a device (**Photo 1**) that can be controlled with two rotational degrees of freedom between input and output segments. We expect that this device can be used in robotic joints, optical platforms and so on. It can also be used alone as a machine element in the connection of parts between the segments.

This paper introduces a device, consisting of a joint (OD49×height 48mm) and two actuators in the input segment.

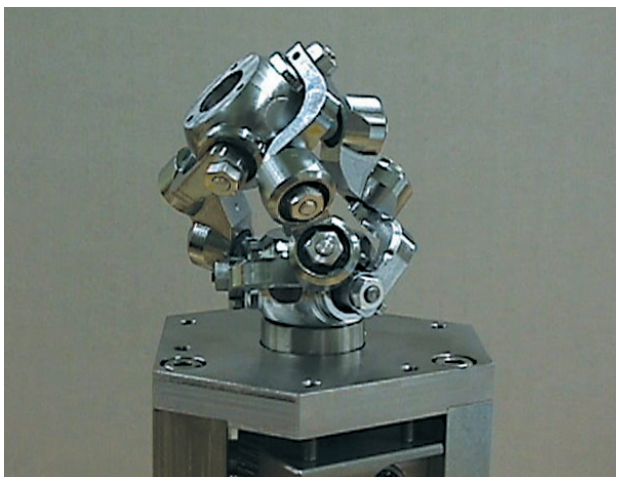

Photo 1 High Angle Active Link

*New Product Planning Department Research & Development Center

2. Structure and Features

2. 1 Joint Mechanism

As shown in **Fig.1,** the joint forms a parallel linkage mechanism, consisting of three linkage systems (input arm, intermediate link, output arm) between the input segment (input-side link hub) and output segment (output-side link hub). Each linkage system includes four rotation pairs and three links. A bearing is used in each rotation pair to reduce rotational resistance and eliminate clearance in the linking areas. Also shown in **Fig. 1**, each linkage system forms the spherical link mechanism (i.e. segments move on spherical surface) and has the input and output segments of the same form. The shafts extending from the input- and output-side arm links are connected at certain crossing angle (angle γ , **Fig, 2**) via the middle link. These linkage systems are located symmetrically to Point A, the cross point of two connecting rods of the middle link toward input- and output-side.

The three linkage systems mentioned above are spaced evenly about a circle, and are constrained to move on a common circle. This means that the cross point A of the two connecting rods inside the middle link of each linkage system lie only on the plane bisecting the angle between the center lines of input and output-side link hub. Therefore, this mechanism has the constant-velocity performance.

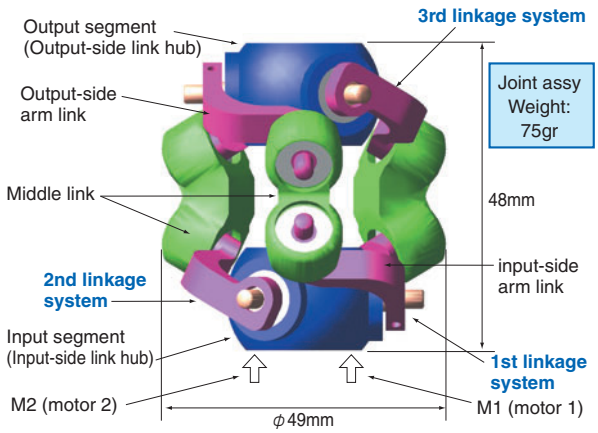

Fig. 1 Joint assy

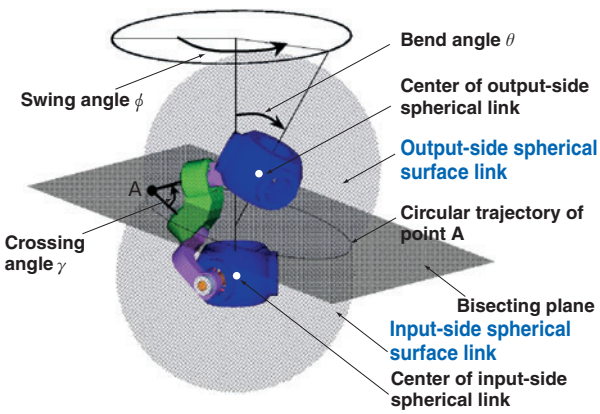

Fig. 2 Operating principle of the joint

2. 2 Unit Configuration

As shown in **Fig.3**, two actuators and reduction gears are located inside the input-side arm connected to the input-side link hub, to control the rotation angle of the arm. Motor 1 is located in the 1st linkage system, motor 2 in the 2nd linkage system, and the 3rd linkage system is used as a passive link **(Fig. 1**). Because of the parallel structure, the output side of each linkage system moves in such way that it maintains symmetrical position to the points on the bisecting plane. This allows positioning of the output segment for two angles (bend angle θ . swing angle ϕ , **Fig. 2**).

Fig. 4 shows the relationship between the input-side arm swing angles (see **Fig. 5)** of the 1st or 2nd linkage system and two angles of output segment. Motor 1 and motor 2 control these input-side arms. It shows that the input-side arms turn within ±45 degrees and the phase difference in the input-side arm swing angle between 1st and 2nd linkage systems is 120 degrees.

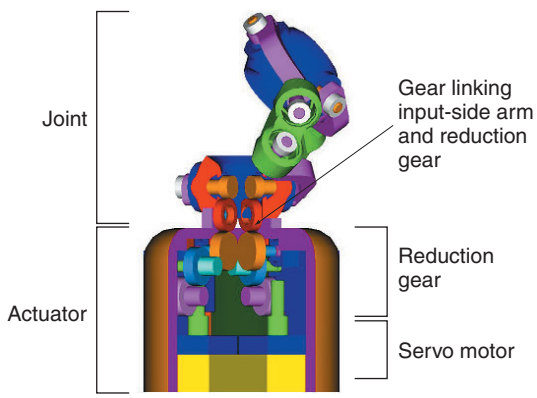

Fig. 3 Unit

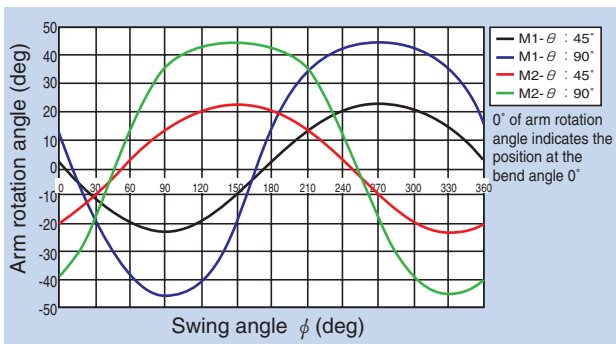

Fig. 4 The relationship between the swing angle (ϕ) and the revolution angle of the arm in the position of the bend angle θ =45° and θ =90°

2. 3 Features

① Operating range

Bend angle θ : ±90˚

Swing angle ϕ : ±360˚× n (No limit)

② The actuator and reduction gear are located in the input-side segment to reduce the weight and size of moving part.

③ Reducing bearing clearance inside the joint promotes accuracy of the motion under low operating resistance.

④ Adoption of constant velocity joint structure allows smooth motion in all direction for inverse input.

⑤ It ensures sealing capability because the parts linking acutuator and joint are located into the joint.

3. Analysis of Mechanism

The general-purpose mechanism analysis software "ADAMS" was used to analyze the mechanism with a 5N perpendicular load exerted at the center on the top of the output segment (**Fig. 5**). The support load on each link bearings and the torque of the motor were calculated. (**Figs. 6**, **7**, **8**)

The maximum load on the bearing was checked, and it was found that both radial and axial loads were approximately 20N and the moment on the bearing was approximately 200 N・mm. It was also found that the larger the bend angle θ the higher the load. (**Fig. 6** shows the moment on the bearing of the passive link (3rd linkage system) of the input-side link hub at the bend angle θ = 0˚, 45˚ and 90˚.)

The maximum torque on the motor is approximately 380 N・mm. In motor 1, the torque has the peak when ϕ is near 30 (ϕ =60˚) and 270˚ as shown in **Fig. 7.** In motor 2, the load has the peak when ϕ is near 30 (ϕ =0˚) and 150 as shown in **Fig. 8**. The positions of patterns A, B and C in **Fig. 9** correspond to these swing angles (ϕ =30˚, 150˚, 270˚). Note that the torque at part 2 and the torque generated by the load are in the same direction. In the case of pattern A, since part 2 corresponds to the passive link, the other

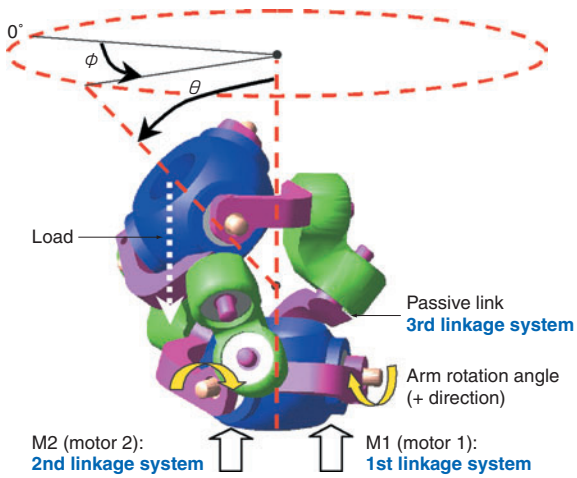

Fig. 5 The model of ADAMS analysis

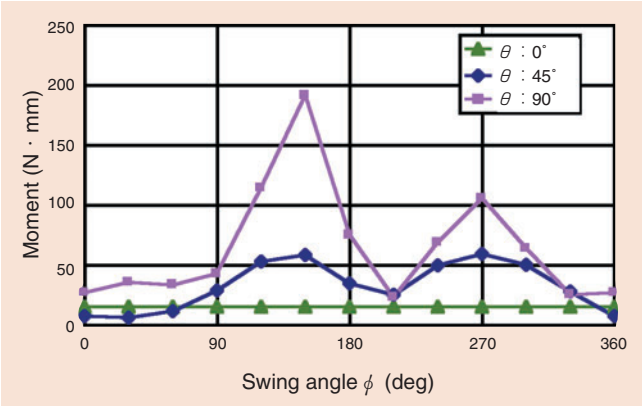

Fig. 6 Bearing load to the swing angle

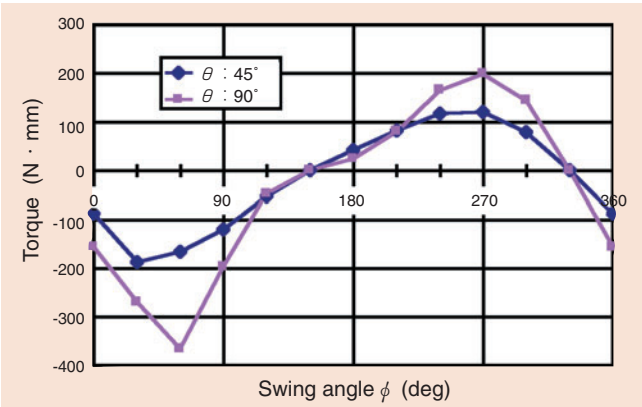

Fig. 7 The required torque of the motor 1 to the swing angle

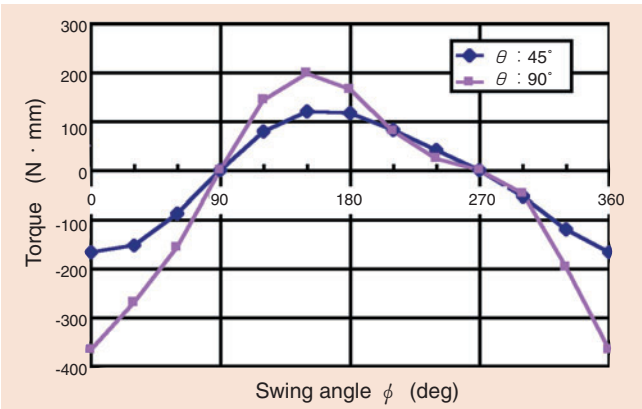

Fig. 8 The required torque of the motor 2 to the swing angle

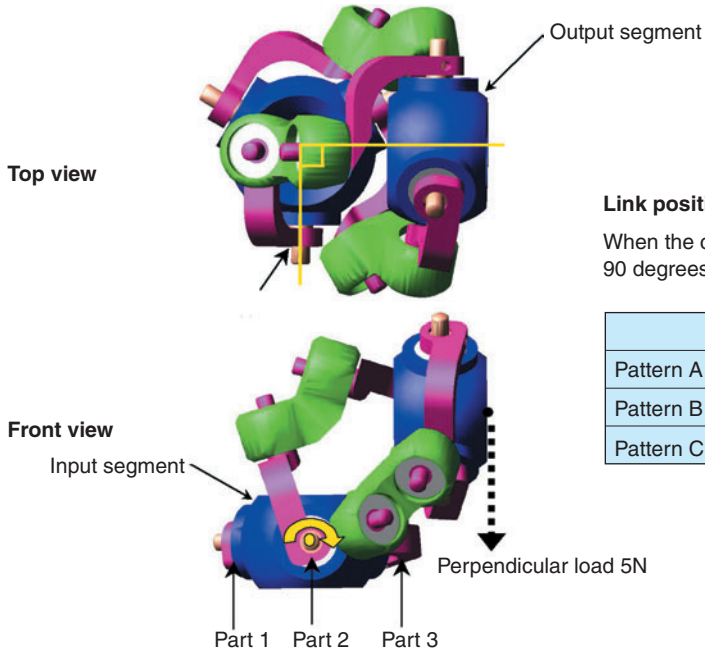

Link positions generating peak torque

When the centerline of input segment bearing is at 90 degrees to the centerline of the output segment

	part 1	part 2	part 3
Pattern A（ϕ:30°）	Motor 1	Passive link	Motor 2
Pattern B（ϕ:150°）	Passive link	Motor 2	Motor 1
Pattern C（ϕ:270°）	Motor 2	Motor 1	Passive link

Fig. 9 The link position when maximum torque is generated

two links share the torque. This causes motor 1 and motor 2 to have the peak load at a 30-degree phase difference. Furthermore, since the torques generated by the load and the motor are in different directions, a larger torque is required. Therefore, each motor is exposed to the maximum torque. The torque at this time is about twice as large as that for patterns B and C (see **Figs. 7** and **8**). These must be taken into account when designing the device.

4. Future Developments

By locating two actuators in the input segment, it has been confirmed that the position of the output segment can be controlled in all directions by two degrees of freedom. We will work on refining the gear reduction mechanism and its control method in order to improve the accuracy and movement of the device. The design will also be made specifically for individual applications in hopes of further development and future business.

Photos of authors

Keisuke SONE

New Product Planning Department, Research & Development Center

Hiroshi ISOBE

New Product Planning Department, Research & Development Center

Koji YAMADA

New Product Planning Department, Research & Development Center

Improvement of Leakage Magnetic Flux Resistance of Integrated Sensor Bearings

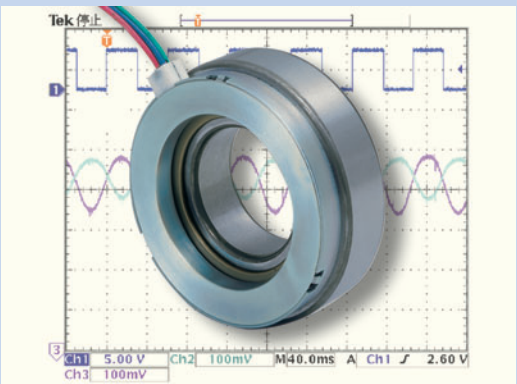

Takashi KOIKE*
Tomomi ISHIKAWA*
Hiroyoshi ITO**
Noriyoshi MIZUTANI**

A recent trend in manufacturing is to utilize electric controls to simplify machines and ensure better reliability of these machines.

Because of this trend, there has been an increasing need in the marketplace for bearings with sensing functions. A bearing with a rotation sensor that uses a magnetic encoder system is currently available. However, when using this sensor bearing near equipment that generates a magnetic flux such as a motor or magnetic clutch, the sensor may operate incorrectly due to leakage magnetic flux.

Therefore, leakage magnetic flux needs to be minimized and mechanisms to improve leakage magnetic flux performance are needed. We have successfully enhanced the function of the integrated sensor bearing by optimizing the mechanical structure through magnetic field analysis. An overview of this process was introduced in **NTN** Technical Review No. 69. In this paper, an electronic technique for further improvement of leakage magnetic flux resistance is introduced.

1. Introduction

A recent trend in manufacturing is to utilize electric controls to simplify and ensure better reliability of machines and to reduce the impact on the environment. Because of this trend, there has been an increasing need for bearings with sensing capabilities.

Integrated sensor bearings with speed detection capabilities have just become available on the market. However, when using a sensor bearing near a device that generates a magnetic flux, such as electric motors and magnetic clutches, the sensor may be influenced by the magnetic field, resulting in malfunctions such as sensor output failure. Therefore, sensors need to have sufficient leakage magnetic flux resistance, so that they are not influenced by magnetic flux generated by nearby devices. **NTN** has been working to enhance the leakage magnetic flux resistance by optimizing the mechanical structure through magnetic field analysis. An overview of this process was introduced in **NTN** Technical Review No. 69. Due to requirements of some applications further improvement of leakage magnetic flux resistance is required.

NTN has established sensor circuit technology with drastically improved leakage magnetic flux resistance compared to conventional bearings. An overview of this technology is introduced in this paper.

2. Integrated Sensor Bearings

Fig. 1 shows a sectional view of an integrated sensor bearing with leakage magnetic flux resistance characteristics that have been designed based on the conventional magnetic field analysis. By deploying a magnetic bypass ring that diverts leakage magnetic flux the amount entering the Hall IC has been minimized.

*Research & Development Center New Product Planning Department
**Industrial Sales Headquarters Industrial Engineering Department

The rotating speed detector of the bearing consists of a magnetic encoder that has alternately magnetized N and S poles, and a magnetic sensor. A Hall IC that can output a rectangular wave is normally used as the magnetic sensor. The Hall IC contains a Hall element, amplifying circuit, Schmitt trigger circuit and output transistor. Two types of Hall IC's are available: the unipolar type and the bipolar type. The unipolar type turns ON/OFF according to the magnitude of the magnetic field, and the bipolar type turns ON/OFF as the N and S poles of the magnet are alternately activated. For a rotary sensor, the latter is often used in order to have an output duty ratio close to 50%. **NTN** uses this type, the bipolar type of Hall IC.

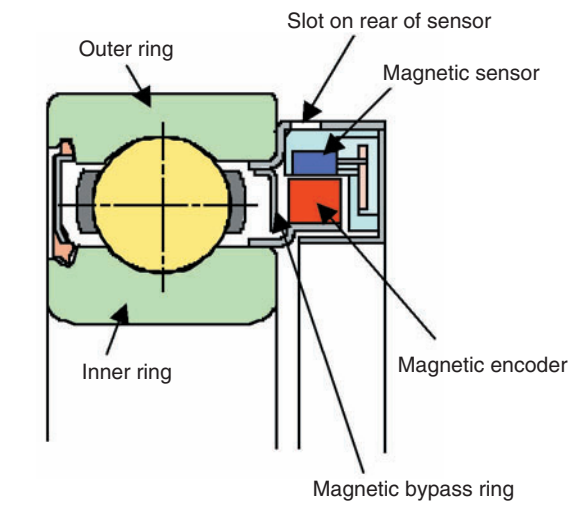

Fig. 1 Sectional view of integrated sensor bearing (Conventional design)

3. Influences of Leakage Magnetic Flux

By taking an example that uses a Hall IC as the magnetic sensor, the influences of leakage magnetic flux on the Hall element inside the Hall IC are explained in **Fig. 2**.

As the inner ring and magnetic encoder rotate, alternating magnetic fields are forced to the Hall element, causing the output voltage to change in the form of a sine wave with a center level (reference voltage) of $V_H/2$, which is half of the power voltage (V_H) supplied to the Hall element (See the sine wave indicated by black line in **Fig. 2**). Since the output signal of the Hall element is compared with this reference voltage (used as the threshold level), a rectangular wave that repeatedly turns ON and OFF is output from the Hall IC. The output duty ratio (T_P/T_n) is approx. 50% (See the rectangular wave indicated by the black line in **Fig. 2**).

If the influence of an external magnetic flux is strong enough, the alternating magnetic field on the Hall element is affected and changes up and down (see the red and blue lines in **Fig. 2**), causing the output duty ratio to change (See the rectangular waves indicated by red and blue lines in **Fig. 2**). If the external leakage magnetic flux increases and the sine wave output changes considerably, loss of pulses on the sensor output may occur.

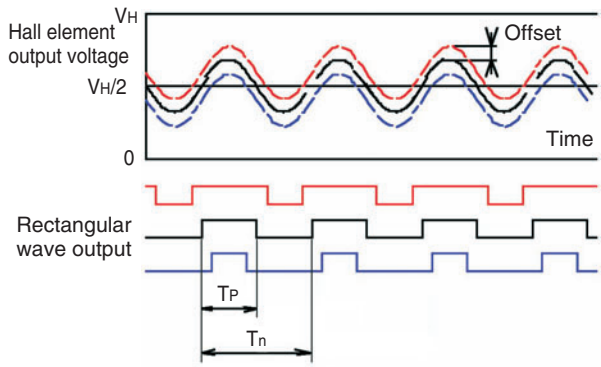

Fig. 2 Hall element and digital output voltage

4. Improvement of Leakage Magnetic Flux Resistance

Malfunction of the sensor output caused by external leakage magnetic flux interference can be prevented by canceling the sensor output that changes due to the external leakage magnetic flux or by increasing the magnetization intensity of the magnetic encoder. Since increase of the magnetization intensity is limited due to the properties of the magnetic material, electric processing to eliminate the offset components was implemented to improve the leakage magnetic flux resistance.

4. 1 Structure

To cancel the influences of the leakage magnetic flux on the magnetic sensor, two analog output type magnetic sensors (e.g. Hall elements) are placed closer to each other at different positions (at 180-degree electrical angles) so that they are equally exposed to the influences of the leakage magnetic flux. The two sensor outputs are differential-output to cancel the offset caused by the leakage magnetic flux, and then subjected to rectangular wave processing to provide single-phase output. This differential output method has doubled the output sensitivity and improved noise resistance.

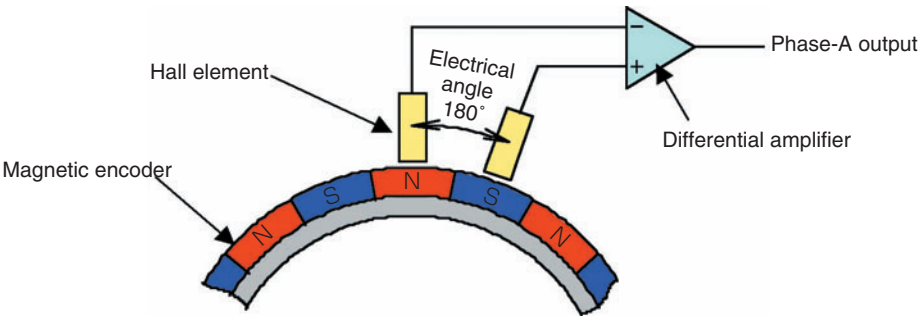

Fig. 3 Schematic view of sensor

4. 2 Circuit

Fig. 4 shows a schematic view of the detector circuit. The structure of the circuit for one phase (phase-A) is shown. To reduce the number of electrical components, a comparator was used to compare the two outputs to provide a rectangular waveform signal. This was used instead of differential amplification of two Hall element outputs.

Typically, an optical encoder is used separately to detect the number of revolutions. If the optical encoder is integrated with the bearing in one unit, both bearing and sensor will be put in the same environment which will often hinder use of the optical encoder. Thus, sufficient care must be paid not to allow the detector circuit to malfunction even if temperature changes in a wide range. The Hall element can easily be affected by the operating temperature, and if the ambient temperature rises, the input resistance inside the Hall element will drop to increase the current, resulting in larger heat generation inside the detector. With this in mind, the Hall element drive voltage was set according to the operating temperature range.

Two Hall element drive methods are available: constant-current drive and constant-voltage drive. The constant-voltage drive method was employed since the constant-current drive method causes the Hall output voltage and unbalanced voltage to change excessively depending on the ambient temperature. The Hall element's reference voltage ($V_H/2$) varies with the Hall element used. If the reference voltage ($V_H/2$) is made equal to all Hall elements, the output offset difference between Hall elements can be reduced, making it possible to approximate the duty ratio of the rectangular output to 50%. Because of this, some ideas were implemented as explained in section 4.4 to provide an equal reference voltage for all Hall elements.

4. 3 Circuit Operation

The integrated sensor bearing with the earlier explained built-in detector circuit was put in the magnetic flux interference test equipment [1)] shown in **Fig. 5**, and waveform was observed at points A, B and C of the detector circuit (**Fig. 4**). The results are given in **Fig. 6**. The test equipment generated a magnetic flux by forcing current into a generating coil and the resulting magneto-motive force (AT, current×number of coil turns) was measured when the sensor output malfunctioned. The result was used as the criterion of judgment for evaluation of the leakage magnetic flux resistance. When the magneto-motive force was increased to expose the bearing to a magnetic flux as shown in **Fig. 6 (b)**, it can be observed that the Hall element's output voltage is changed upward. However, by adopting the method that obtains differential output of two Hall elements, a rectangular waveform output with the same duty ratio can be obtained even if the output is exposed to the leakage magnetic flux.

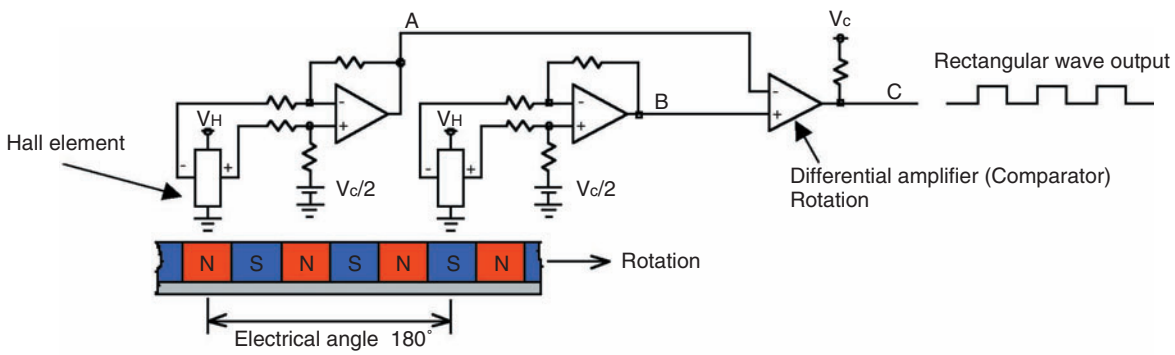

Fig. 4 Schematic view of detector circuit

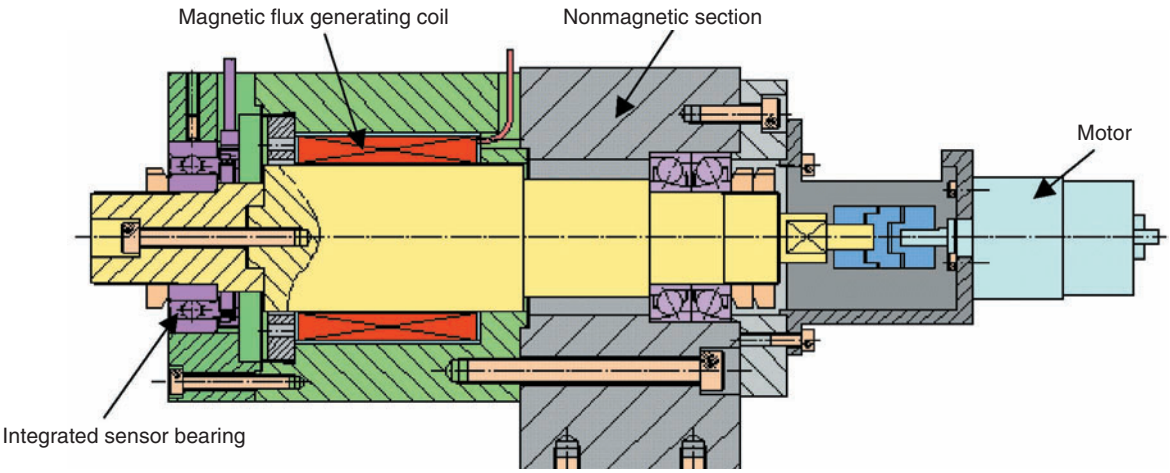

Fig. 5 Magnetic flux leakage durability test equipment

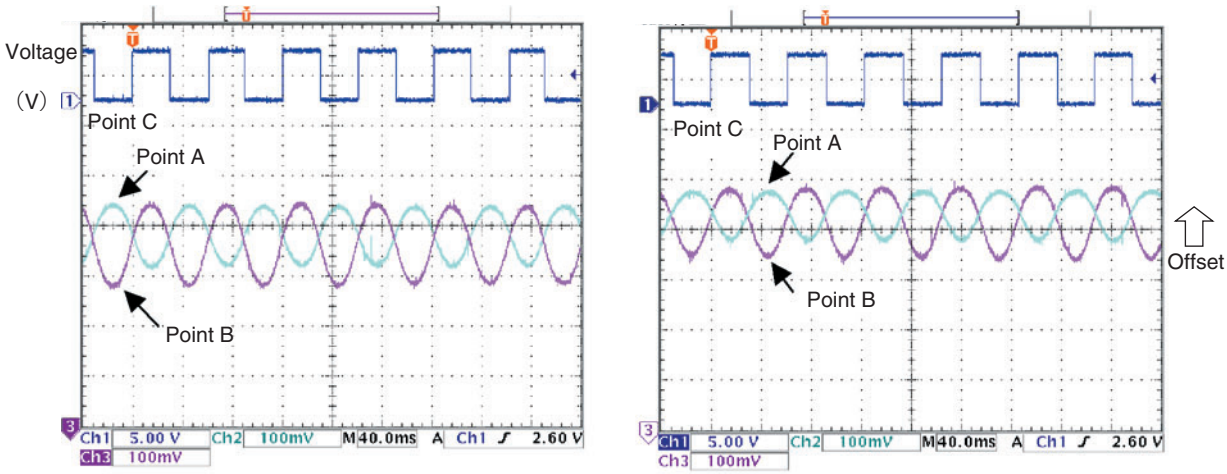

(a) Without external magnetic field (Magneto-motive force: 0AT)

(b) With external magnetic field (Magneto-motive force: 400AT)

Fig. 6 Waveform of detector circuit

4. 4 Influence on Reference Voltage

The reference voltages of two Hall elements comprising a differential circuit change according to the leakage magnetic flux. This change was measured and shown in **Fig. 7**.

From the figure, it can be understood that the reference voltages of two Hall elements change due to influence of leakage magnetic flux (magneto-motive force). This change of the reference voltages is an offset caused by the leakage magnetic flux, and the sensors interference resistance can be improved by minimizing the difference in the reference voltages of Hall elements. We have succeeded in almost equalizing the reference voltages by adopting a circuit that causes the reference voltage of a Hall element to match that of another element.

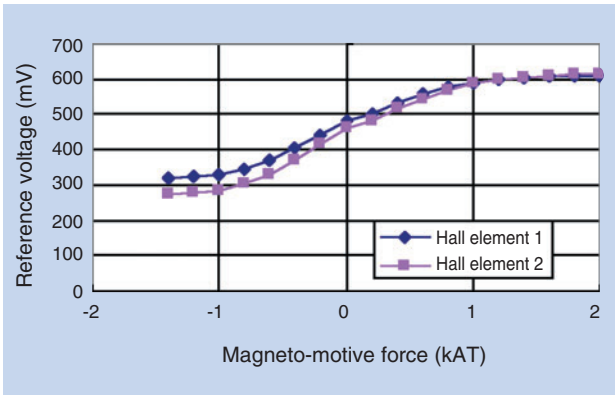

Fig. 7 Influence on reference voltage

5. Evaluation of Leakage Magnetic Flux Resistance

The Hall element's sensitivity varies with the elements used. With our method of forming a differential circuit, the leakage magnetic flux resistance is also influenced by the individual difference (sensitivity difference) of two Hall elements that were used. Evaluation testing was conducted under three different conditions shown in **Table 1**, with the possible maximum sensitivity difference limited to 20%. **Fig. 8** shows the evaluation results of the leakage magnetic flux resistance of the integrated sensor bearing equipped with a differential circuit. For comparison, the evaluation results for conventional bearings equipped with a magnetic bypass ring (**Fig. 1**) are also given.

Table 1 Sensitivity test condition

Test condition	Hall element sensitivity difference (%)	Magnetic bypass ring
1	0	Not used
2	10	Not used
3	20	Not used
Conventional type	- (Hall IC)	Used

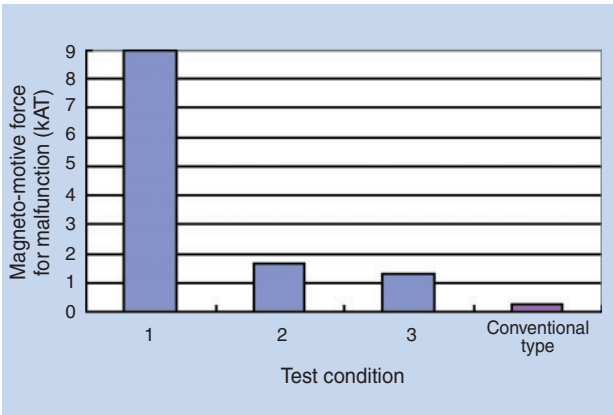

Fig. 8 Magnetic flux leakage durability

5. 1 Influence of Sensitivity Difference on LeakageMagnetic Flux Resistance

From **Fig. 8**, it is understood that the leakage magnetic flux resistance can be improved by decreasing the sensitivity difference between two Hall elements comprising a differential circuit. Test condition 3 is the worst possible condition. However, under this condition, it was found that the leakage manetic flux resistance was five times better or more than the conventional type, and sufficient performance was obtained without screening Hall elements. The magneto-motive force that causes malfunction under test condition 1 was set to 9 kAT. However, this is the maximum magneto-motive force that the test equipment can produce, and the new integrated sensor bearing can withstand even higher leakage magnetic flux. The performance can be improved up to 30 times compared to the conventional type by minimizing the difference between Hall elements.

5. 2 Influence of Leakage Magnetic Flux on Duty Ratio

Fig. 9 shows the results of the test conducted to determine the influences of leakage magnetic flux on the duty ratio under three conditions given in **Table 1**. When the sensitivity difference between two Hall elements is set to zero, like condition 1, the change of the duty ratio is small. Even in the magneto-motive force range of ±9kAT, the change of the duty ratio is within ±15%. When a duty ratio of 50±15% is set as the allowable range, even under conditions 2 and 3, the magneto-motive force is 1kAT or larger, which is sufficiently improved compared to the conventional type.

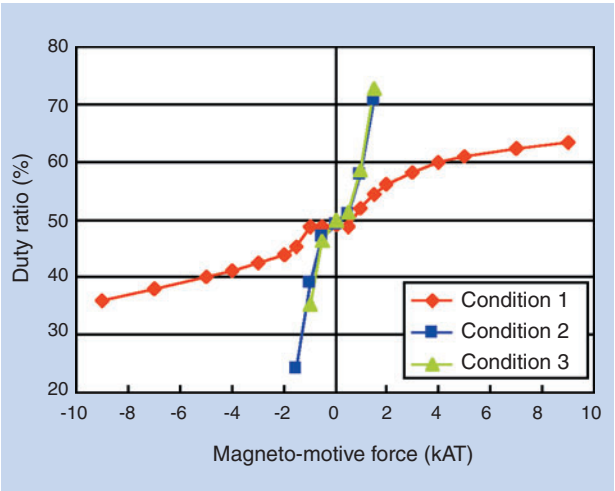

Fig. 9 Impact on duty ratio

6. Conclusion

This paper has introduced the electrical method to improve the leakage magnetic flux resistance of integrated sensor bearings. Compared to the conventional method that uses a magnetic bypass ring, the leakage magnetic flux resistance is five times better or more. Adoption of this method eliminates the need for the magnetic bypass ring, and this simplifies the structure of the bearing, resulting in easier assembly work. In addition, it is found that this method is influenced by sensitivity difference between Hall elements composing a differential circuit, but the duty ratio of the sensor output does not change so much.

Since employment of this technology enables installation of integrated sensor bearings into devices, such as motors and magnetic clutches, that generate strong magnetic fields, the application range of integrated sensor bearings is expected to expand.

References

1) Takashi KOIKE, Yoshitaka NAGANO, **NTN** Technical Review No.69 (2001)

Photos of authors

Takashi KOIKE
New Product Planning Department, Research & Development Center

Tomomi ISHIKAWA
New Product Planning Department, Research & Development Center

Hiroyoshi ITO
Industrial Engineering Department Industrial Sales Headquarters

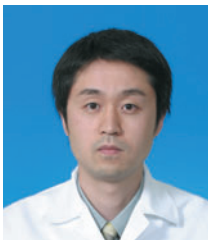

Noriyoshi MIZUTANI
Industrial Engineering Department Industrial Sales Headquarters

Introduction of Grinding Swarf Recycling

Kanji NAKAMURA*

NTN has developed a system to recycle grinding swarf. Recycling has already begun.
NTN has also started a new company, **UNI TOP**, which will supply briquetting machines and support recycling of briquettes.
UNI TOP will contribute to society by reducing the environmental load of grinding swarf.

1. Introduction

Companies like **NTN** who produce precision machinery use many grinding machines in their manufacturing processes. This machinery produces a lot of grinding swarf or industrial waste, most of which is dumped into landfills. Being an ISO14001-certified company, **NTN** thought that it was responsible for helping establish recycling technology and contributing to our recycle-based society. **NTN** has been working on the development of grinding swarf-recycling technology since 1999 and has succeeded in its practical use. In addition, not only is this system friendly to the environment, it also helps reduce rising disposal costs.

2. Recycling System

Fig. 1 shows a comparison between the conventional grinding swarf dumping system and the recycling system **NTN** developed. Briquettes obtained from this new system are delivered to steel manufactures, where the briquettes are reused as raw material in steel production. In addition, the coolant separated in the process is returned to the coolant tank to be reused again.

3. Briquette Technology and Test Results

Grinding swarf primarily contains grinding sludge (metallic components), coolant (oil-based or water-based) and a small amount of grinding powder. During the process, coolant is separated from the swarf and the metallic components are solidified into briquettes. After completed, both the coolant and the metallic components are ready to be reused again. In addition, the technology **NTN** developed produces briquettes from grinding swarf without the use of a binder (see **Fig. 2**). **Fig. 3** shows a magnified view of grinding swarf.

Fig. 4 shows a composition comparison between grinding swarf and a briquette. The figure shows that a large amount of coolant is squeezed out of the grinding swarf in order to create the briquettes.

*Engineering Department, Unitop Corporation

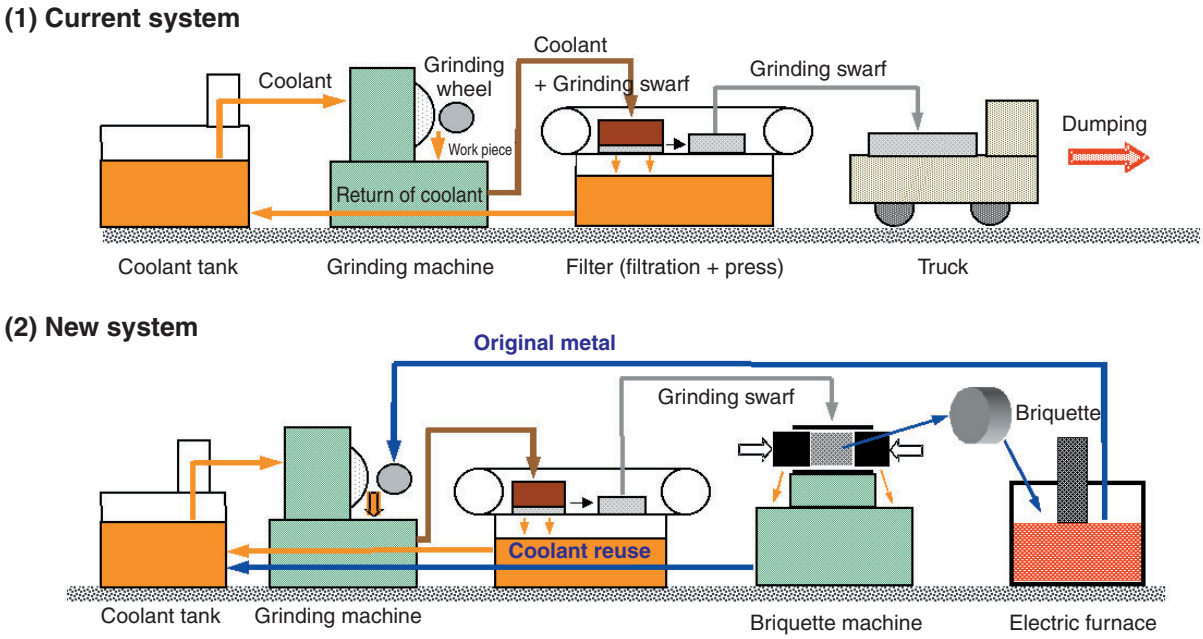

Fig. 1 Comparison of current system and new system

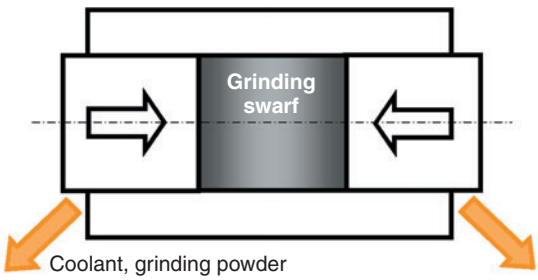

Fig. 2 Briquette method

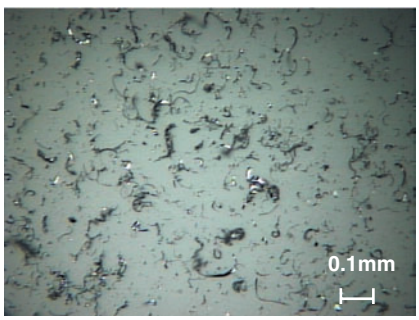

Fig. 3 Magnified view of grinding swarf

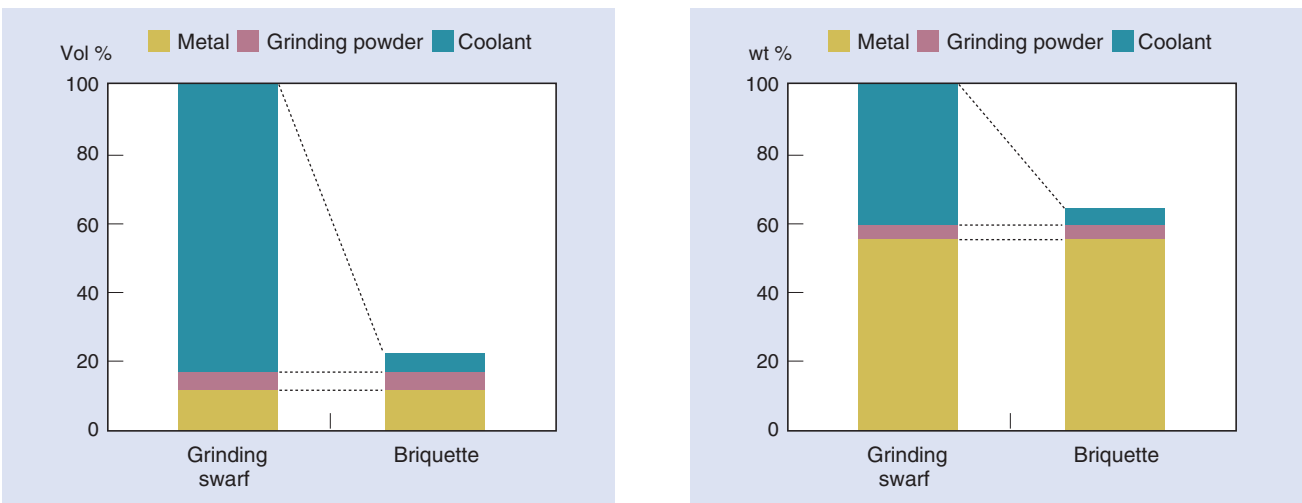

(1) Volume comparison (2) Weight comparison

Fig. 4 Comparison of compositions between grinding swarf and briquette

4. Examples of Practical Applications

NTN has been promoting swarf recycling using the briquette technology described earlier. **Figs 5**, **6** and **7** show the benefits of recycling oil-based coolant using the swarf recycling process. The examples below are result of recycling that was started in April, 2001 on a preliminary basis and was fully implemented in October, 2001.

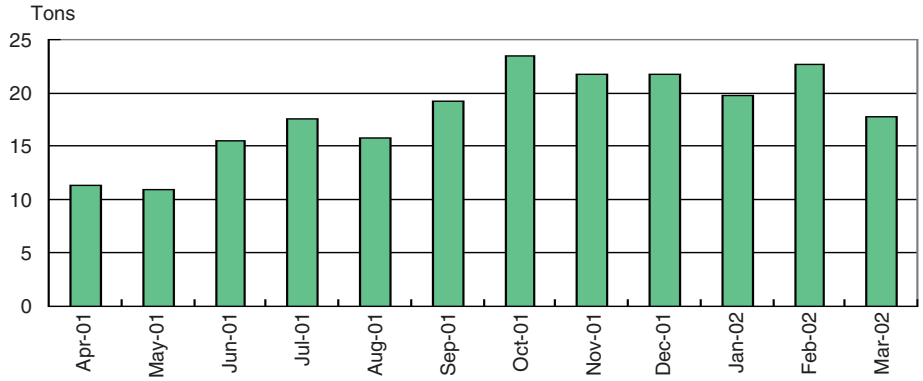

Fig. 5 Grinding swarf processed per month

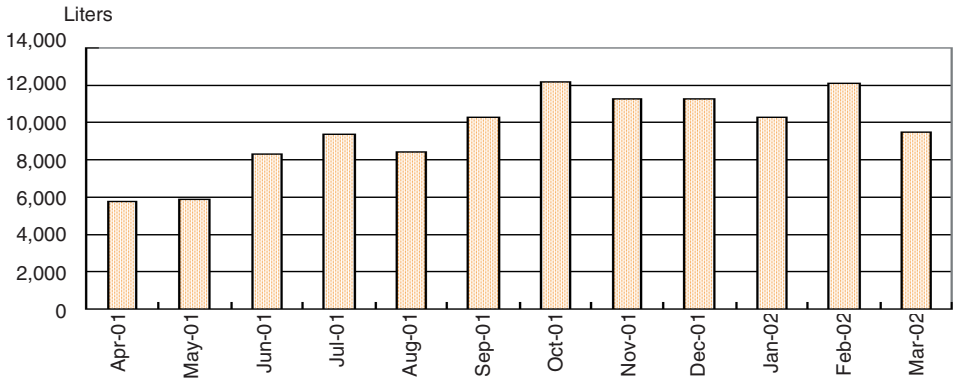

Fig. 6 Oil-based coolant reused per month

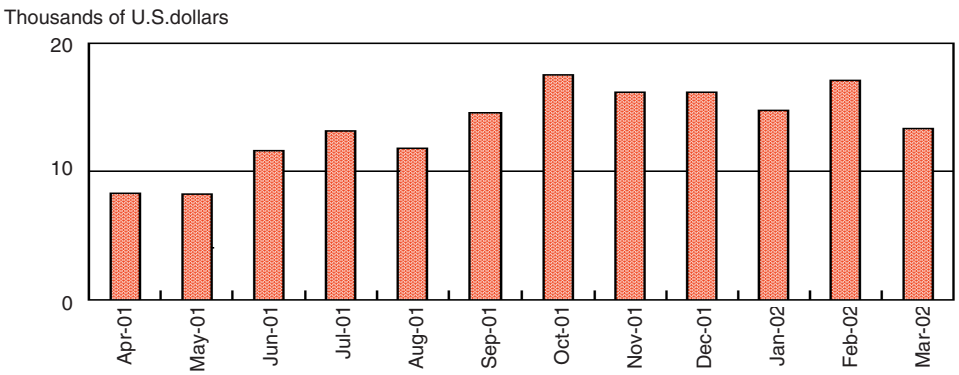

Fig. 7 Monthly cost savings

5. Establishment of Unitop Corporation

Since grinding swarf briquette technology could be used for various kinds of grinding swarf, it may be difficult for machine manufacturers to assume leadership in the practical application of this technology. Unlike these manufacturers, **NTN** produces a large amount of grinding swarf and is in an advantageous position to develop briquette technology.

To further develop this technology. **NTN** established Unitop Corporation in May, 2002 with Noritake Co., Ltd., a manufacturer of grinding wheels, and Nicotec Co., Ltd., a manufacturer of machines.

Briquette machines developed by Unitop have been supplied to **NTN**, where they have made considerable achievements in reducing both cost and the toll on the environment. In the future, **NTN** plans to promote full-scale sales activities in order to supply these machines to industrial companies.

6. Conclusion

Worldwide interest in environmental conservation is growing. Today, companies not focused on reducing environmental burdens will not only find their corporate image diminished, but will also find it difficult to manufacture their products efficiently. In this sense, the grinding swarf recycling technology that **NTN** has invented and put into practical use is very important because it can help many companies reduce their environmental burdens on the environment.

To solve issues regarding the disposal of industrial waste, **NTN** would like to help preserve the global environment by providing the know-how gained through work on grinding swarf briquette technology.

Photo of the author

Kanji NAKAMURA

Engineering Department,
Unitop Corporation

Received the Minister of Economy Trade and Industry (METI) Award in the Recycling and Systems Category in 2002, sponsored by the Ministry of Economy, Trade and Industry.
(March 11, 2003)

Hub Bearing with Wireless ABS Sensor

The wireless ABS sensor module is a single unit containing a hub bearing, hub joint, high-efficiency generator, and wireless transmitter. Use of the generator output as a power supply and sensor signal allows wireless transmission of the wheel speed signal.

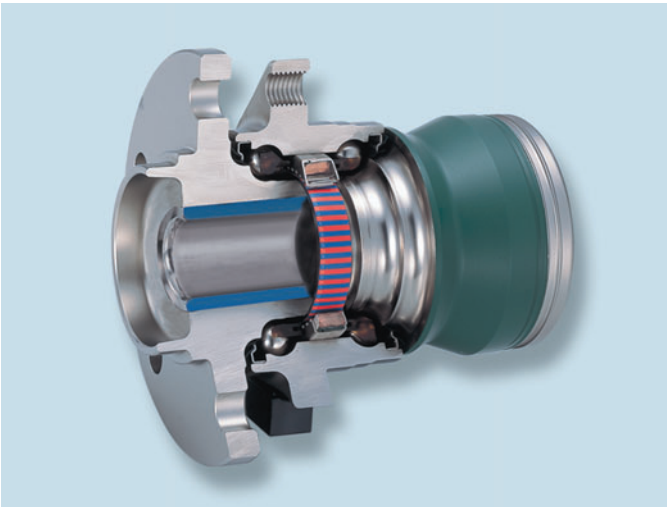

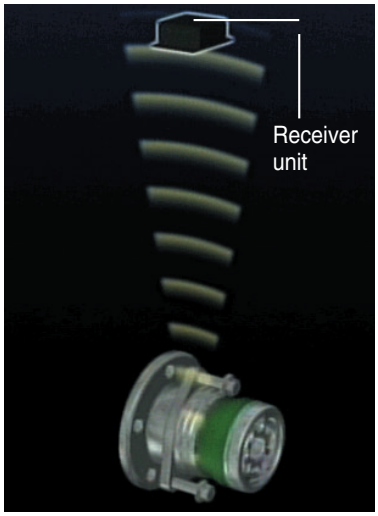

Features

- **Compact**
  Hub bearing, hub joint, and sensor are integrated into one unit.
- **Reduced assembly time**
  No wiring is required between the wheel and tire housing.
- **Improved safety (Prevention of accidents caused by damaged or broken wires)**
  No wiring is used in moving parts.
- **Improved design flexibility**
  Entire sensor is integrated into a single unit.
- **Possible to activate ABS function at very low speeds.**
  It also detects wheel slippage during acceleration.

Structure

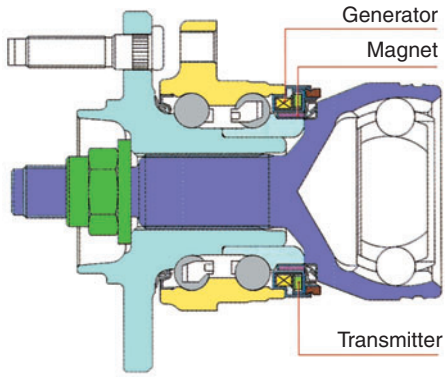

GEN3 hub bearing type

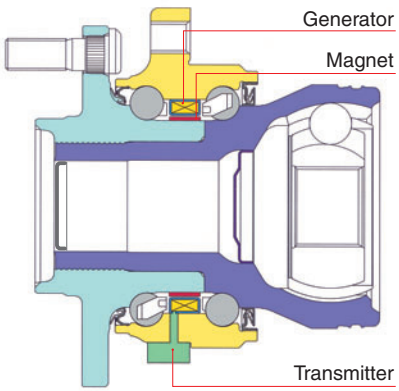

GEN4 hub joint type

GEN2 Tapered Hub Bearing for Large Commercial Vehicles

The outer ring and hub are integrated into a single lightweight greased and sealed unit with high-reliability features.

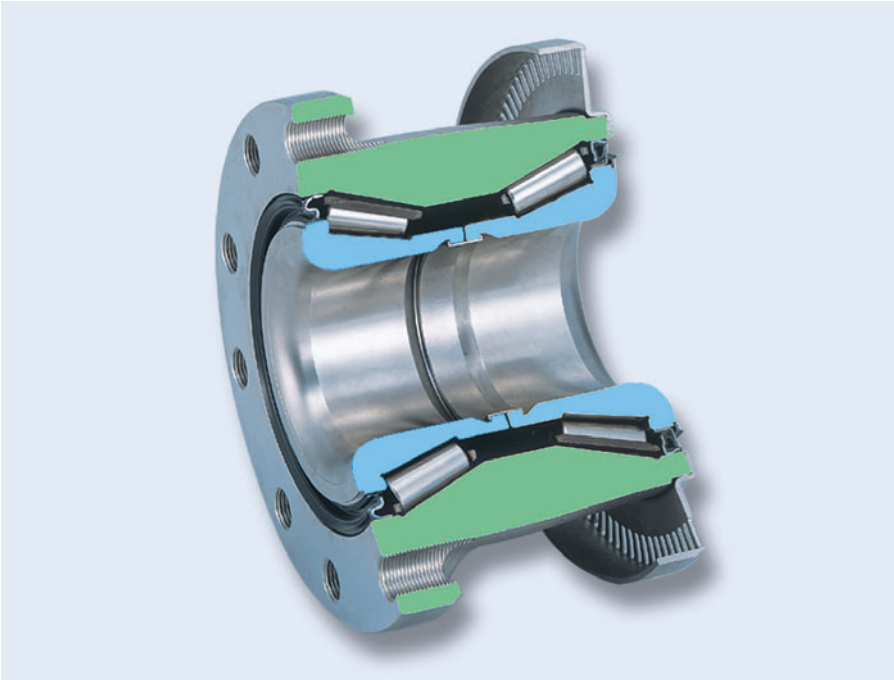

Features

- Requires no preload adjustment (Unit is designed to have the appropriate preload after assembly on the vehicle).
- Ease of assembly, maintenance, and inspection.

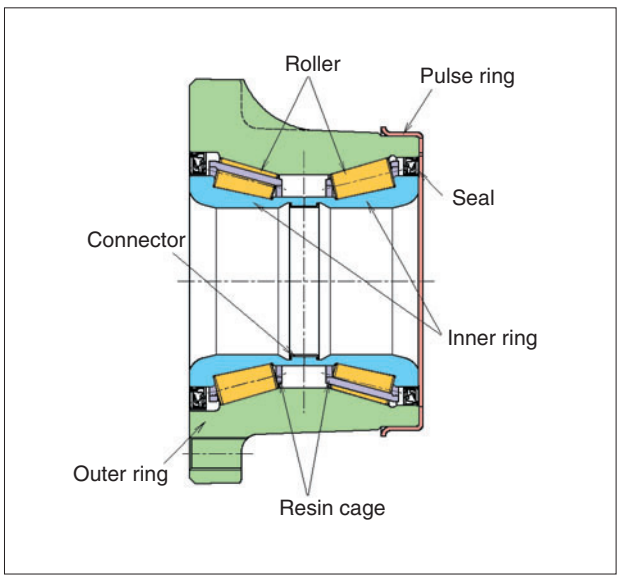

Bearing Specifications

- Outer ring material: **NTN**'s unique SC steel with excellent fatigue strength and shock resistance
- Inner ring and roller material: **NTN**'s unique long-life carburized steel with excellent hardness, toughness, and shock resistance
- Lubrication: Long-life Urea grease with high fretting resistance
- Fluorocarbon rubber seals with excellent high-temperature endurance and seal lips resistant to muddy water

GEN3 Hub Bearing with Brake Rotor

GEN3 hub bearing and brake rotor are integrated into a single unit, resulting in drastically reduced rotor runout.

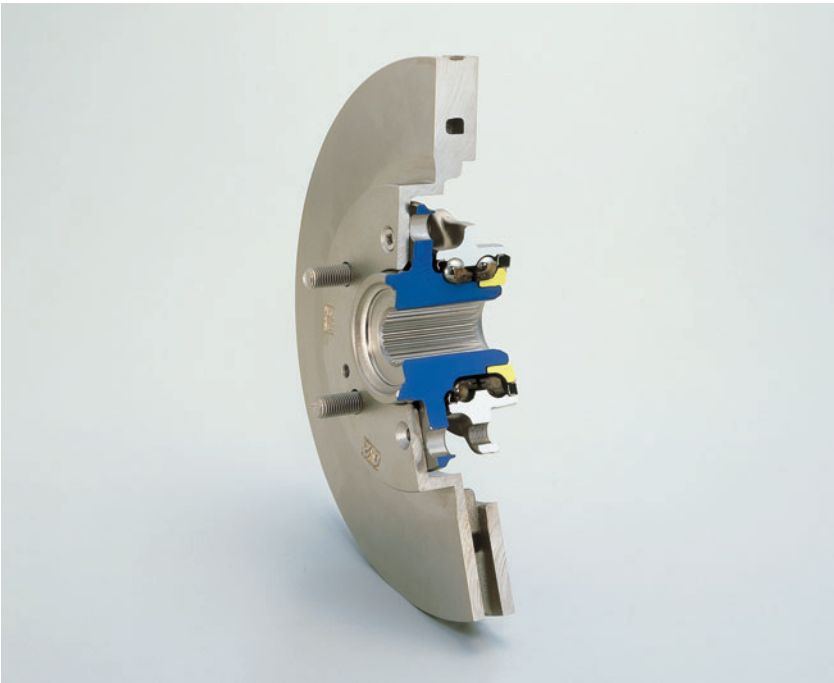

Features

- Not as susceptible to brake shudder
- Decreases drag and reduces fuel consumption
- Eliminates the need for matching brake rotor to hub

Applications

- Axle unit for passenger cars

Structure

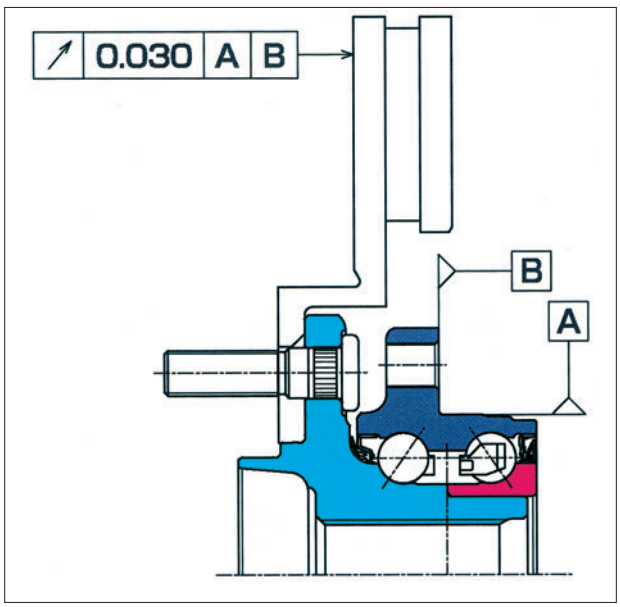

GEN4 Hub Joint

The third generation hub bearing is integrated with the new "E Series" constant-velocity joint, resulting in a compact, lightweight design.

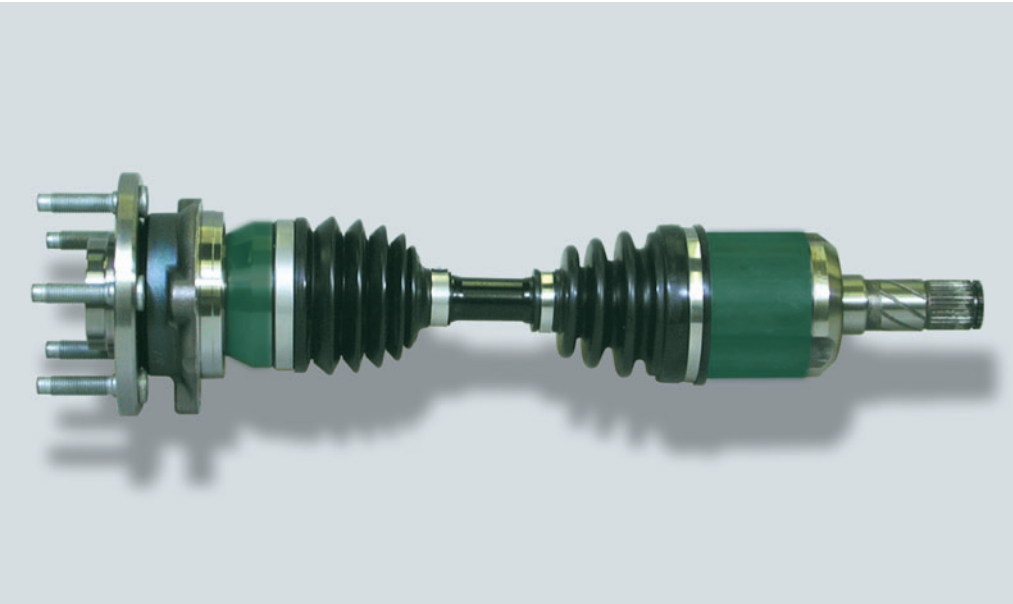

Features

- **High efficiency and low heat generation**
  Adoption of the new "E Series" constant-velocity joint improves transmitted torque by 30% during power conveyance. Heat generation has also been reduced by 20˚C compared to the conventional type.
- **Smaller axial dimension**
  Integration of the new constant-velocity joint and bearing reduces the distance between the flange and CVJ center by 20% or more.
- **Lightweight**
  Integration of the CVJ and bearing, adoption of a hollow joint shaft, and use of the new CVJ bearing tightening method reduces the weight by 10% or more.

Structure

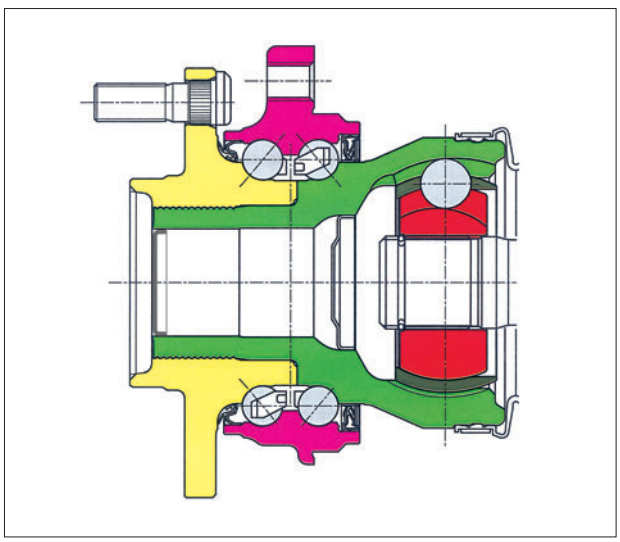

ECO series High Efficiency Compact Constant Velocity Joints - E Series

This E series constant velocity joint provides high levels of functionality and environmental solutions by offering reduced weight, compactness, and high transmission efficiency.

Fixed type

EBJ（θ＝47˚）

EUJ（θ＝50˚）

Plunging type

EDJ

ETJ

Comparison with NTN's conventional CVJ product

	EBJ	EUJ	EDJ	ETJ
Weight (%)	-15	-15	-10	-12
Outer diameter (%)	-7	-7	-4	-8
Temperature rise (˚C)	-20	-20	-20	—

PTJ (Super-Shudderless Constant Velocity Joints)

New plunging type constant velocity joints with low, constant vibration.

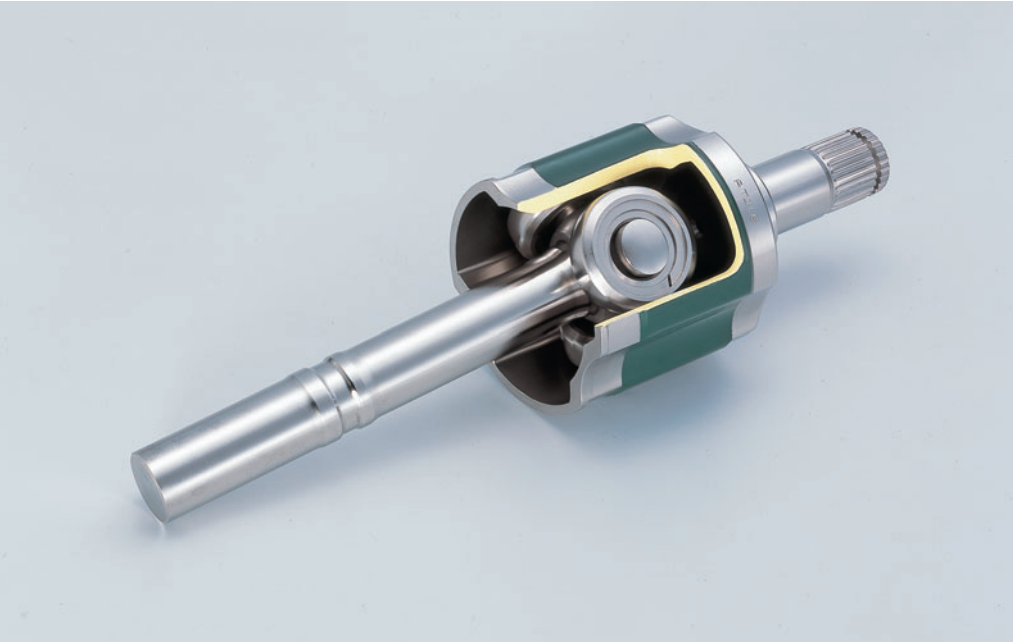

Features

- Minimized vibration for drive shafts.
- Constant induced cyclic axial load not related to the working angle.
- 50% lower induced cyclic axial load in comparison with SFJ.
- Identical outer diameter to SFJ

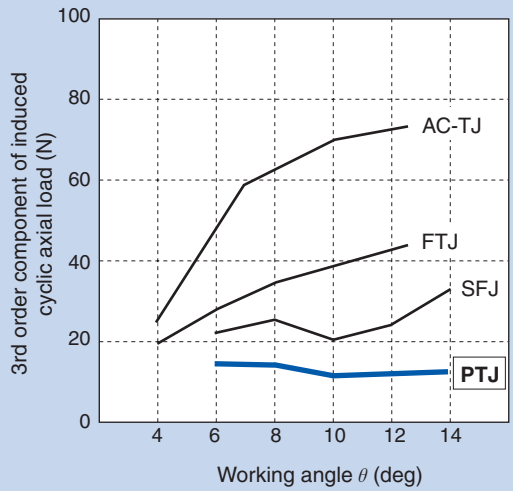

Super High Speed AT Spindle

Aero-static bearing spindle that can be attached to the machining center main spindles

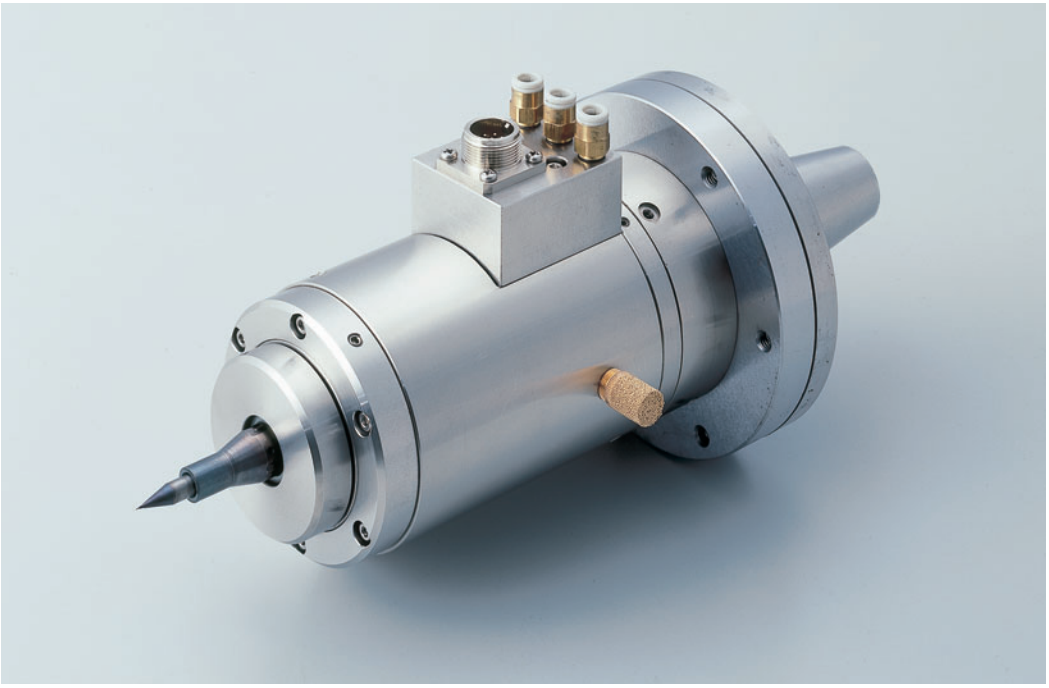

Features

- Can be attached to the machining center spindles (special machine tools are not needed).
- Use of aero-static bearings deliver super-high speeds up to 150,000 min^{-1} with high rotational accuracy.
- Use of a shaft-integrated shrink fit chuck enables high-accuracy and high-stiffness chucking.
- Low vibration, low noise level, and long life

Specifications

Maximum speed	150,000 min^{-1}	Motor	Rated Power 0.6kW Three-phase induction motor：200V AC Water-cooled：1 to 2 L/min
Load capacity	Axial ：20 N		
	Radial：40 N	Applicable tool diameter	ϕ 1mm or smaller
Static stiffness	Axial ：1.0 N / μm	Tool chucking method	Shaft-integrated shrink fit chuck (ϕ 6)
	Radial：1.8 N/ μm	Supply air pressure	0.49 MPa
Spindle weight	5 kg (excluding mounting shank)	Air consumption	100 L/min (A.N.R.)

＊The radial load capacity and static stiffness are measured at a position 14mm from the spindle end.

BEAREE Slide Guide

Lightweight and compact linear guide with optimal utilization of BEAREE material.

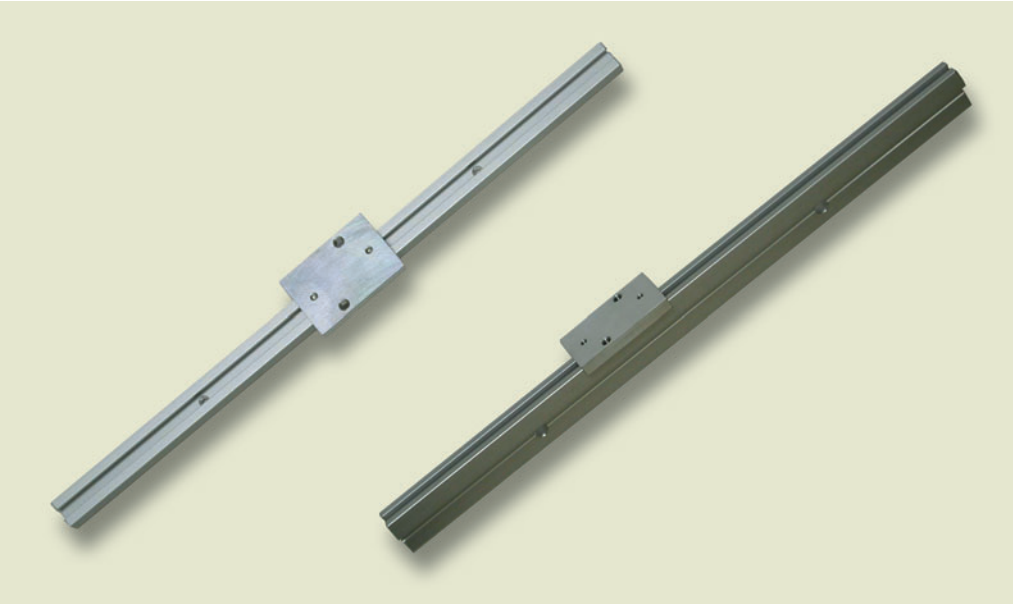

Features

- Low friction at loads up to 50N
- Lighter (approx. 1/3) and less expensive than the conventional linear guide with balls
- Allows custom design of various shapes

Structure

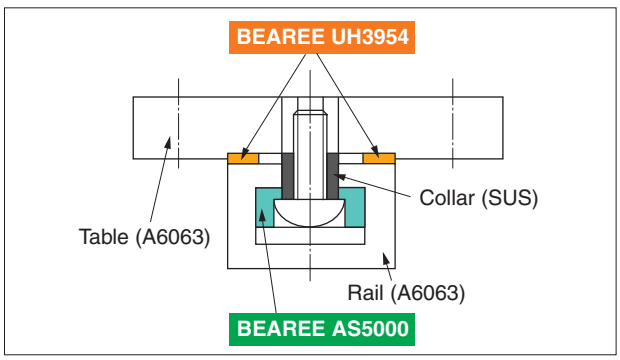
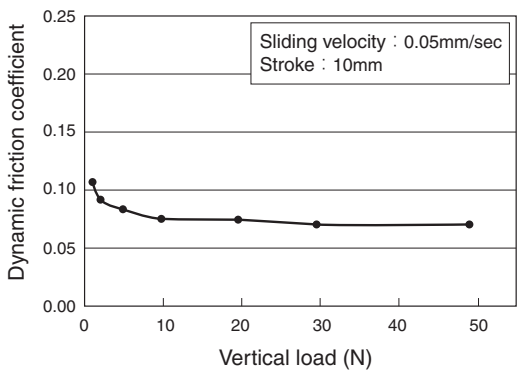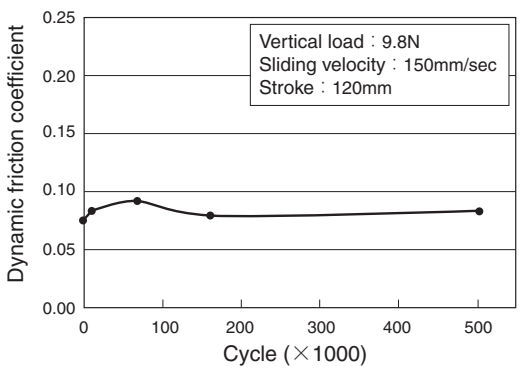
Friction data (Reciprocating testing device)